



Quantitative Identification of Electro-physical Properties of Oxide Based Hetero-interfaces at Extreme Environments

FA9550-12-1-0441

Start Date (Nov, 2012)

Alp Sehirlioglu – Department of Materials Science and Engineering, CWRU

Walter Lambrecht, Xuan Gao – Physics Department, CWRU

Marie-Hélène Berger – Mines-ParisTech, France

Wei Lu – Department of Electrical Engineering and Computer Science,
University of Michigan





Quantitative Identification of Electro-physical Properties of Oxide Based Hetero-interfaces at Extreme Environments

Grant No. FA9550-12-1-0441

STATUS QUO

Oxide Heterointerfaces

- A new type of hetero-interface in perovskite oxides (2004)
- LaAlO_3 on $\langle 001 \rangle$ oriented Ti-terminated SrTiO_3 single crystals.
- Interface electrical conductivity is tunable (2006).
- The origin of the conductivity and tunability under debate to date.

Investigating “real” interfaces for extreme environments.

- The focus will be on parameters below:
 - Composition of the film,
 - Interfacial Strain,
 - Interface composition,
 - Anisotropy
 - Surface conditions
 - Electrodes,
 - Temperature.

These parameters are not isolated from each other and cross-cutting effects will also be investigated.

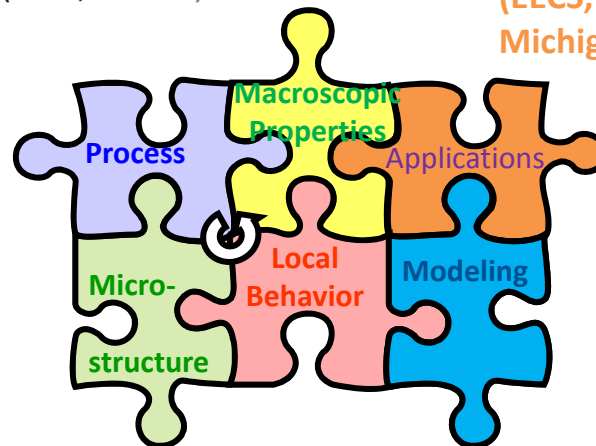
MAIN ACHIEVEMENTS:

The proposed approach is a fully integrated schedule that will provide the electrical property measurements on the exact same films that are characterized for non-stoichiometry, interface strain, intermixing, point defects and dislocations. A strong international team has been built to address these challenges:

Alp Sehrioglu
(MSE, CWRU)

Xuan Gao
(Physics, CWRU)

Wei Lu
(EECS,
Michigan)

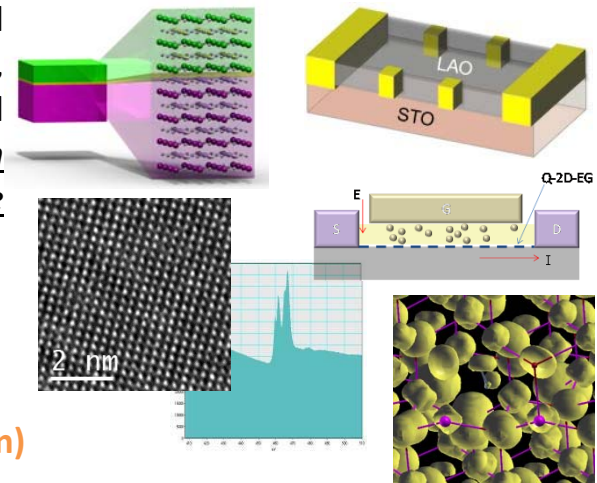


Marie Helene Berger
(Mines-Paris Tech)

Walter Lambrecht
(Physics, CWRU)

Planned Impact

- Quantitative understanding of the electro-physical behavior of the oxide based hetero-interfaces.



- 1-Processing and film characterization
- 2- Electrical characterization
- 3- Modeling
- 4- High Temperature effects
- 5- Proof of concept applications

Research Goals

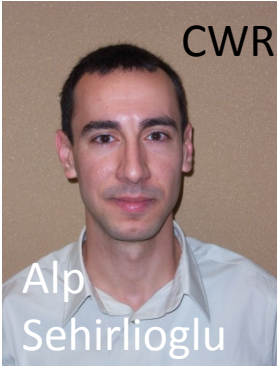
- The proposed approach will fully characterize every film and relate the observed and quantified parameters to electrical properties.

NEW INSIGHTS

QUANTITATIVE IMPACT

END-OF-PHASE GOAL

Research Team



CWRU- MSE

Alp
Sehirlioglu

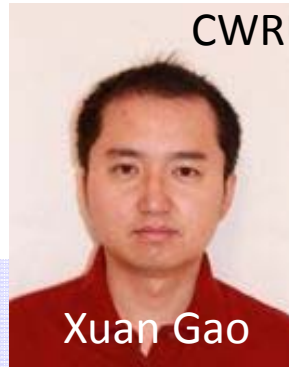
STO Substrate orientation
STO Surface preparation
Target material
Deposition conditions (p_{O_2} , plume, angle, temp...)
Annealing

Substrate termination
Local stoichiometry
Domains
Strain development/relaxation
Intermixing
Ti valence profile
Point defects
+ Temperature dependence

Mines-ParisTech



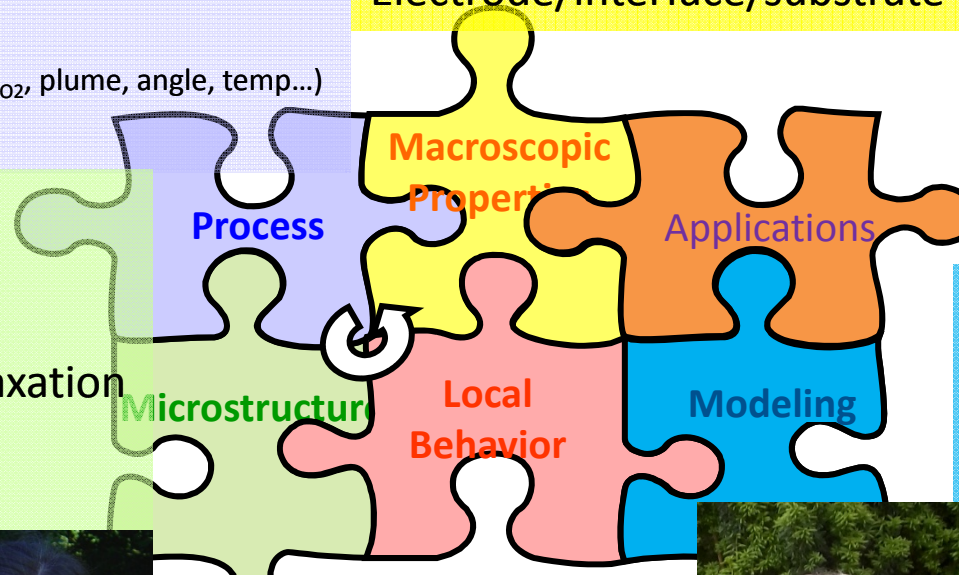
Marie Helene
Berger



CWRU- Physics

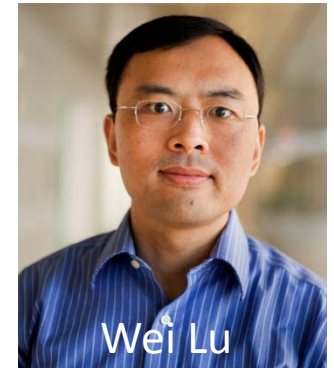
Xuan Gao

Charged carrier density
mobility
Temperature dependence
Electrode/interface/substrate



Transport mechanism:
-Polar discontinuity
-Dipoles
-Scattering sites
-Domain boundaries

UM- Electrical Eng.



Wei Lu

Defect based devices
Resistive switching
Modeling and
experimental
prototype devices.

Defects and Impurities
Strain
Polarization
Compositional
variations
Charge balance
mechanisms.
Charge carrier
development

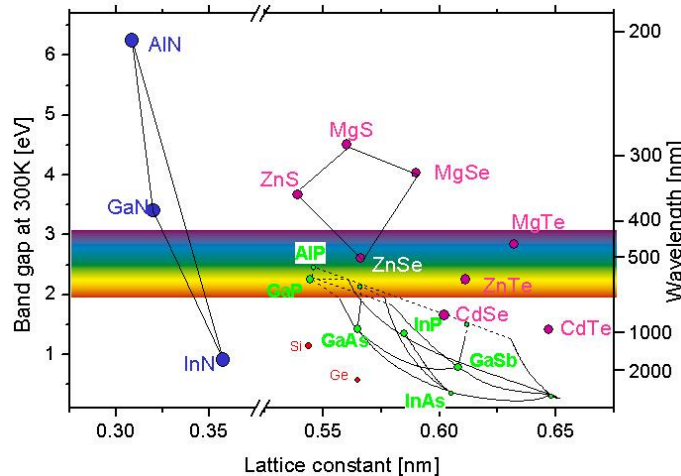


Walter
Lambrecht

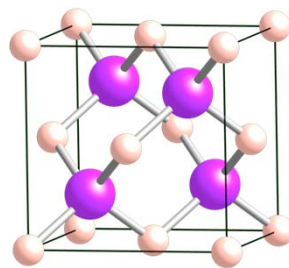
CWRU- Physics

Electronic materials

Semiconductors

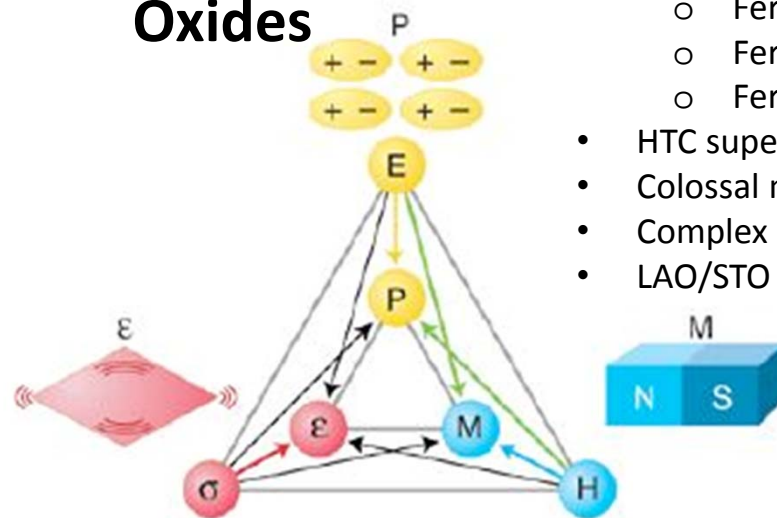


- Band gap
- Opto-electronics
- Transport, doping
- Transistor, Diode
- **Spintronics**



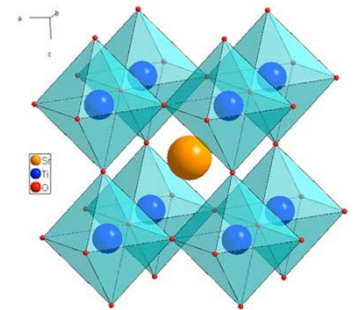
Zinc blende

Oxides



- Multifunctional
 - Ferroelectric
 - Ferromagnetic
 - Ferroelastic
- HTC superconductors
- Colossal magneto resistance
- Complex ABO_3
- LAO/STO 2DEG

- Complex structure leads to various instabilities and complex ordering phenomena
 - Magnetism
 - Jahn-Teller distortions
 - Orbital ordering
 - Superconductivity
- Transition metal element d-electrons lead to strongly correlated electron behavior
- These are the fundamental origin of the multifunctional behavior

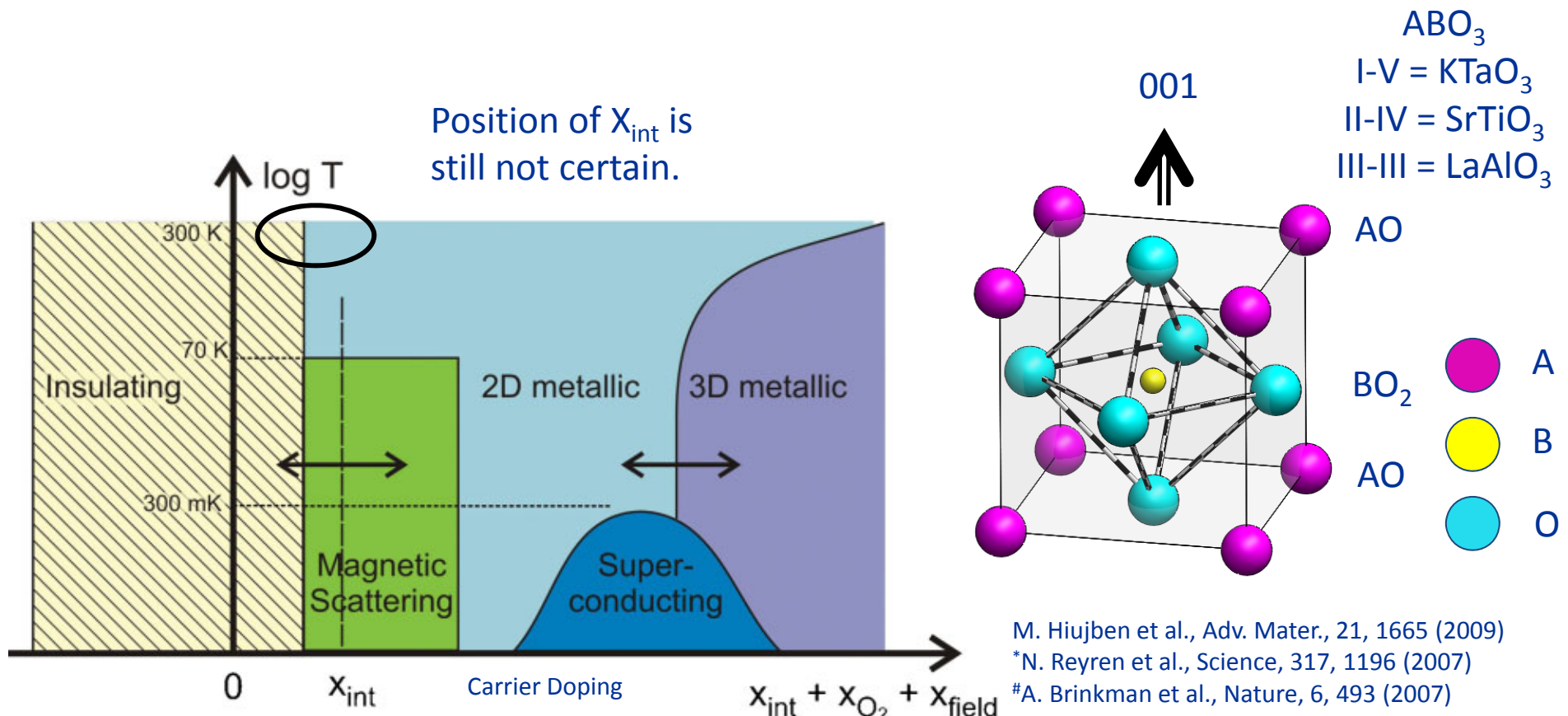


Perovskite

Objectives

- Quasi-two-dimensional electron gas: Recently discovered
Investigated for nano-device applications
- The science behind Q-2D-EG is still not clear.
- **We aim to elucidate the fundamentals of Q-2D-EG formation by isolating effects that contribute to charge at the interface.**

Science will lead to optimization of the device → Stability and Reproducibility



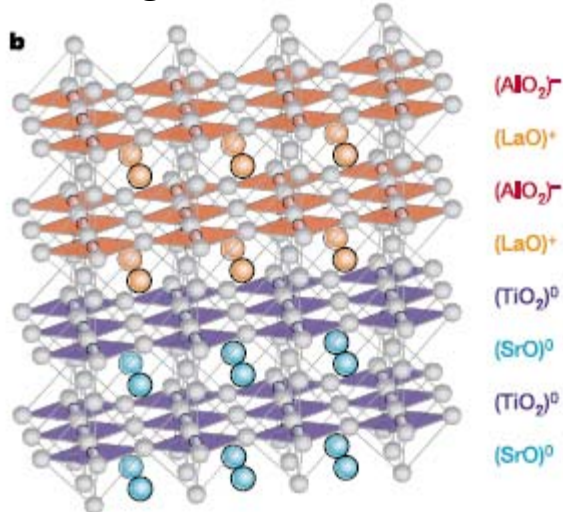
M. Huijben et al., Adv. Mater., 21, 1665 (2009)

*N. Reyren et al., Science, 317, 1196 (2007)

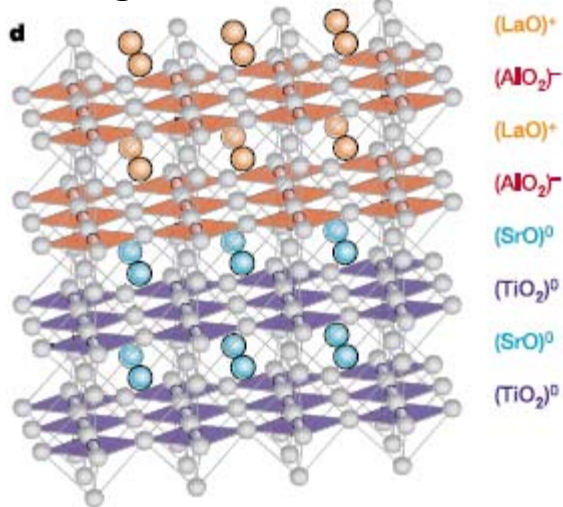
#A. Brinkman et al., Nature, 6, 493 (2007)

Q-2D-EG

Conducting interface



Insulating interface



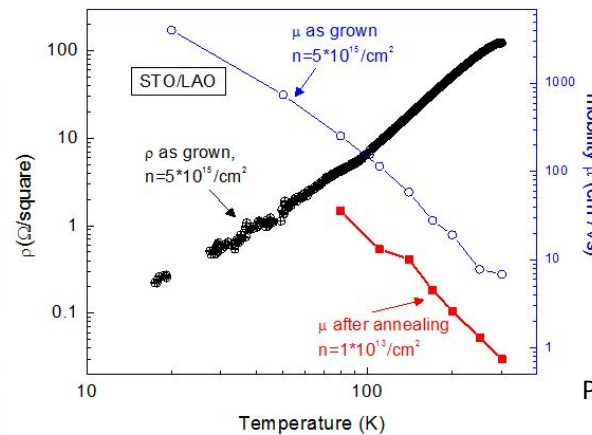
* Wide band gap insulator,

Insulator – borderline semiconductor

A. Ohtomo and H.Y. Hwang, "A high mobility electron gas at the LaAlO₃/SrTiO₃ interface," Nature, **427**, 423 (2004).

	LaAlO ₃	SrTiO ₃
Band gap	5.6 eV [*]	3.2 eV [#]
Similar lattice parameters	3.768 Å	3.905 Å

Larger band gap of both LAO and STO make them attractive for extreme environment applications such as (i) High temperature and (ii) exposure to radiation.



- Our film resistivity ρ shows metallic behavior and mobility of as grown sample approaches $10^4 \text{ cm}^2/\text{Vs}$ at low T for as grown sample.

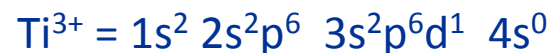
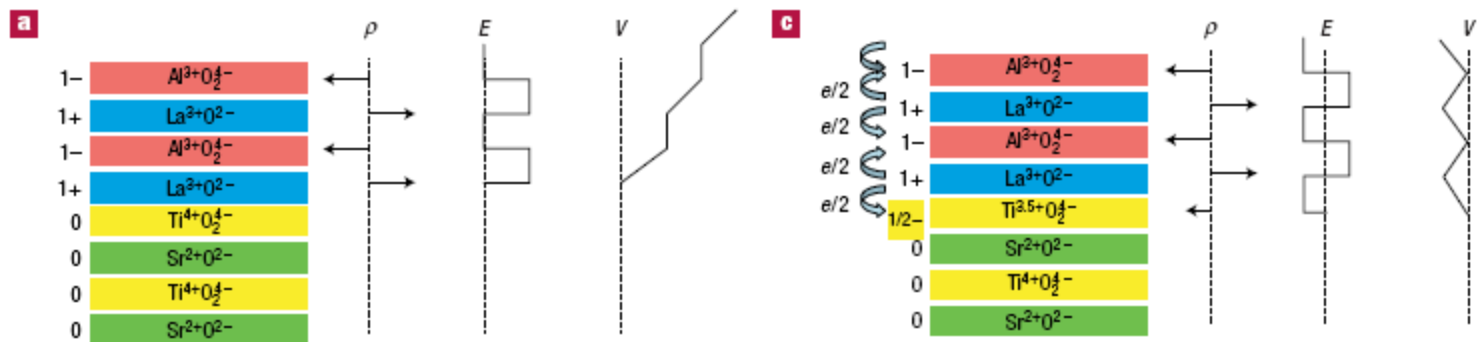
Prof. Xuan Gao – Physics Department (CWRU)

- The high electron density in as grown sample can be reduced to $10^{13}/\text{cm}^2$ regime by annealing in O₂.
- The annealed sample still has metallic behavior and mobility above $1 \text{ cm}^2/\text{Vs}$ (red dots).
- These values are similar to other reports in literature.

Intrinsic vs. Extrinsic effect

- Polar catastrophe, electronic reconstruction

N-type interface, conducting, charge rearrangement unlike semiconductors



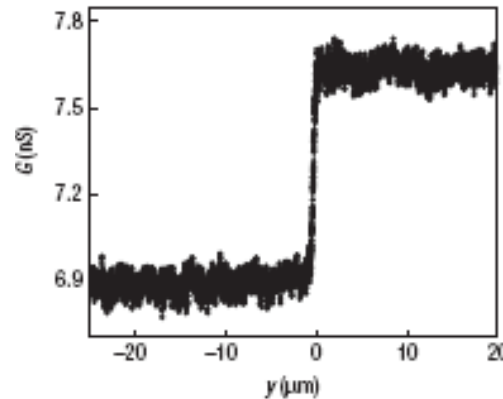
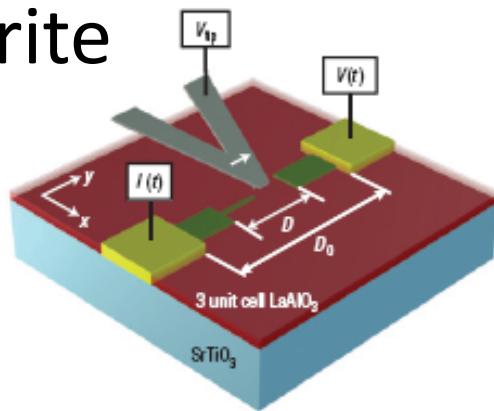
Ti termination is necessary for Q-2D-EG formation

Nakagawa et al., Nature Materials, 5, 204, 2006. Eckstein, Nature Materials, 6, 473, 2007

- Upper limit for charge carrier density for $\frac{1}{2} e^-$ per unit cell = $3.5 \times 10^{14} \text{ cm}^{-2}$ (for stoichiometric LAO)
- Measured charge carrier densities: $1 \times 10^{13} - 4 \times 10^{16} \text{ cm}^{-2}$
- Interface charge carrier density and resistance depends on partial pressure of oxygen during deposition ($10^{-3} - 10^{-6} \text{ Torr}$)
- High energy particles from PLD sputtering off oxygen.

Tunability

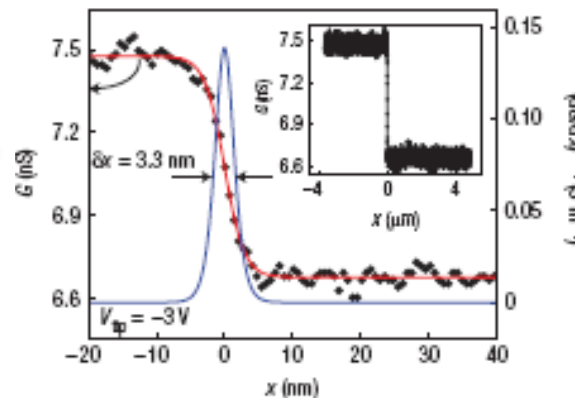
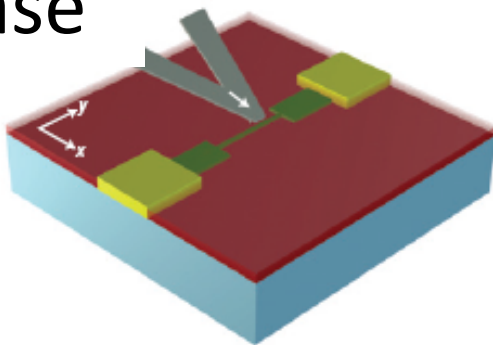
Write



- Layer thickness LAO < Critical thickness
- Write and Erase cycles possible
- Wire thickness is a function of tip voltage
- Features as small as 1nm can be written

Cen et al., Nature Materials, 7, 298 (2008)

Erase



- The electronic reconstruction at the interface requires reconstruction at the surface of the film; structurally, electronically, or chemically.
- Electronic reconstruction requires holes forming at the surface, however, such p-type surface conduction was never observed.
- In structural and chemical reconstruction the two most significant factors are: (i) oxygen vacancies and (ii) adsorbed humidity on the surface.
- STO capping of the films allowed circumvention of structural or chemical reconstruction and allowed electronic reconstruction on the surface.

Factors that contribute to Q-2D-EG

1. Polar catastrophe at the polar LAO/non-polar STO interface,
2. Structural distortions at the interface
3. Oxygen vacancies introduced into the LAO/STO hetero-structure during the growth of LAO
4. Preferential cationic intermixing at the interface.

None of these factors are exclusive of each other.

•In addition to the (i) surface termination, (ii) deposition conditions, and (iii) oxygen annealing other factors can effect the presence and/or magnitude of interface conductivity and tunability.

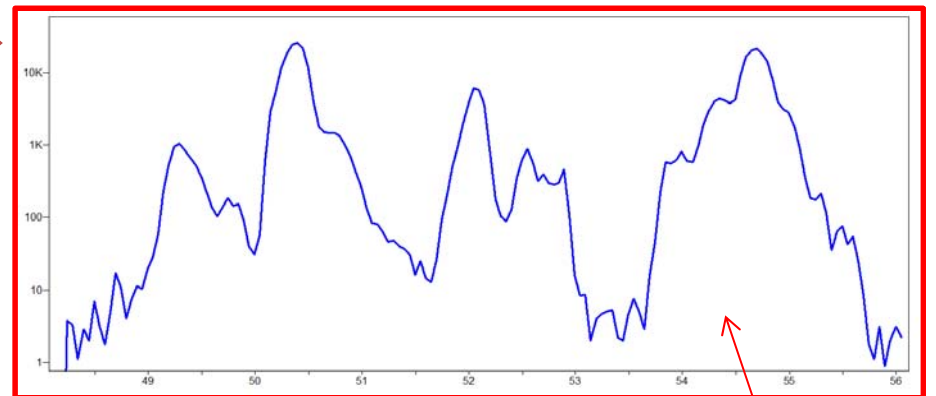
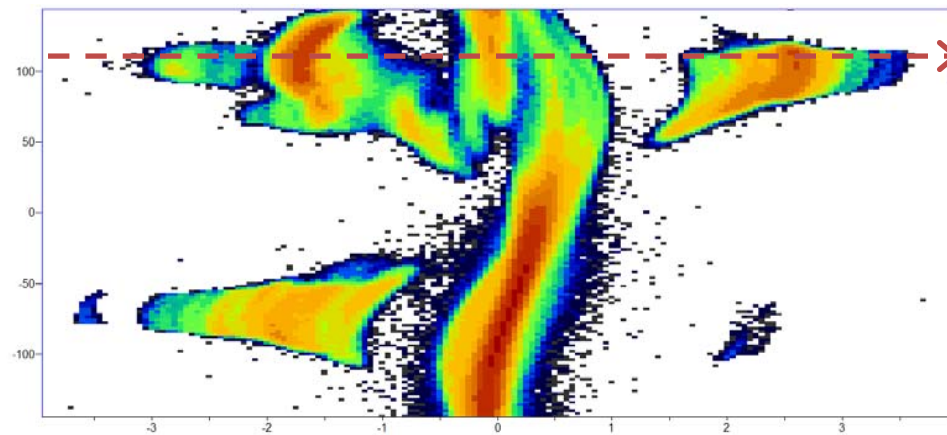
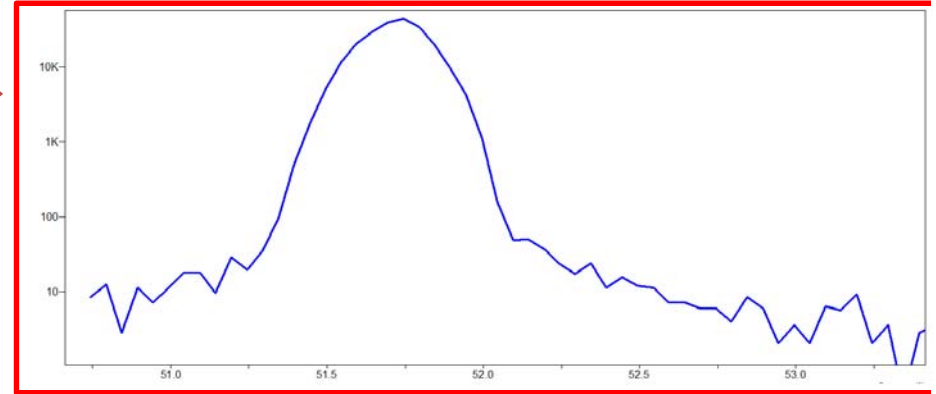
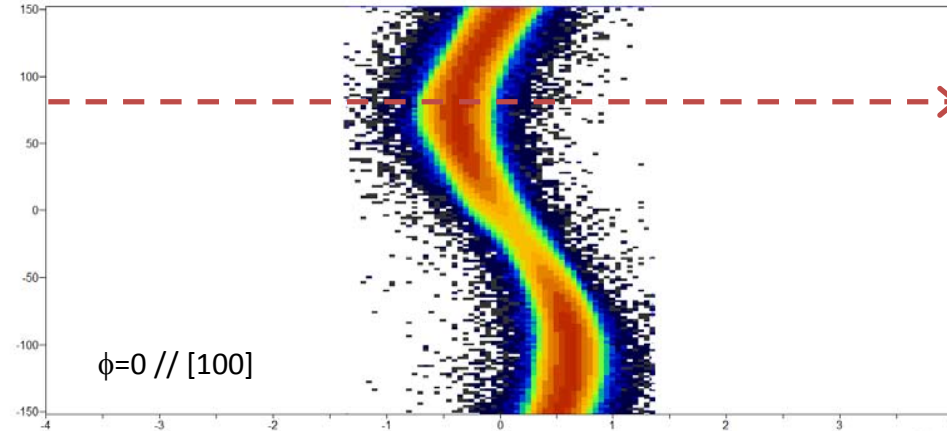
•A large number of parameters can effect both the existence and the magnitude of the interface conductivity.

- Substrate quality
- Film composition
- Defects
- Strain development
- Film thickness
- Electrode materials
- Film surface conditions
- In plane anisotropy.

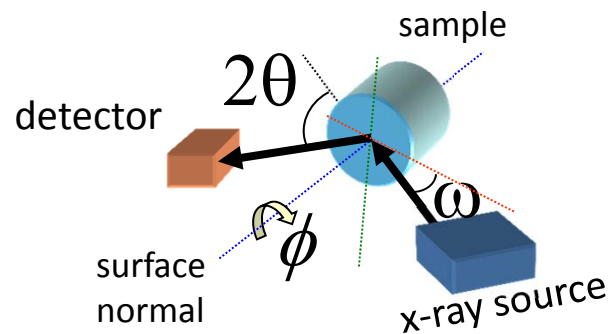
All have different dependence on temperature.
Therefore any extreme environment application
requires quantitative analysis of these parameters.

SrTiO₃ (001) substrate domain distribution

ϕ (degrees)



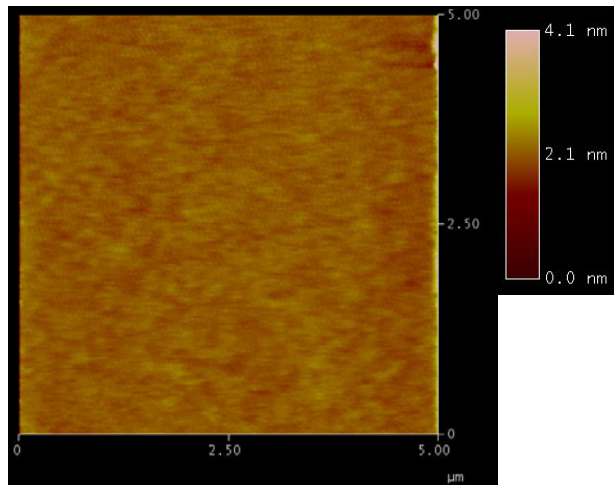
ω (degrees)



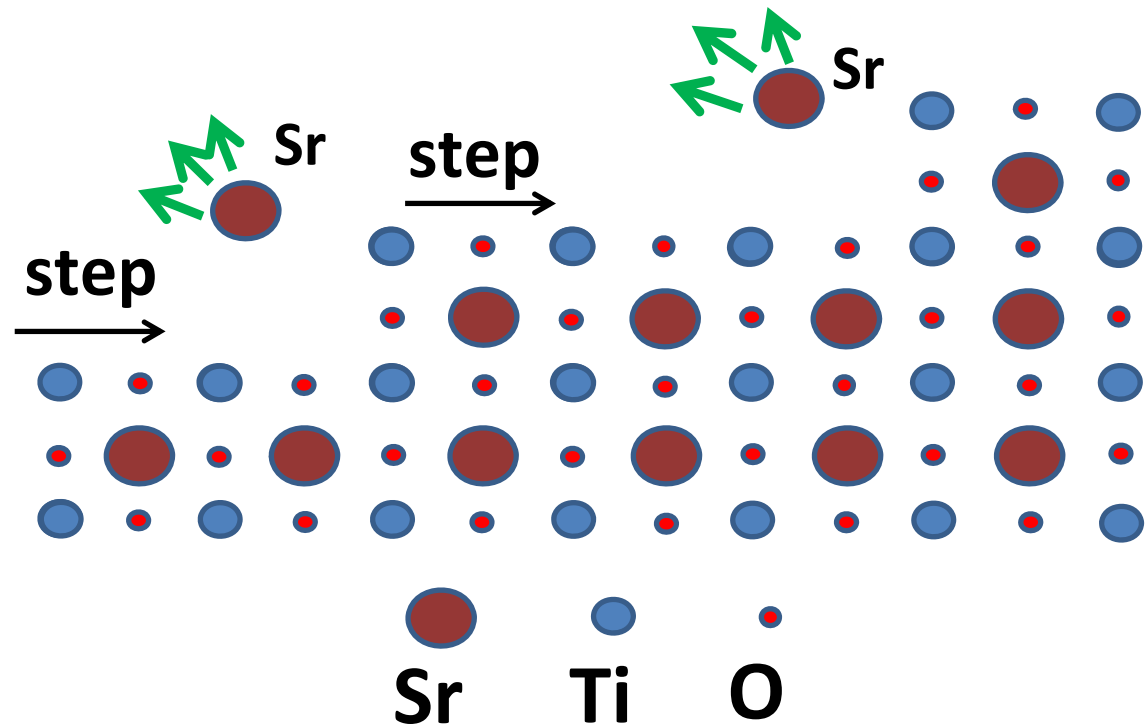
Multiple domains

Surface Preparation

As-received



SrTiO_3 surface etching process



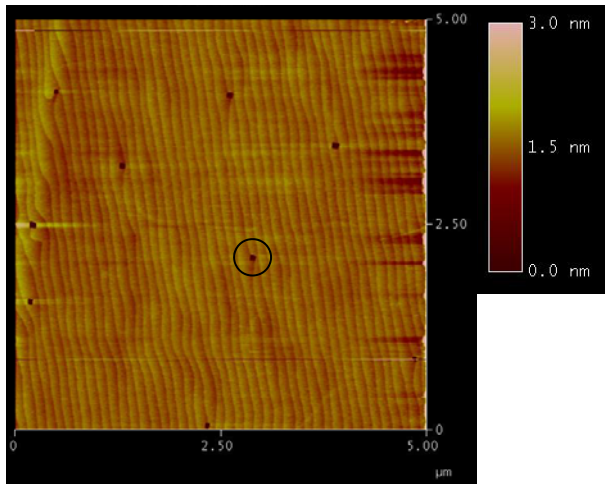
Ultrasonic soaking
in water
(SrO , $\text{Sr}(\text{OH})_2$)

Etching by NH_4F -HF
(pH = 6)
30 sec

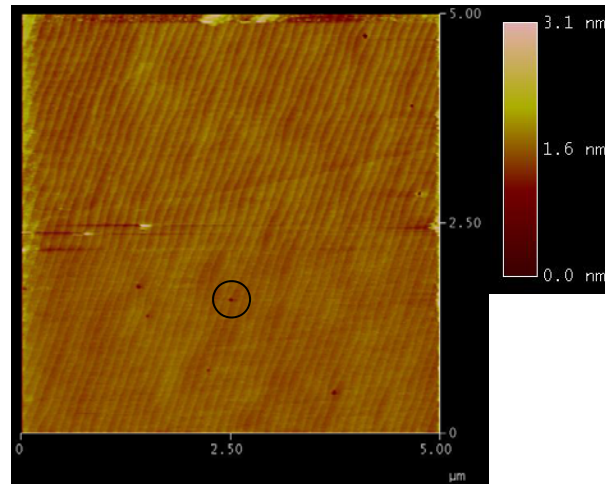
Annealing
950 °C 2 hrs

Surface Preparation

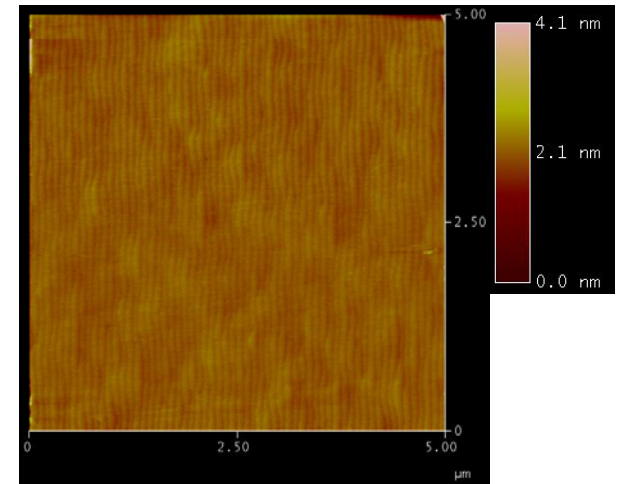
pH = 5.7



pH = 5.8

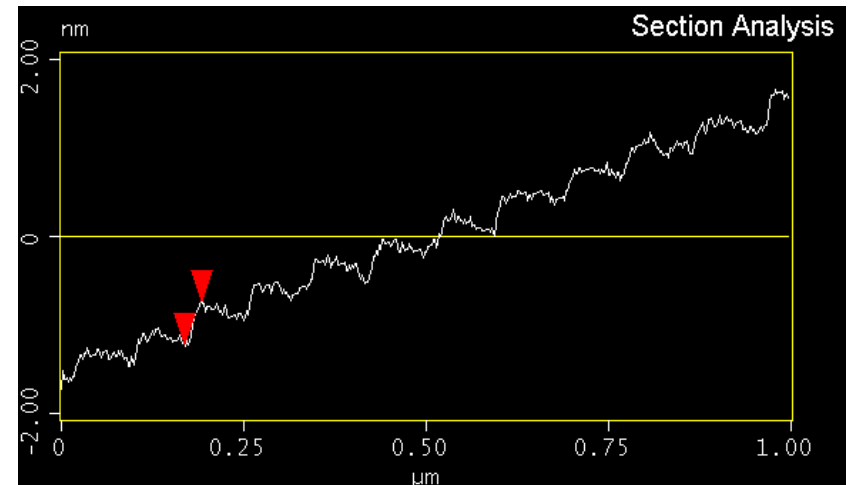
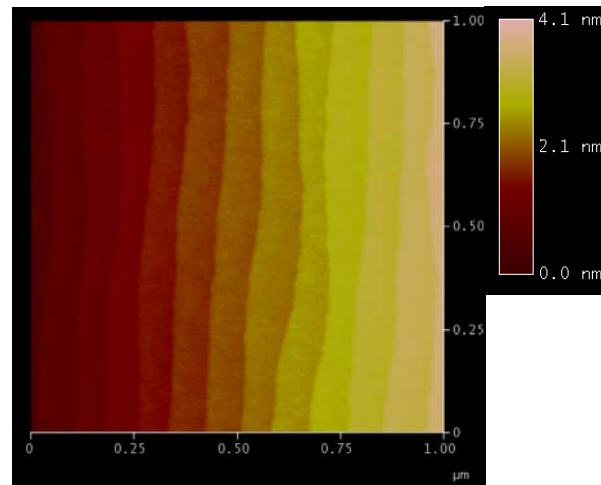
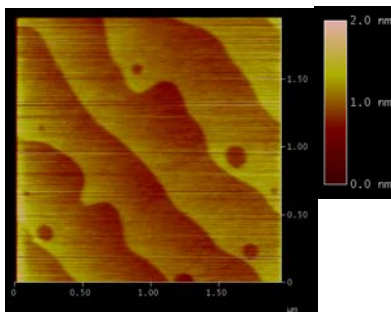


pH = 6.0

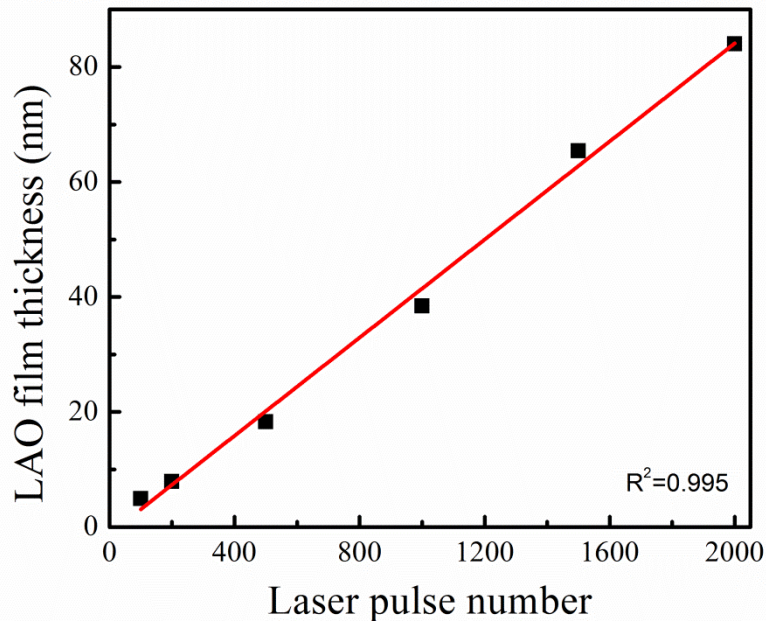
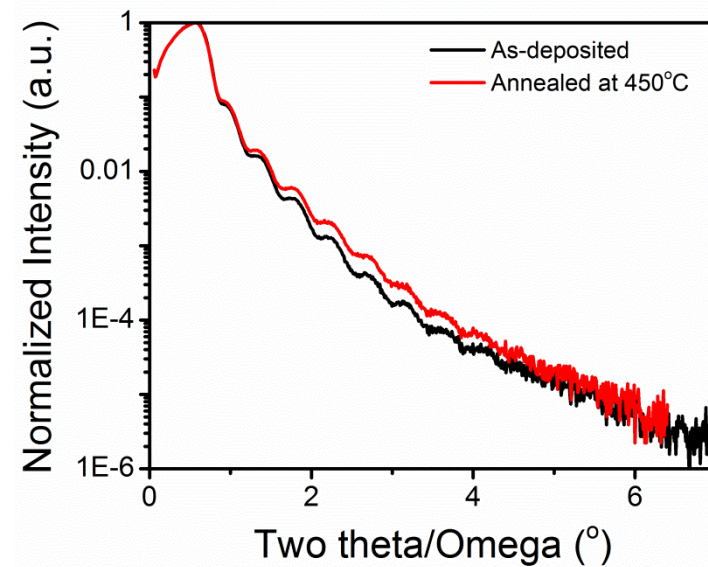
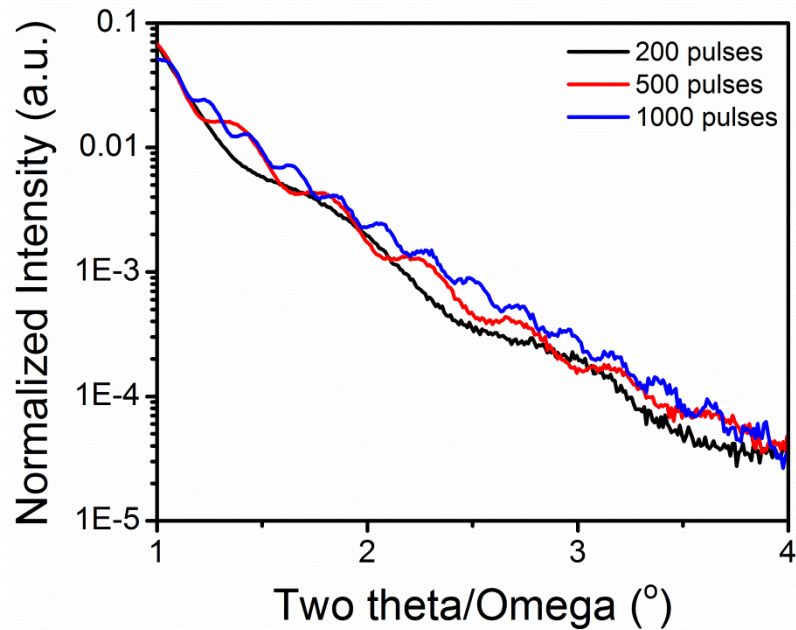


Steps

Commercially
terminated

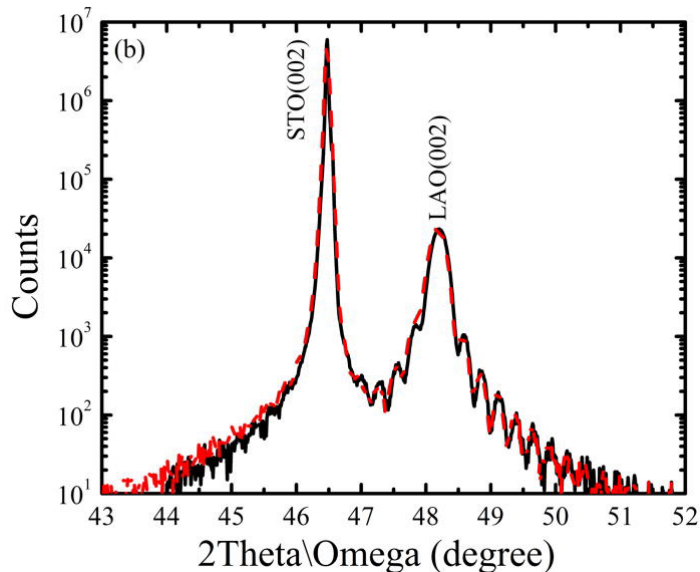
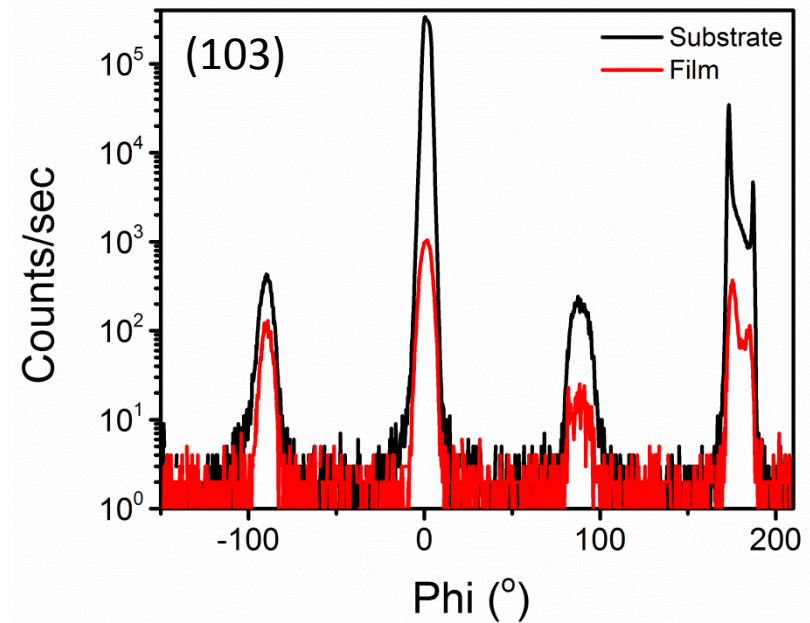
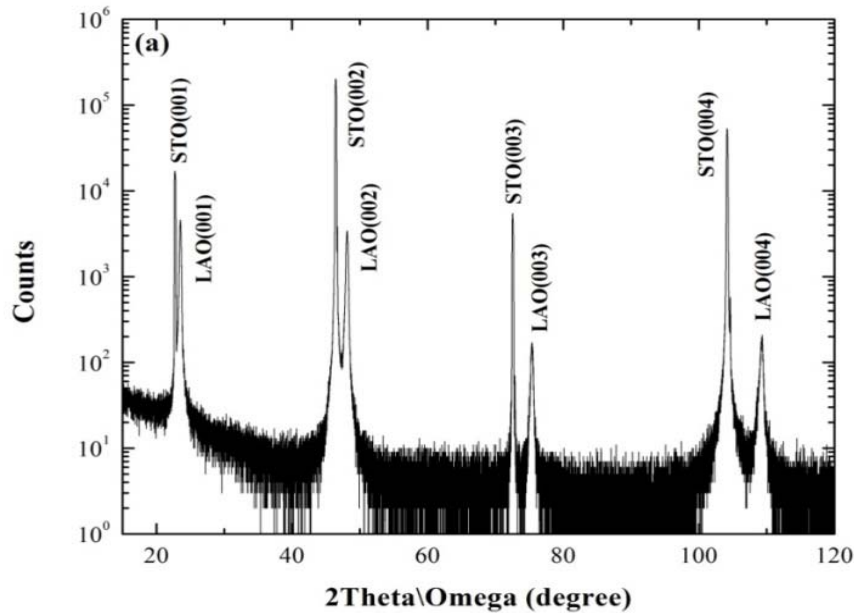


Film thickness



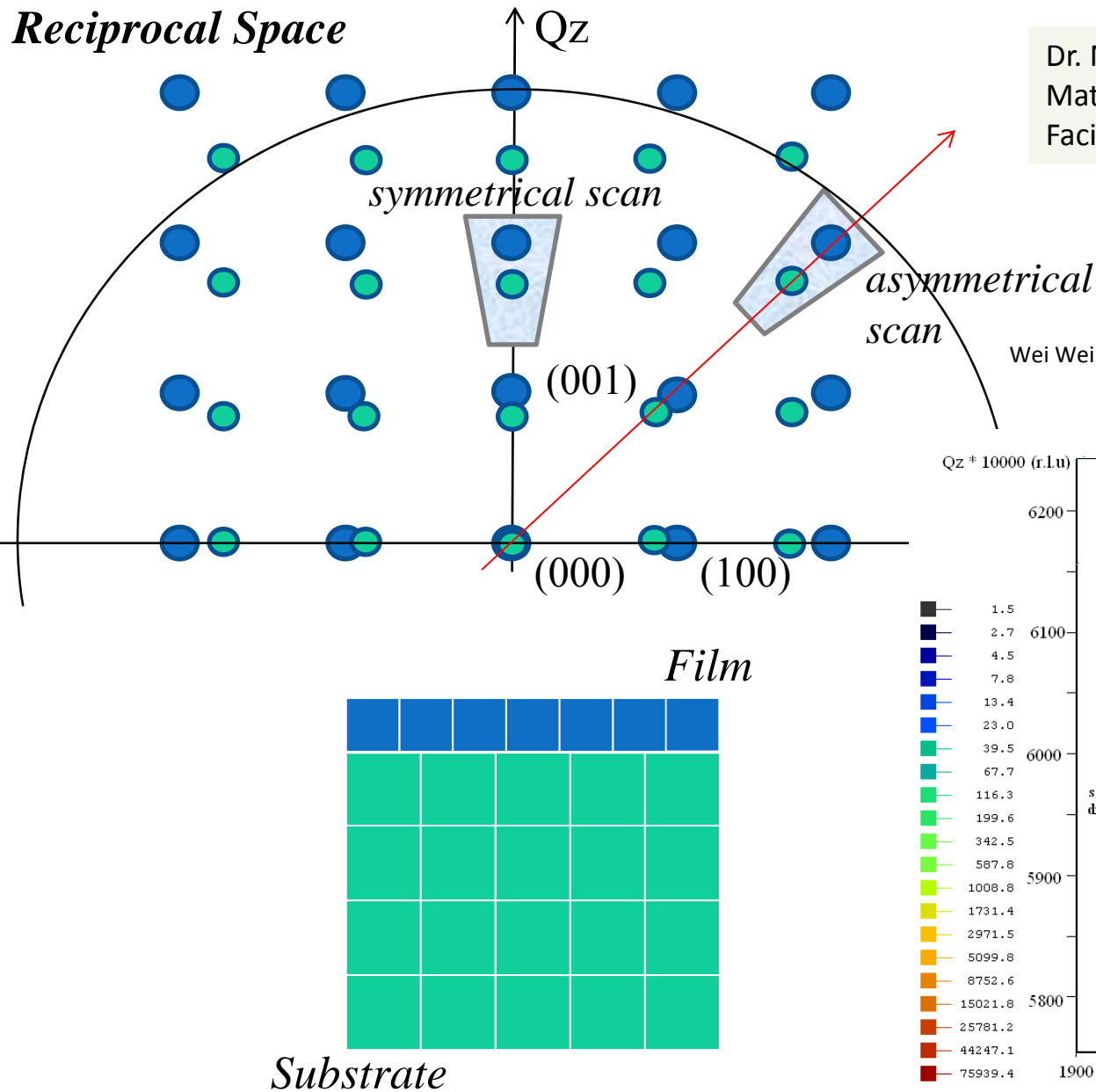
- Sharp interfaces (roughness rms < 0.3 nm).
- Critical angle in XRR curves is about the same for each sample as-grown and after annealing (450°C) suggesting no change in the film density.
- XRR curve decays slightly slower in the annealed samples compared to the as-grown samples, suggesting a slightly improvement in the interface sharpness of the films with annealing.

Epitaxial films



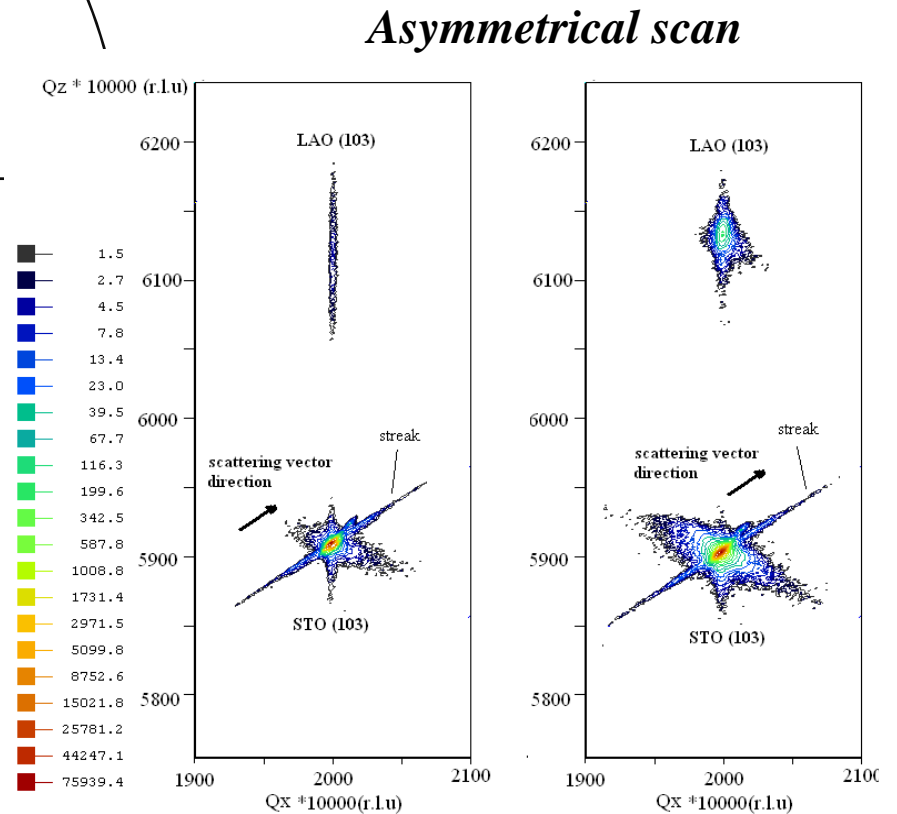
- The films are strongly oriented with the substrate in the film growth direction.
- No new phases or orientations were induced by the 450°C annealing.
- A smaller atomic spacing “d” for the film in the growth direction compared to the substrate.
- Thickness fringes are also observed in each sample, indicating that the film interfaces are sharp.
- Four-fold symmetry due to the cubic structure.
- Films are epitaxial with the substrate.
- with the crystallographic relationship [001]STO//[001]Film and [100]STO//[100]Film.

Reciprocal space mapping

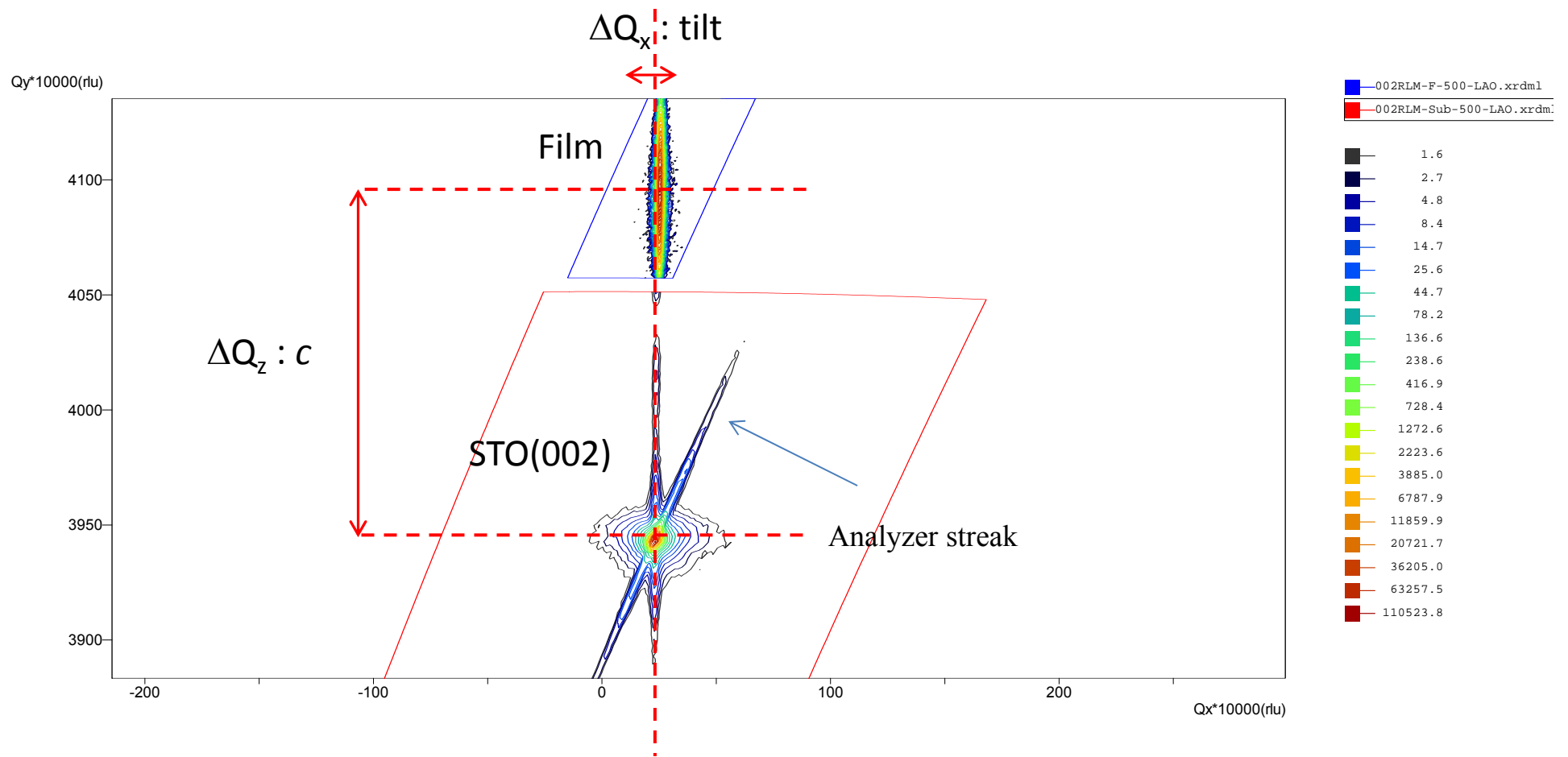


Dr. Mauro Sardela in the Frederick Seitz
Materials Research Laboratory Central
Facilities, University of Illinois

Wei Wei and Alp Sehirlioglu, Appl. Phys. Lett., **100**, 071901 (2012)



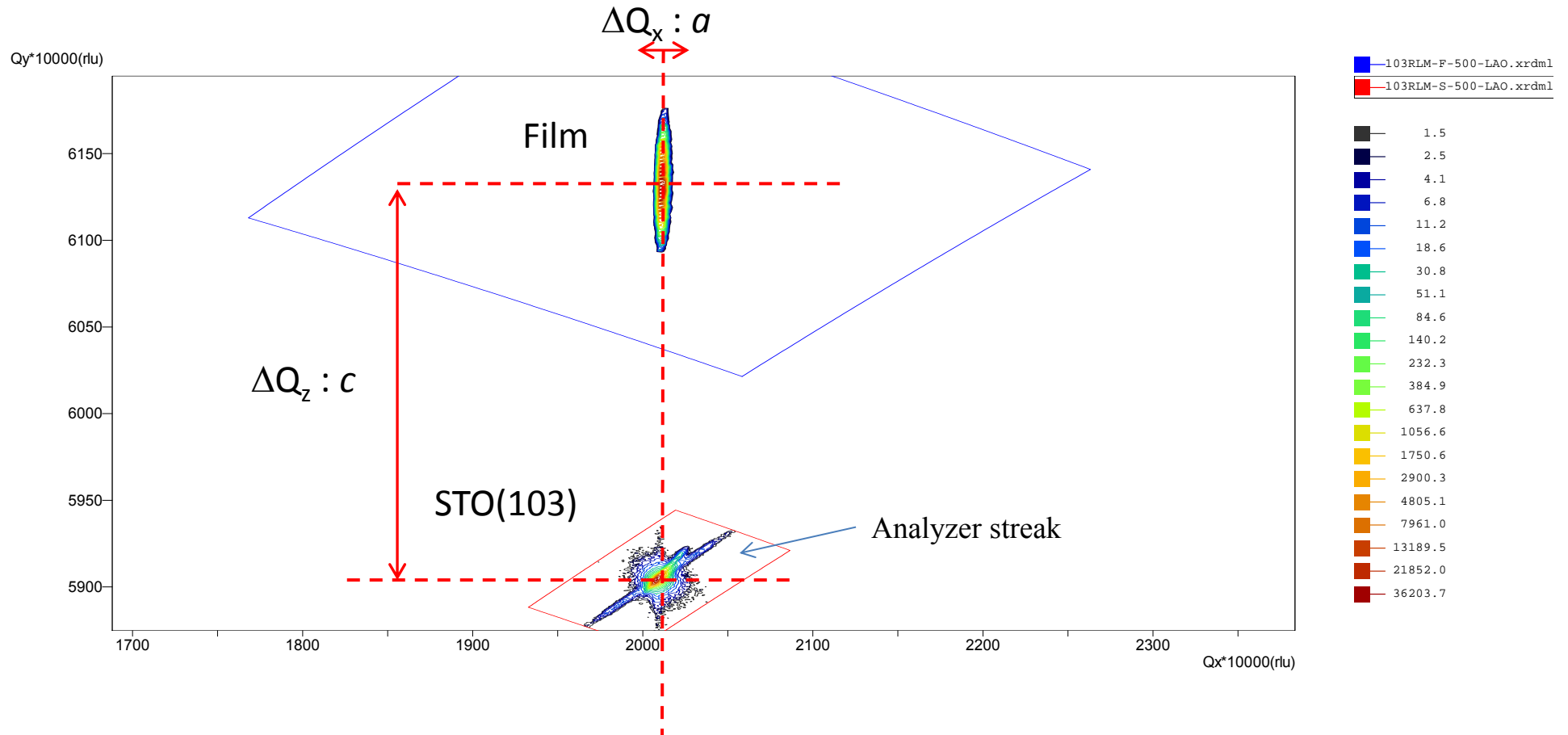
RLM near STO(002): sample 500# - LAO



Q_z [001]

Q_x [100]

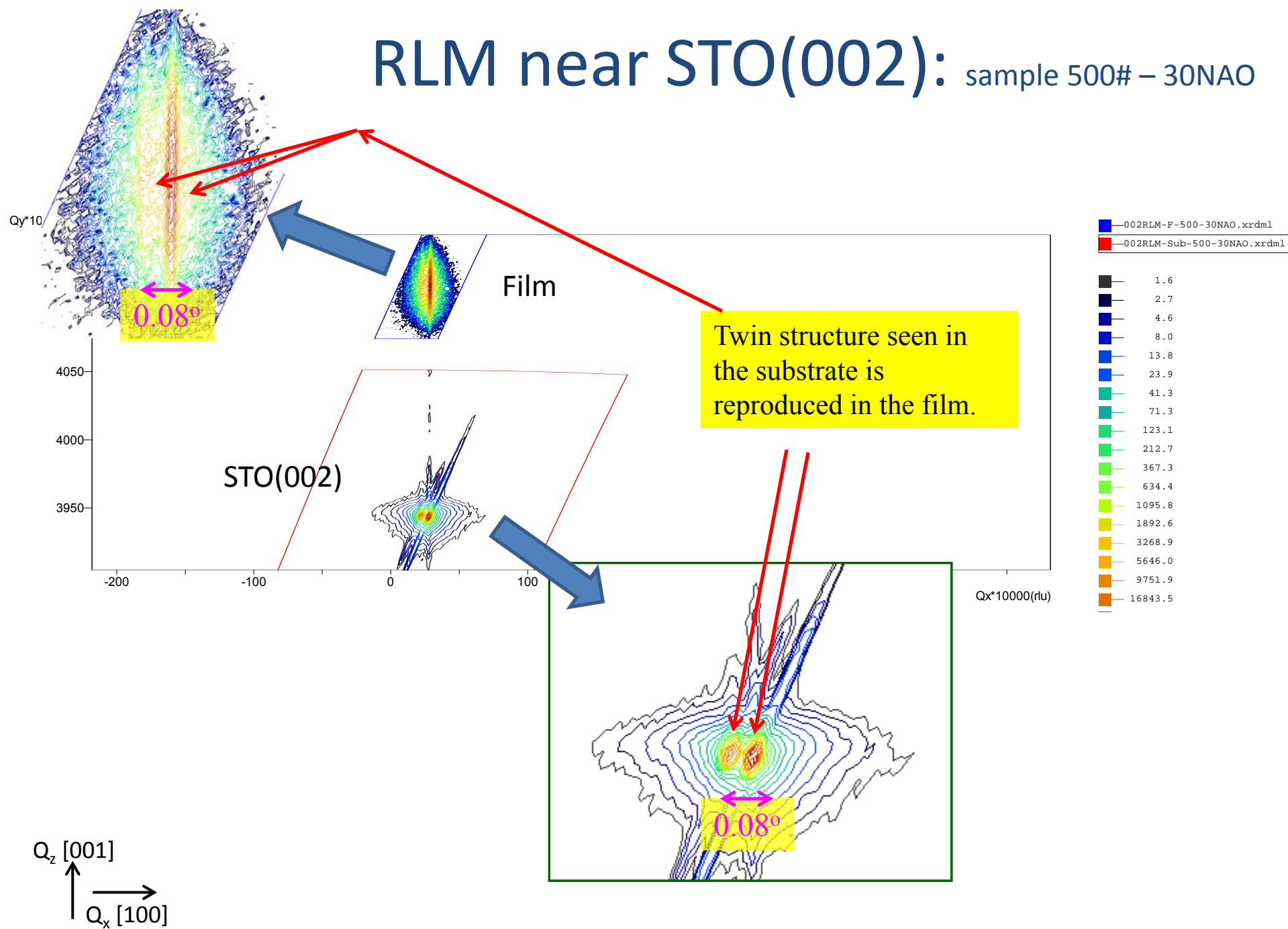
RLM near STO(103): sample 500# – LAO



Q_z [001]

Q_x [100]

RLM near STO(002): sample 500# – 30NAO



Reciprocal space mapping

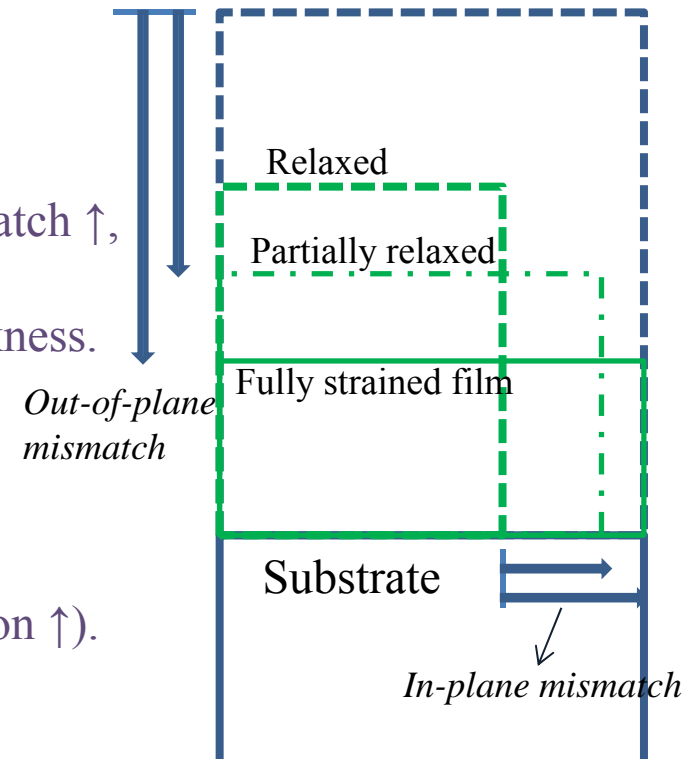
Bulk LAO: 0.3791 nm Bulk STO: 0.3905 nm

In-plane direction:

- LaAlO_3 films are under tensile strain.
- As thickness increases: Stress \uparrow , Lattice constant \downarrow , Mismatch \uparrow , Strain \downarrow
- Partial relaxation in LaAlO_3 films with increasing film thickness.
- Above 80nm film thickness: Plastic deformation due to large strain. Residual film remains highly strained.

Out-of-plane direction:

- LaAlO_3 films are tetragonally distorted.
- Degree of tetragonality is decreased as thickness \uparrow (relaxation \uparrow).
- Residual film above 80nm is still tetragonally distorted.



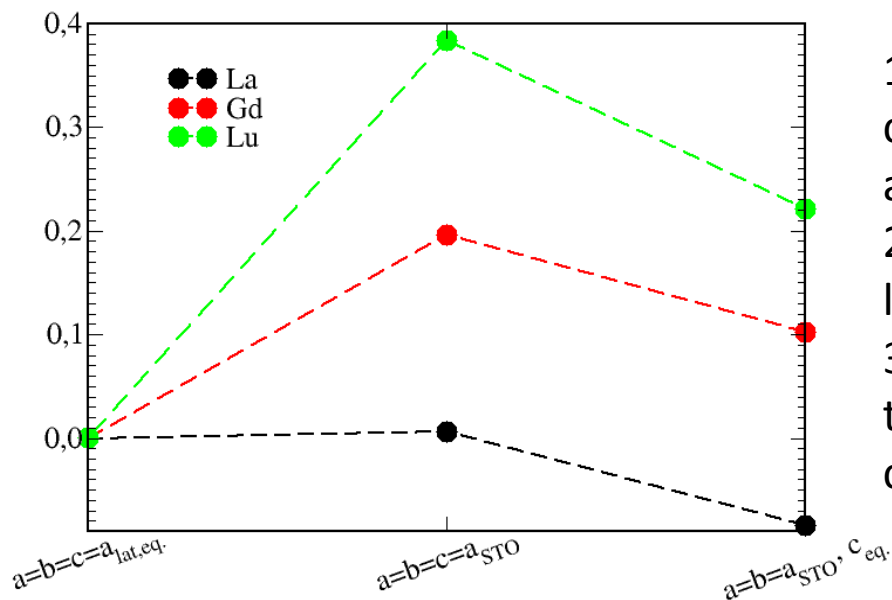
Wei Wei and Alp Sehirlioglu, Appl. Phys. Lett., **100**, 071901 (2012)

Laser pulse	Thickness (nm)	f_{pp}	f_{pl}	ϵ_{pp}	ϵ_{pl}	a_{pp} (nm)	a_{pl} (nm)	Relaxation rate	a_{pp}/a_{pl}
100	4.9	- 0.03958		- 0.00913		0.375045			
200	7.9	- 0.03522	- 0.00056	- 0.00437	0.03139	0.376750	0.390280	1.83%	0.965332
500	18.3	- 0.03358	- 0.00076	- 0.00268	0.03119	0.377390	0.390202	2.48%	0.967165
1000	38.4	- 0.03326	- 0.00100	- 0.00261	0.03067	0.377513	0.390109	3.26%	0.967711
1500	65.4	- 0.02987	- 0.00117	- 0.00321	0.03050	0.377284	0.390041	3.83%	0.967293
2000	84	- 0.03322	- 0.00052	- 0.00257	0.03117	0.377529	0.390298	1.68%	0.967283

Lanthanides

- Can the strain at the interface be changed without changing the electronic reconstruction mechanism (for a given thickness)

Theoretical case of Gd and Lu at the place of La: In order to see best the effect of the known systematic size reduction of rare-earth atoms in the periodic system, the “lanthanide contraction”, both the central rare-earth element Gd and the right-most element Lu were selected for the substitution of the left-most original element La.



1- Cubic bulk structure with the equilibrium lattice constant a_{lat} of the specific LnAlO_3 crystal:

$$a=b=c=a_{\text{lat}}$$

2- Cubic bulk structure enlarged to the equilibrium lattice constant a_{STO} of STO: $a=b=c=a_{\text{STO}}$.

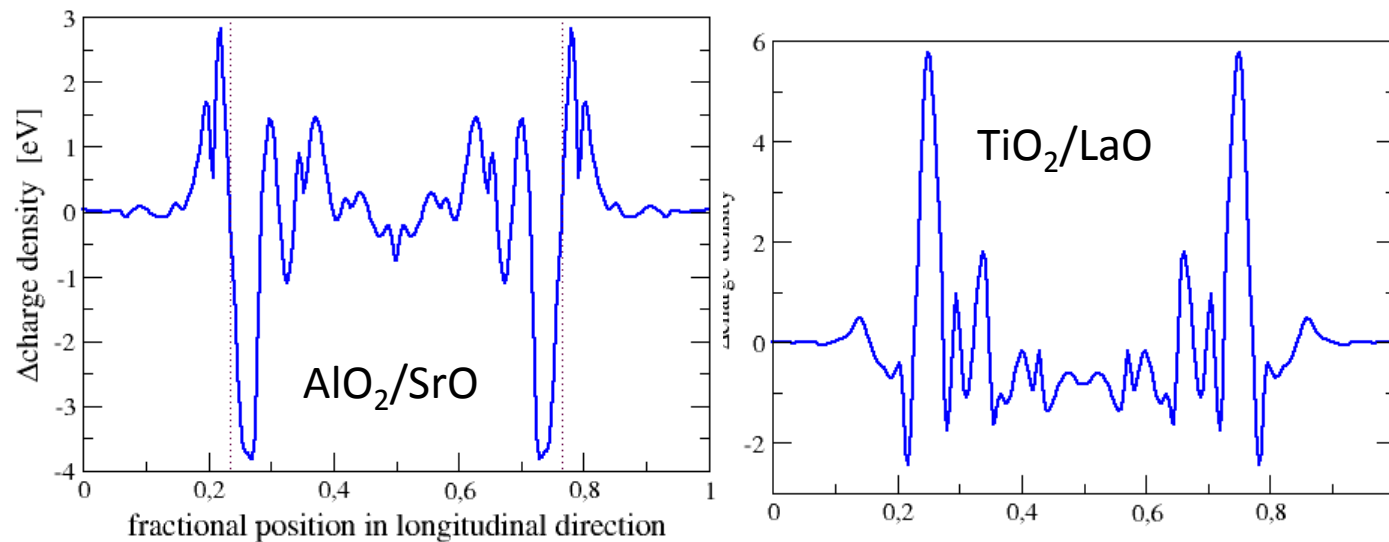
3- Tetragonal structure of type no. 2. stretched in the axial direction by the ratio c/a_{STO} : $a=b=a_{\text{STO}} / c=c_{\text{eq}}$.

Energetical view on the equilibrium bulk structures LnAlO_3

Theoretical calculations by Christian Elsaesser (FRAUNHOFER-INSTITUT FÜR WERKSTOFFMECHANIK IWM)

Lanthanides

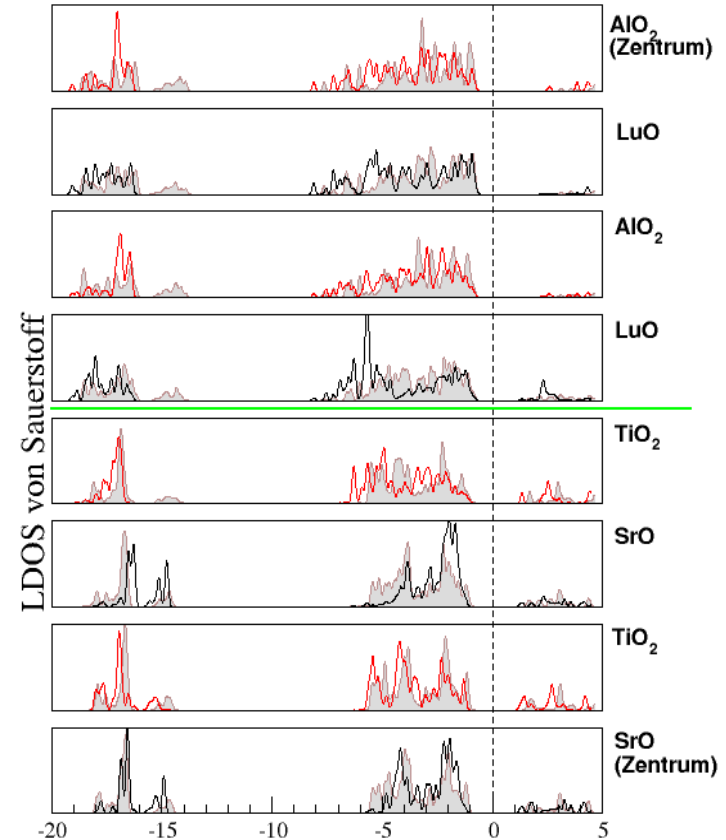
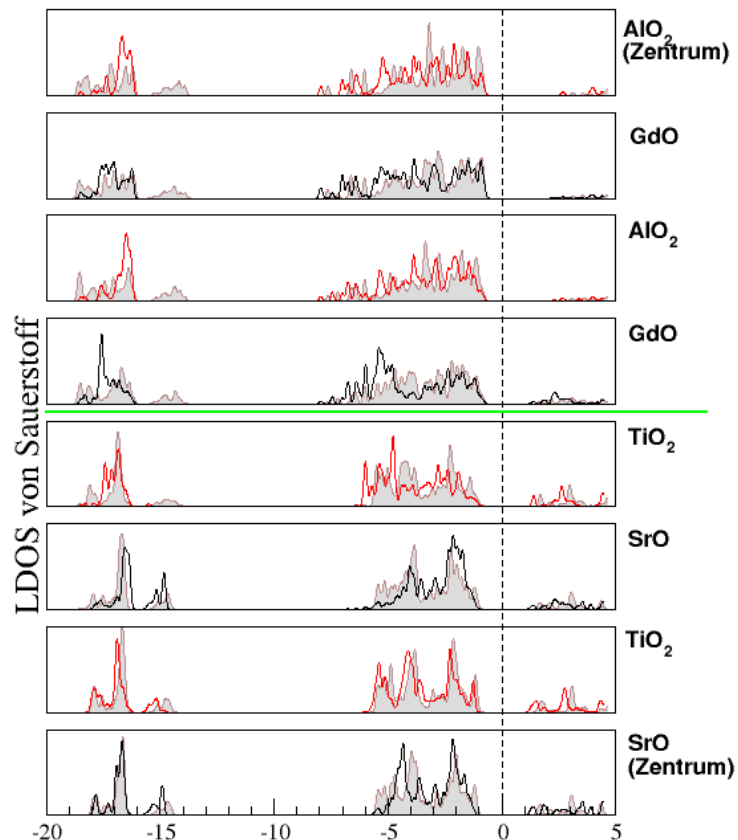
The different ionic radii of the lanthanides influence the stability of the bulk structures laterally fixed to the STO lattice constant. At the interface the LAO site seems to be more stable thermodynamically and with respect to the electron charge transfer: It is the STO atomic structure adjusting the volume (getting thus stretched out of equilibrium), and it is the electrons on the STO site compensating for the charge dipole at the interface far into the bulk.



The difference of the charge densities is directly related to the corresponding difference in the potential. The integral of this difference along the z direction is defined as the interfacial dipole associated with the electronic rearrangement during the formation of the interface. On the LaAO side of the interface, the charge transfer is limited to a close vicinity of the interface. On the STO side of the interface the charge transfer is decreasing with increasing distance to the interface, but is not yet zero in the center of the STO.

The charge dipole at the interface becomes larger for LuAO.

Lanthanides

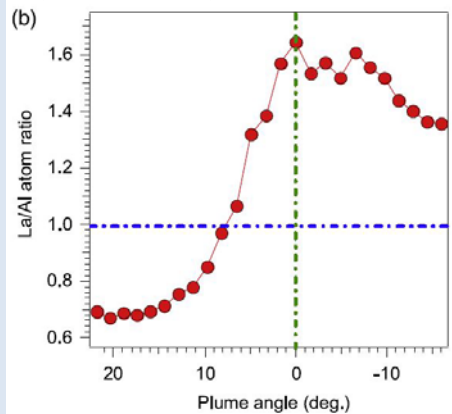


All figures contain the corresponding oxygen LDOS from the non-substituted case ($\text{Ln}=\text{La}$) as shaded gray/brown background for comparison.

There is no significant change in the electronic structure caused by the La substitution, or in the behavior of the absolute charge difference caused by the interface. Hence, the atomic structure at the interface can likely be tuned via the different ionic radii of rare-earth elements without losing the desired particular electronic properties of the interface.

Composition

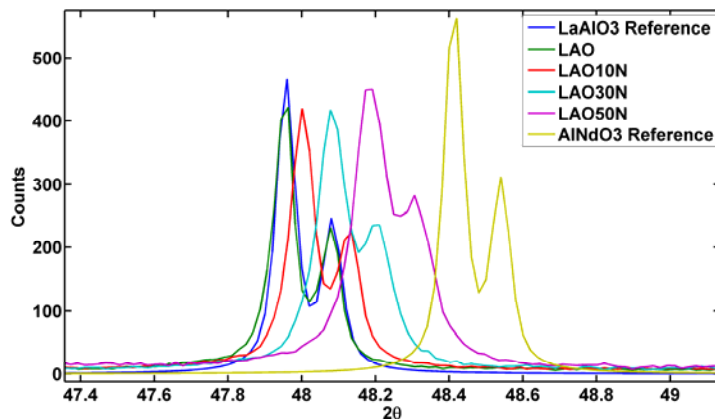
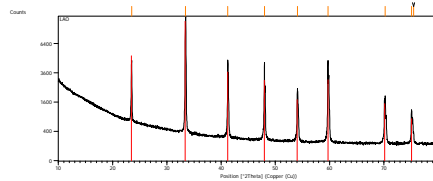
La/Al ratio in the film and the level of intermixing can depend on plume angle



T.C. Droubay, et al. Appl. Phys. Lett. **97**, 124105 (2010).

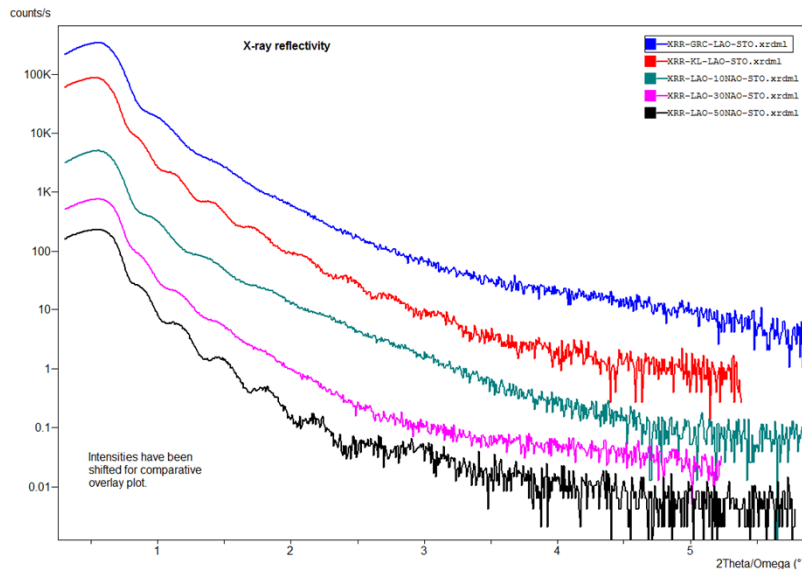
- The composition of target and the film can be different when multiple single-site cations exist.
- The composition of the film can be different for targets of same composition but different source.

Film composition	O	La	Nd	Al	(La + Nd)/Al	Nd/La
LAO-CWRU	66.13	20.25	0	13.62	1.48	0
LAO-Kurt Lesker	62.85	25.93	0	11.22	2.31	0
LAO-10NAO	67.03	18.88	0.69	13.39	1.46	0.036
LAO-30NAO	67.38	18.13	5.14	9.35	2.48	0.28
LAO-50NAO	65.93	15.54	8.97	9.56	2.56	0.57



- Targets were single phase with decreasing lattice parameters with increasing Nd content.
- The composition change in the target did not translate perfectly to the film
- As the Nd/La ratio increased (La+Nd)/Al ratio also increased.

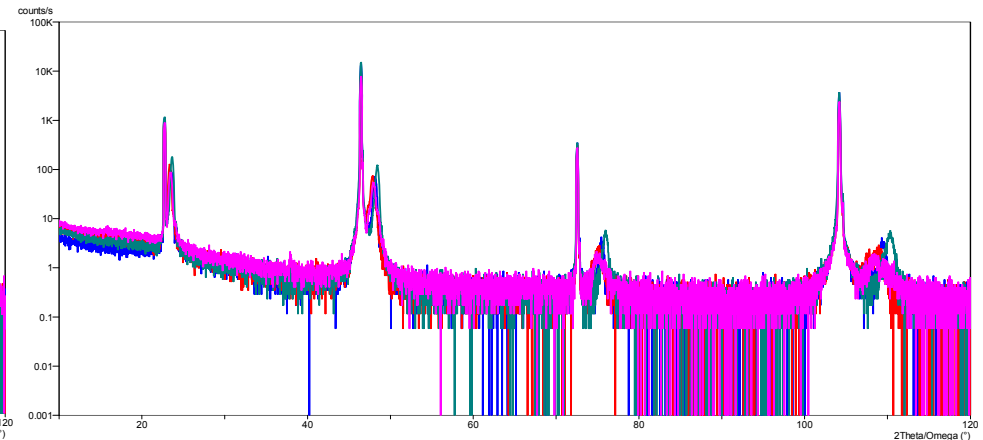
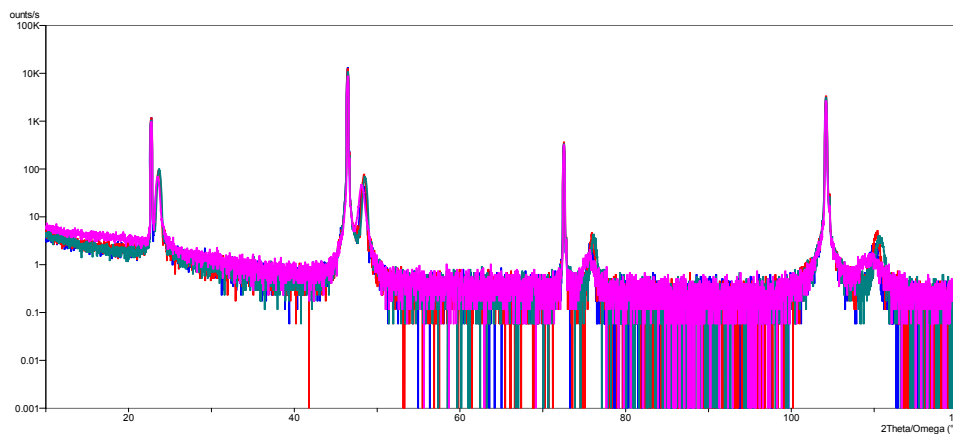
(La,Nd)AlO₃



Sample (#500)	Film thickness, nm
LAO	17.0
10NAO	20.5
30NAO	21.0
50NAO	24.0

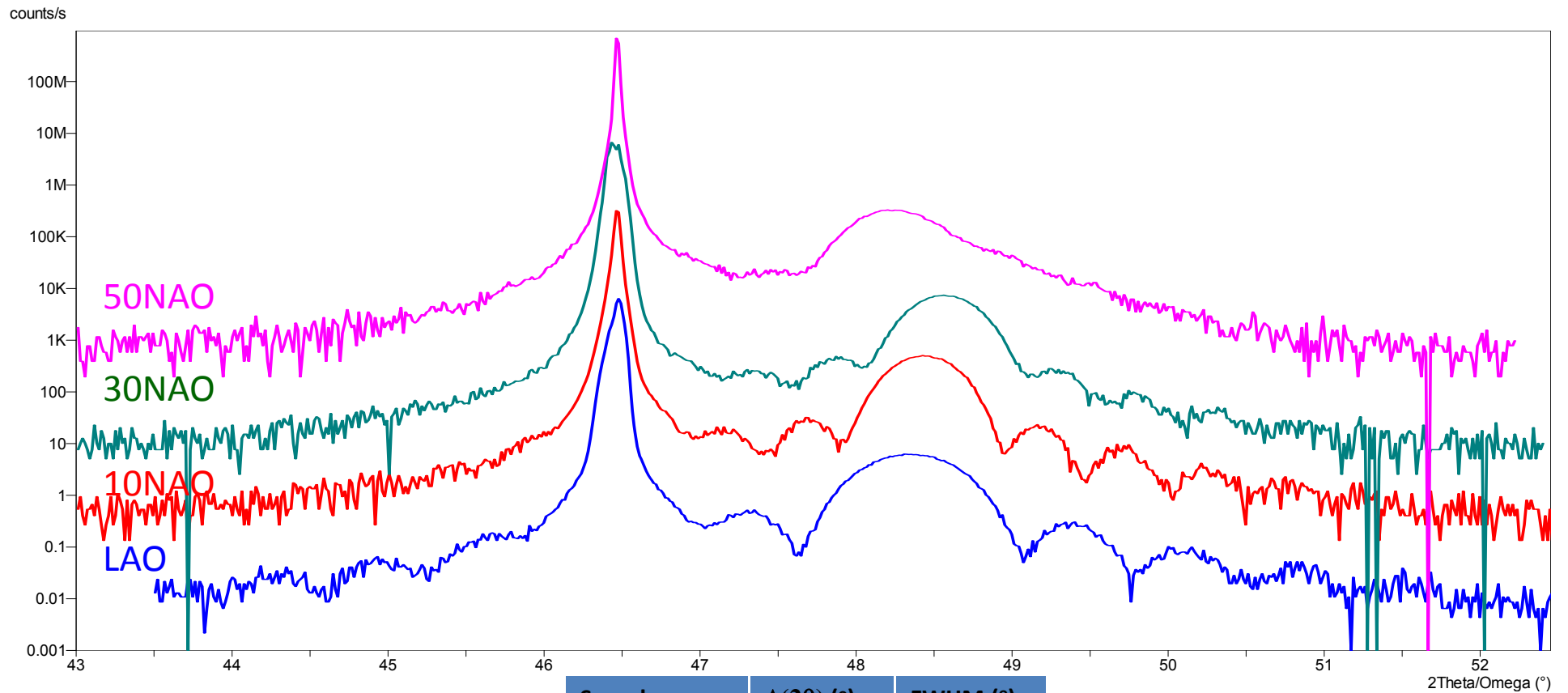
Sample (#750)	Film thickness, nm
LAO	19.5
10NAO	28.0
30NAO	28.5
50NAO	24.0

- Deposition rate increases with increasing %NAO
- 50NAO acts as an outlier in many of the observations



- The films are strongly oriented with the substrate in the film growth direction.
- A smaller atomic spacing “d” for the film in the growth direction compared to the substrate.
- Four-fold symmetry due to the cubic structure.

(La,Nd)AlO₃



Sample	$\Delta(2\theta)$ (°)	FWHM (°)
500Hz-LAO	1.912	0.65
500Hz-10NAO	1.966	0.45
500Hz-30NAO	2.128	0.48
500Hz-50NAO	1.776	0.57

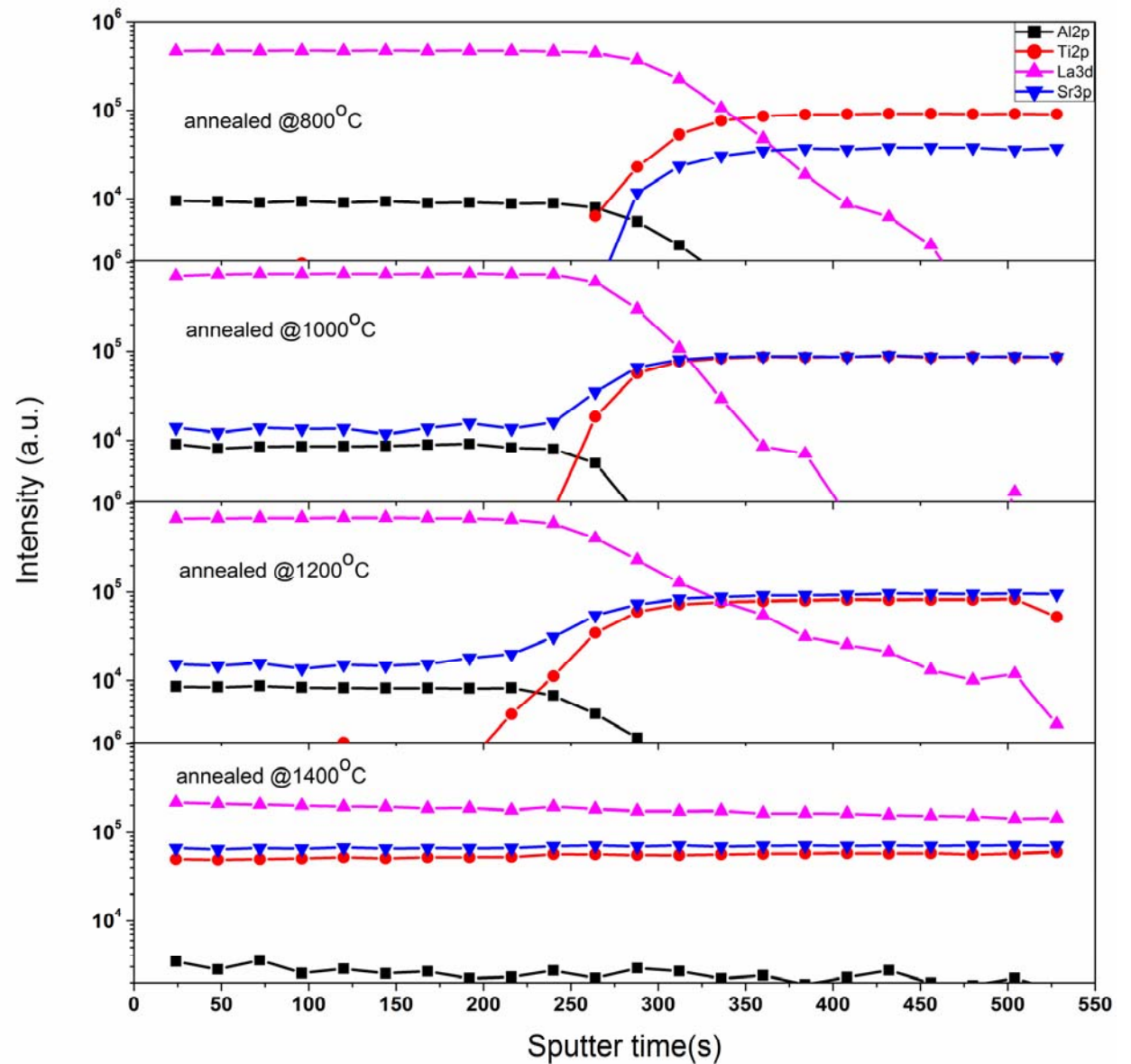
Summary of RLM results:

Sample (500#)	LAO	10NAO	30NAO	50NAO
Crystallographic tilt	0.000199	0.000116	0.000099	0.000234
Surface-normal lattice mismatch	-0.03730	-0.03882	-0.04128	-0.03475
Surface-normal lattice constant, c (nm)	0.375936	0.375341	0.374378	0.376932
Surface lattice mismatch	-0.00033	-0.00147	-0.00081	0.00021
Surface lattice constant, a (nm)	0.390370	0.389925	0.390182	0.390584

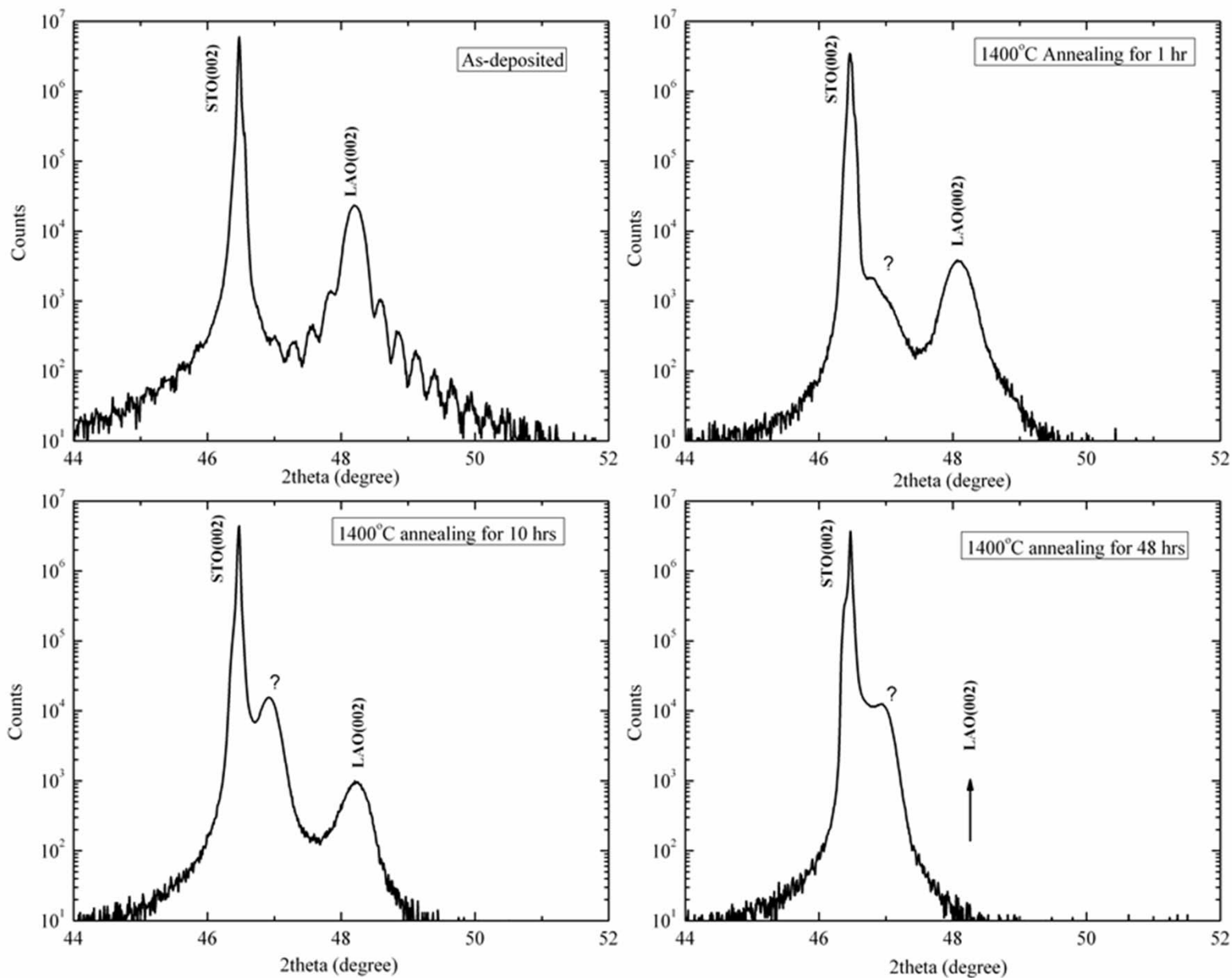
Sample (750#)	LAO	10NAO	30NAO	50NAO
Crystallographic tilt	0.000079	0.000037	0.000117	0.000053
Surface-normal lattice mismatch	-0.03343	-0.03184	-0.04055	-0.02813
Surface-normal lattice constant, c (nm)	0.377444	0.378067	0.374664	0.379517
Surface lattice mismatch	-0.00028	0.00026	-0.00301	-0.00522
Surface lattice constant, a (nm)	0.390392	0.390600	0.389324	0.388460

Diffusion

- No diffusion up to 1000 °C.
- Sr diffuses into film first.
Mechanism unknown
(substitutional vs. interstitial)
- La starts diffusing at 1200 °C.
- Complete diffusion at 1400°C.
Interface destroyed.



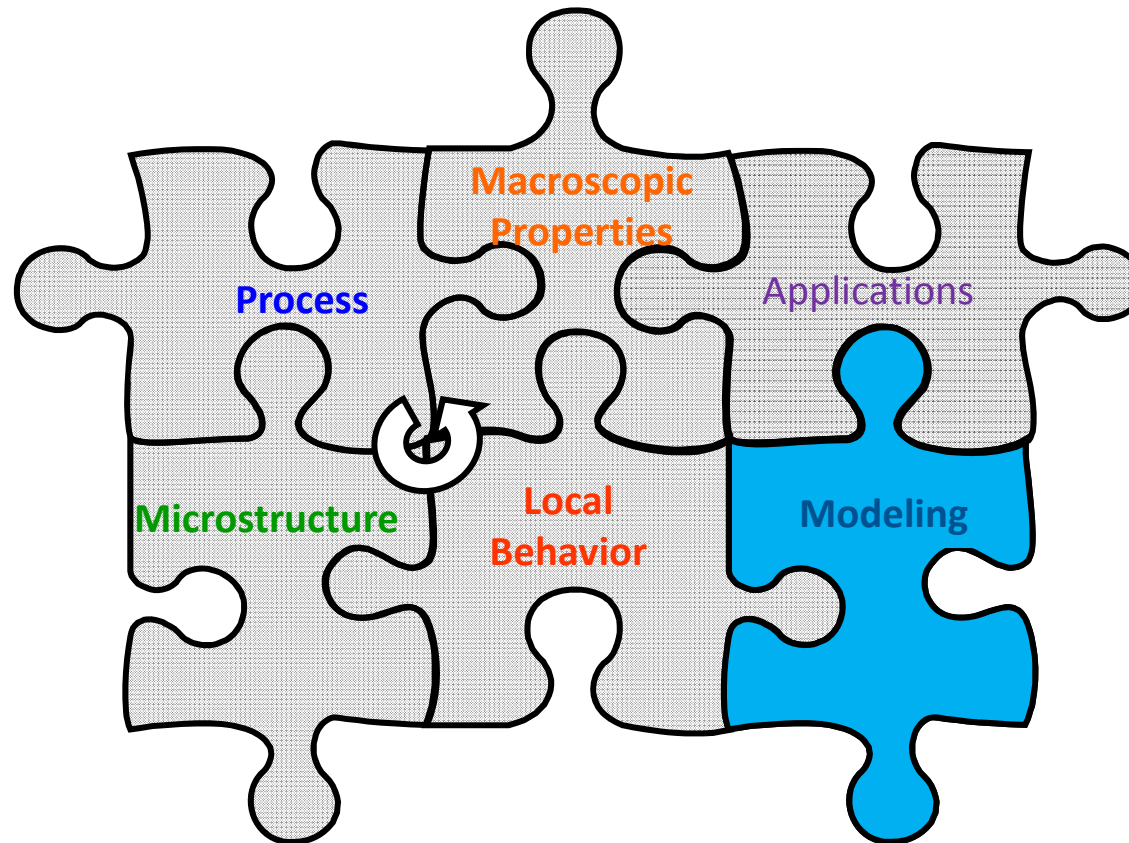
High Temperature Stability



Quantitative identification of electro-physical properties of oxide based hetero-interfaces at extreme environments

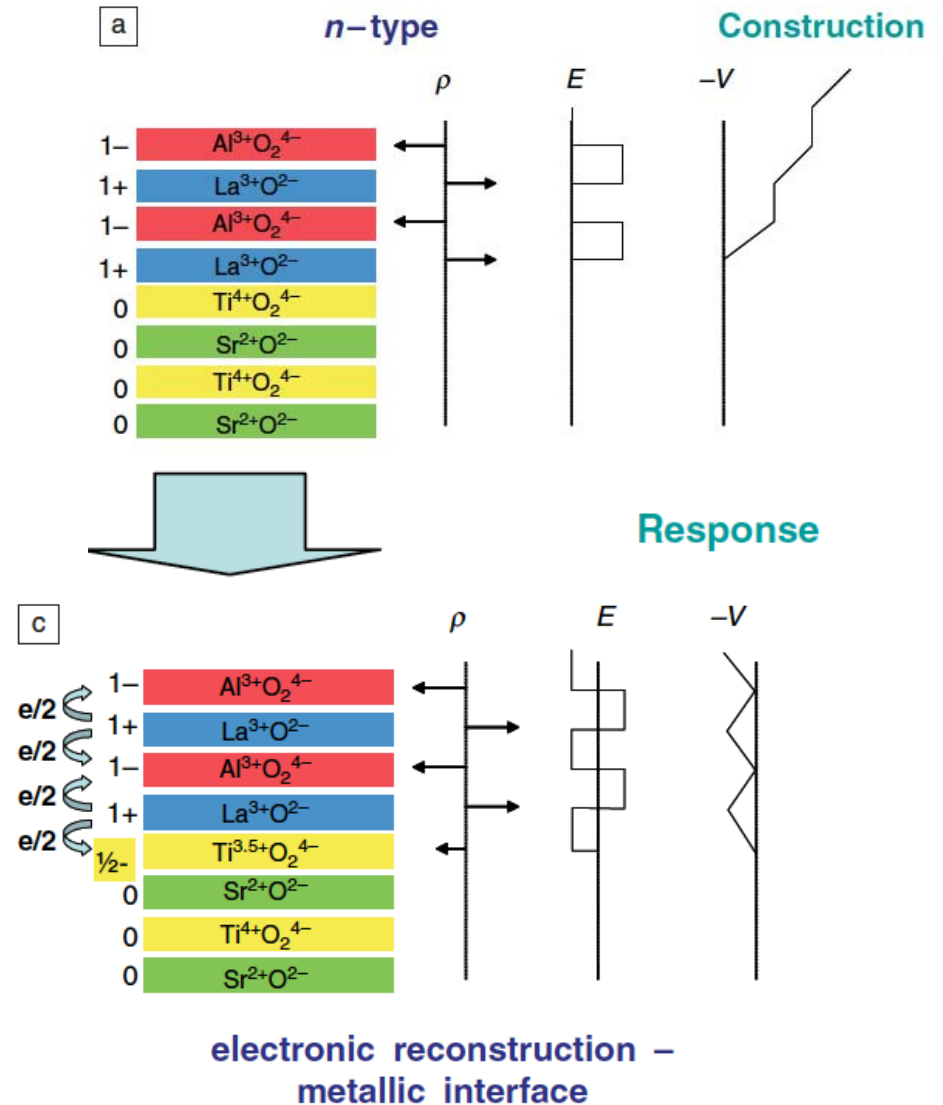
Electronic structure and point defects in oxides: computational challenges

Walter Lambrecht, Department of Physics, CWRU



2DEG formation at oxide interfaces

- Polar catastrophe model
 - Explains why only for (001) TiO_2 terminated layer
 - Critical thickness existence
- But ... there are alternative theories
 - What is the role of oxygen vacancies?
 - Surface adsorbates, defects
- Which lead to the interface charge
- What is role of strain?
- Atomic reconstruction, relaxation, interdiffusion
- What is role of off-stoichiometry between La, Al?



Focus of our planned research

- Study the effects of various point defects and impurities on these phenomena
 - Oxygen vacancies as function of distance from the interface
 - Oxygen vacancies and adsorbates at the surface
 - La-Al stoichiometry deviations
- Strain effects: relation to piezo induced fields and interface charges
- Quantitative comparison with experiment to understand the relative role of each of these contributing factors
- Explore new questions arising from the experimental studies

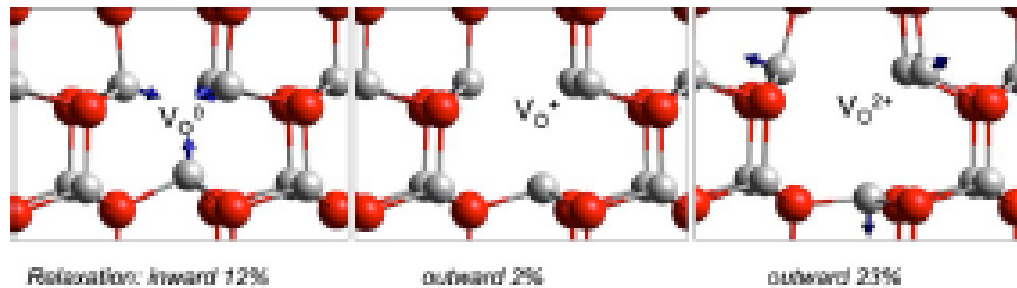
Computational Methods

- Density functional theory
 - Local density approximation and beyond
 - LSDA +U
 - Quasi-particle Self-consistent GW
- Density functional perturbation theory
 - Phonon normal modes
 - Elasticity, piezo, spontaneous polarization, stress, strain
- Band structure methods: FP-LMTO, PAW-method
- Supercell models for point defects, interfaces, surfaces

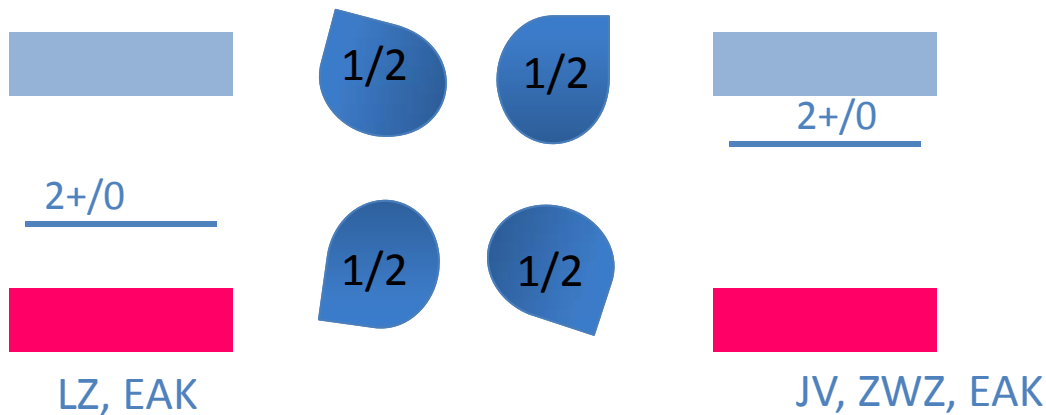
EXAMPLES OF PRIOR WORK

- Defects in ZnO
- Properties of LiGaO_2
- 2D materials: MoS_2
- Strongly correlated materials

The oxygen vacancy in ZnO



One of the most studied and controversial defects



Depending on how the gap underestimate is corrected, the transition level can lie in upper or lower half of the gap!

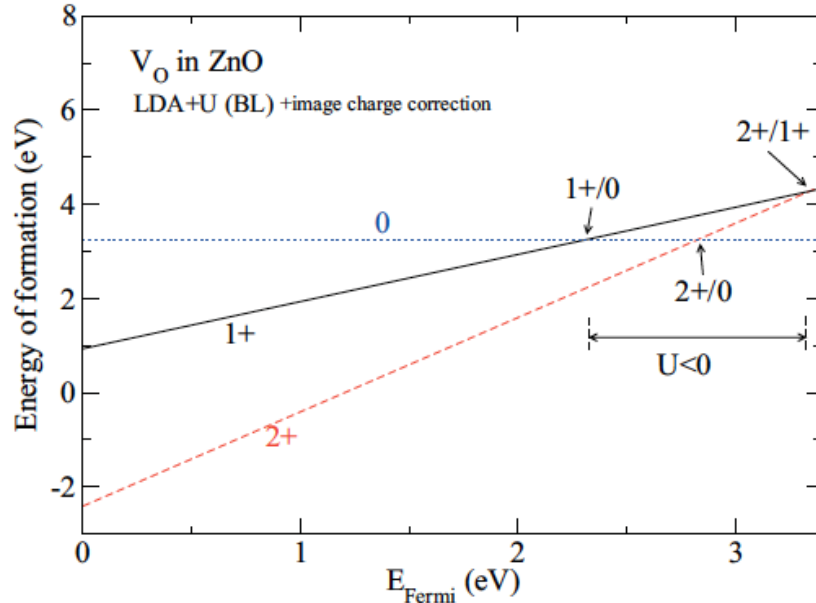
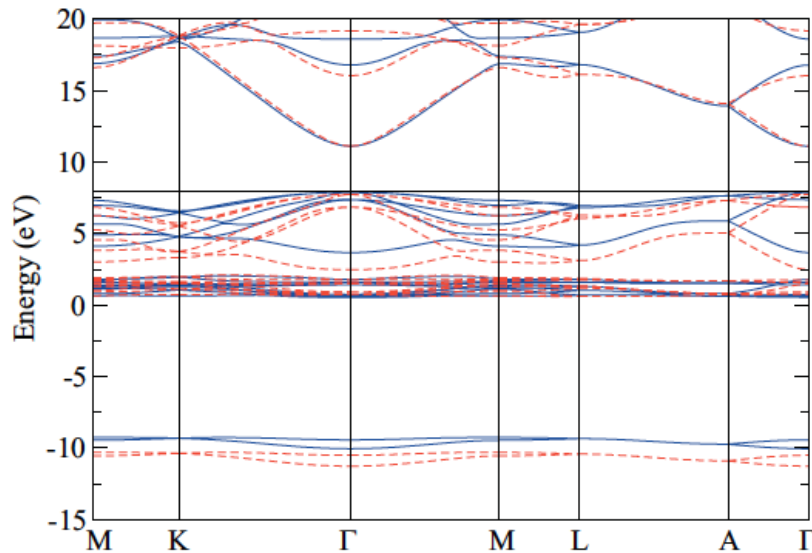
LZ: S. Lany + A. Zunger

EAK: P. Erhart, K. Albe, A. Klein

JV: A. Janotti + C. Van de Walle

ZWZ: SB Zhang, SH Wei, A. Zunger

Our solution



LDA+U with U on Zn-d, Zn-s, Zn-p
O-s, O-p adjusted to QSGW
band structure corrects not only
the gap but also the absolute
position of bands and the CB
effective mass.

Defect state expanded in host states
has mixed CB and VB character and
because deep involves several k-point
Bloch states

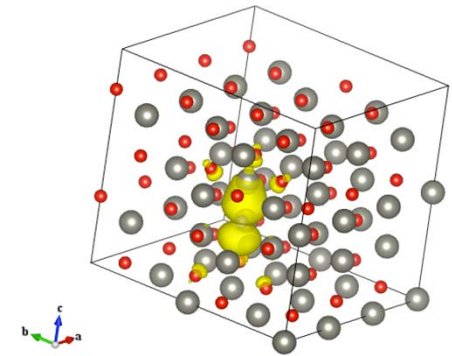
Excellent agreement with expt.
E4(DLTS) 2+/0 at 2.87 eV, ours 2.82 eV
E4R(DLTS) 2+/- at 3.26 eV, ours 3.34 eV

D.M. Hofman et al. Appl.Phys. A 88, 147
(2007)

A. Boonchun and WL Phys Stat Solidi (b)
248, 1043 (2011)

The problem of p-type doping in ZnO

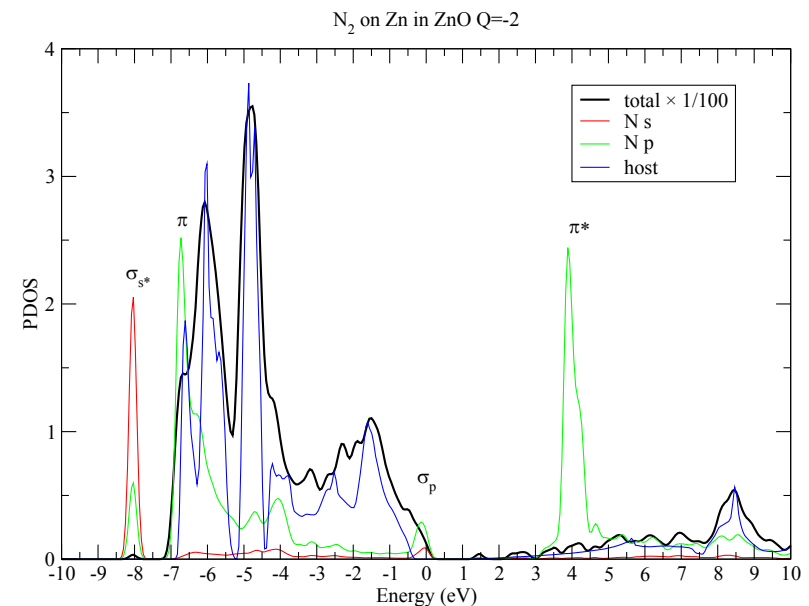
- N_O deep level because of orbital polarization
... but shallow level related to N known experimentally from donor acceptor pair recombination PL
- What is the nature of this unknown defect?
- N_2 is known to lead to an EPR signal but are these related and what is the site of the N_2 ?



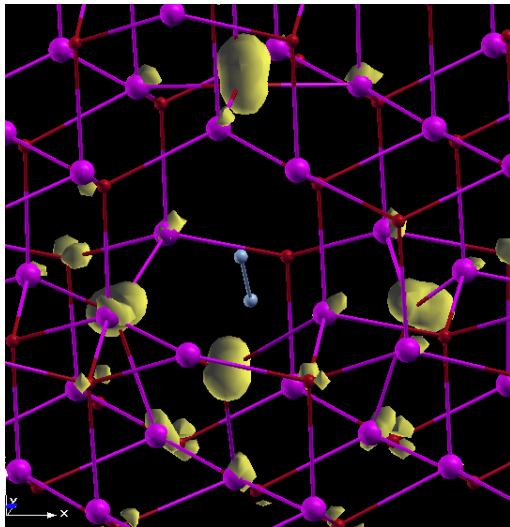
Our solution

N_2 on Zn site:

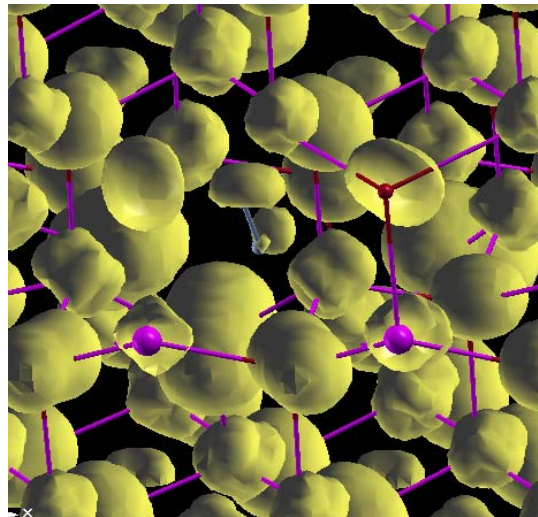
- 2 electrons removed from HOMO σ_g^+ state
- Alignment with ZnO bands leads to shallow acceptor level
- when occupied with 1 electron it can explain EPR g-factor and hyperfine structure



Shallow nature of the wavefunction



Charge density peak
is located on neighboring
O dangling bonds



But the tail of this
distribution is very
delocalized

Two pictures of the
 σ_g^+ resonance at two
different isovalues of the
charge density, illustrating
the shallow acceptor nature

Relation to EPR center

TABLE I: Calculated g-tensor components in N_2^+ , compared to measured ones for the EPR center observed by Garces et al. [11]. Also shown are the measured g-tensor for N_2^- in MgO and KCl[21].

	present	Bruna	Garces	MgO	KCl	
g_{\parallel}	2.0023	2.0021	2.0036	1.9833	1.9065	g_{zz}
g_{\perp}	1.9997	1.9996	1.9935	2.0043	1.9971	g_{xx}
				2.0021	2.000	g_{yy}

The g-tensor describing the effective spin splitting in a magnetic field measured by Garces for N_2 in ZnO agrees better with that for an N_2^+ molecular radical corresponding to the Zn site than with that for N_2^- , corresponding to the O site

Hyperfine splitting

- The σ_g^+ nature of the wavefunctions allows s-electron contribution at the nucleus and hence isotropic hyperfine interaction with ^{14}N $I=1$ nuclear spin.
- In contrast, in the π_g state of the N_2^- radical, the isotropic hyperfine structure should be negligible

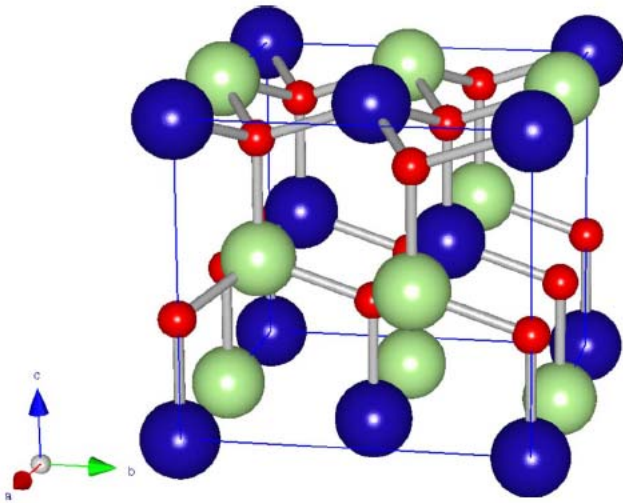
TABLE II: Hyperfine parameter comparison

	Garces	N_2^+ (Bruna)	N_2^- in MgO	
A_{iso} (MHz)	16.7	88	4.5	A_{iso}
A_{dip} (MHz)	-3.4	28	-7.8	T_{xx}
			17.7	T_{yy}
			-9.9	T_{zz}

Why this is important!

- The N_2 on Zn site is a perfect candidate to explain an already known experimental shallow level at 165 meV related to N and observed by Zeuner et al. but until now unidentified
- In its negative charge state, when occupied with 1 electron this same center can explain the EPR center observed by Garces et al. but until now believed to correspond to N_2 on O site.
- This suggests a new direction for achieving p-type doping in ZnO. Grow in Zn-poor conditions and dope with N_2 rather than atomic N or N^*

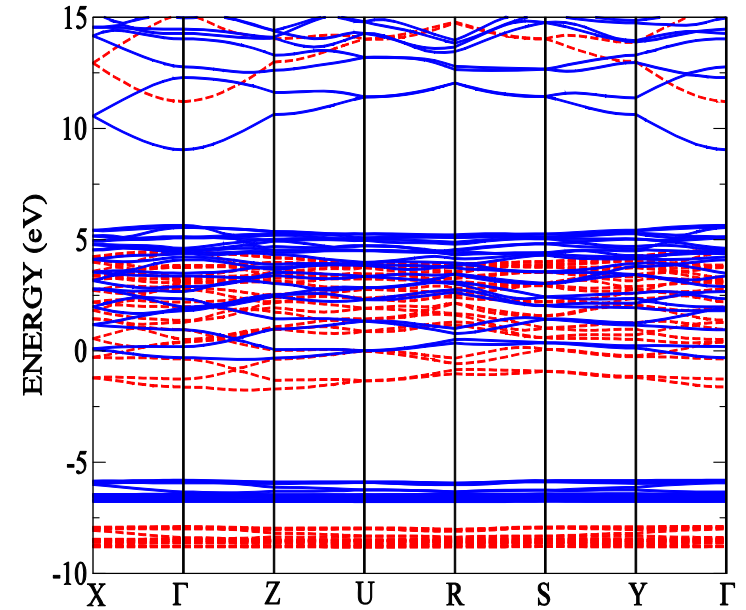
LiGaO_2 an extremely wide gap semiconductor oxide related to ZnO



Crystal structure related to that of ZnO , ordered Arrangement of Li (I), Ga (III) on cation sublattice of wurtzite



Can be grown by Czochralsky growth method



Our calculations predict a band gap of 6.25 eV

Lattice dynamical properties of LiGaO₂

- Phonon calculations of IR spectra in good agreement with experiment.
- Calculations provide insight in nature of vibrational normal modes
- Elastic constants and piezo electric properties were calculated.

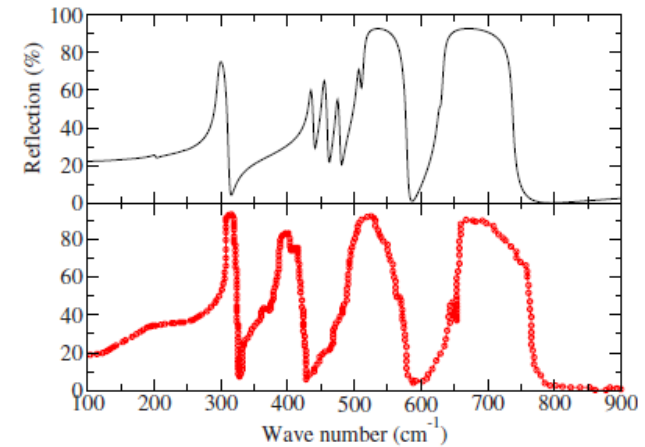
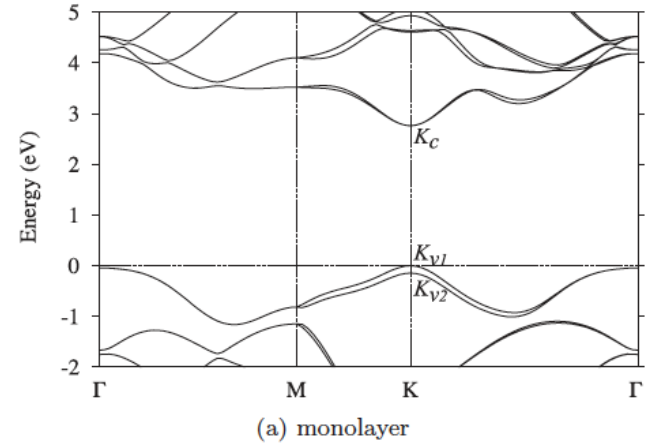
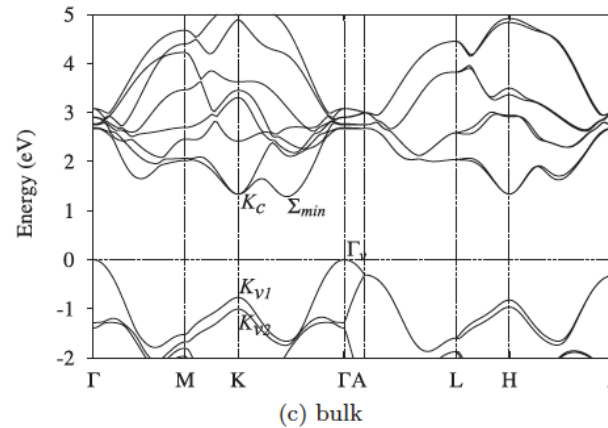
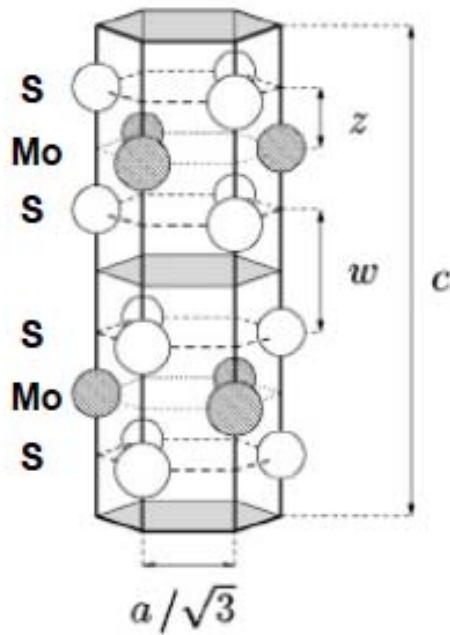


TABLE VI. Combinations of elastic compliances (10^{-12} m²/N) and stiffnesses (GPa) directly measured by experiment.

	Present	Expt. ^a	Expt. ^b
e_{15} (C/m ²)	-0.29	-0.34	-0.29
e_{24}	-0.30	-0.32	-0.30
e_{31}	-0.21	-0.31	
e_{32}	-0.09	-0.17	
e_{33}	0.52	0.96	0.90
d_{15} (pm/V)	-6.04	-6.0	
d_{24}	-7.41	-6.9	
d_{31}	-2.92	-4.7	
d_{32}	-0.87	-2.5	
d_{33}	4.80	8.6	

	Present	Expt. ^a	Error (%)
s_{11}	9.58	9.1	5
s_{22}	7.37	7.3	1
s_{33}	8.0	8.0	0
$\frac{9s_{11}+6s_{12}+s_{22}+3s_{66}}{16}$	3.03	3.04	1
$\frac{s_{11}+6s_{13}+9s_{33}+3s_{55}}{16}$	8.13	7.6	7
$\frac{s_{22}+2s_{23}+s_{33}+s_{44}}{4}$	9.15	8.4	9
c_{44}	40.5	47.4	15
c_{55}	48.0	57.1	16
$\frac{c_{44}+c_{66}}{2}$	58.2	45.1	29

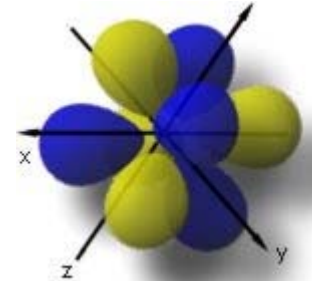
2D materials: MoS₂

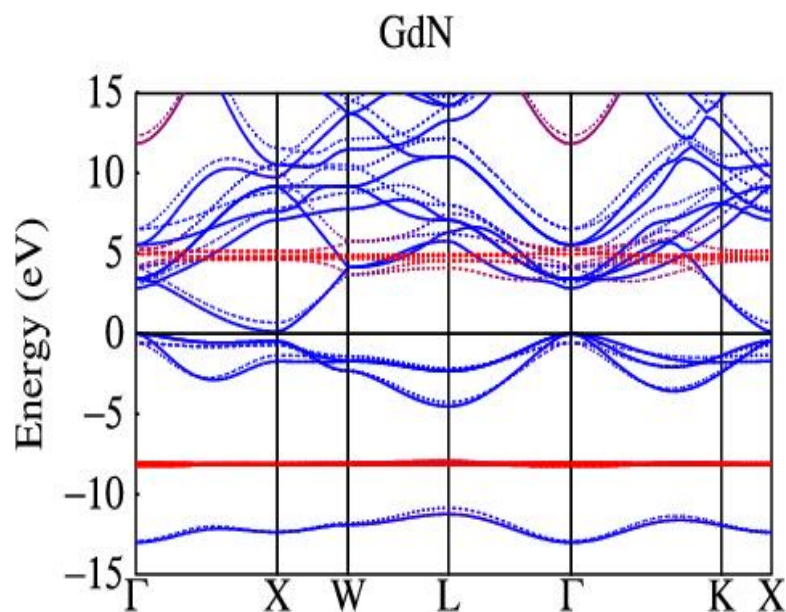


MoS₂ is a layered material from which monolayers can be exfoliated. The gap changes from indirect in bulk to direct in the monolayer. We calculated band gap changes with QSGW and found large exciton binding energies due to reduced screening explain why the monolayer does not have a much larger gap than the bulk.

Rare-earth nitrides: strongly correlated f-electron materials

- We studied the electronic structure and formation of magnetic moments due to orbital and spin moment in the RE-N series
- Using the LSDA+U method
- Analyzed Xray Absorption Spectroscopy and XEmission experiments and Resonant XES
- Studied magnetic exchange interactions in GdN
- Studied Gd doped GaN





Band structure of GdN indicating the f-electrons in red strongly split between up and down spin by Hubbard U interaction

Induced magnetic moments on Gd d orbitals and N p are opposite as in an Anti Ferromagnet but imply f-moments on Gd are ferromagnetic

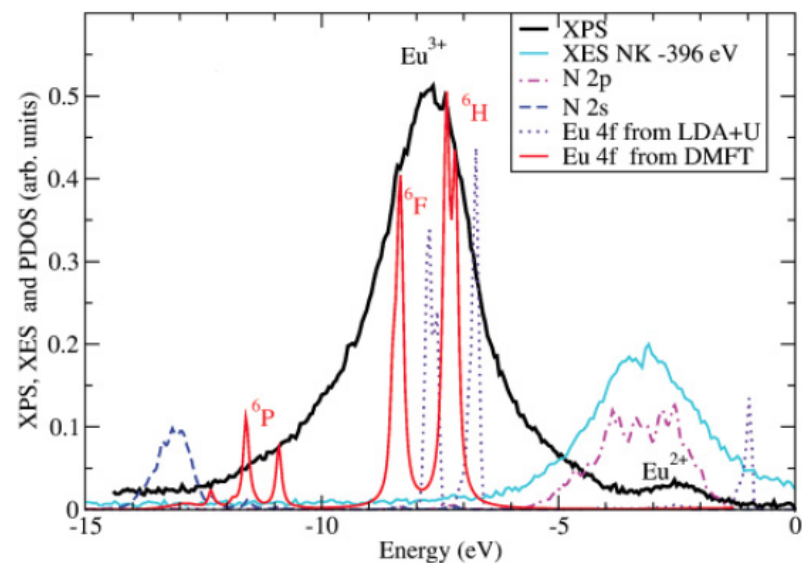
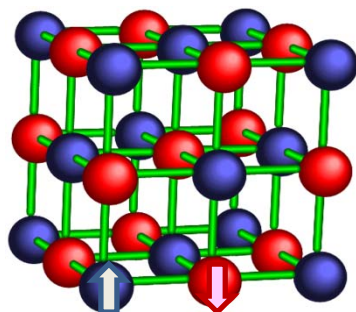
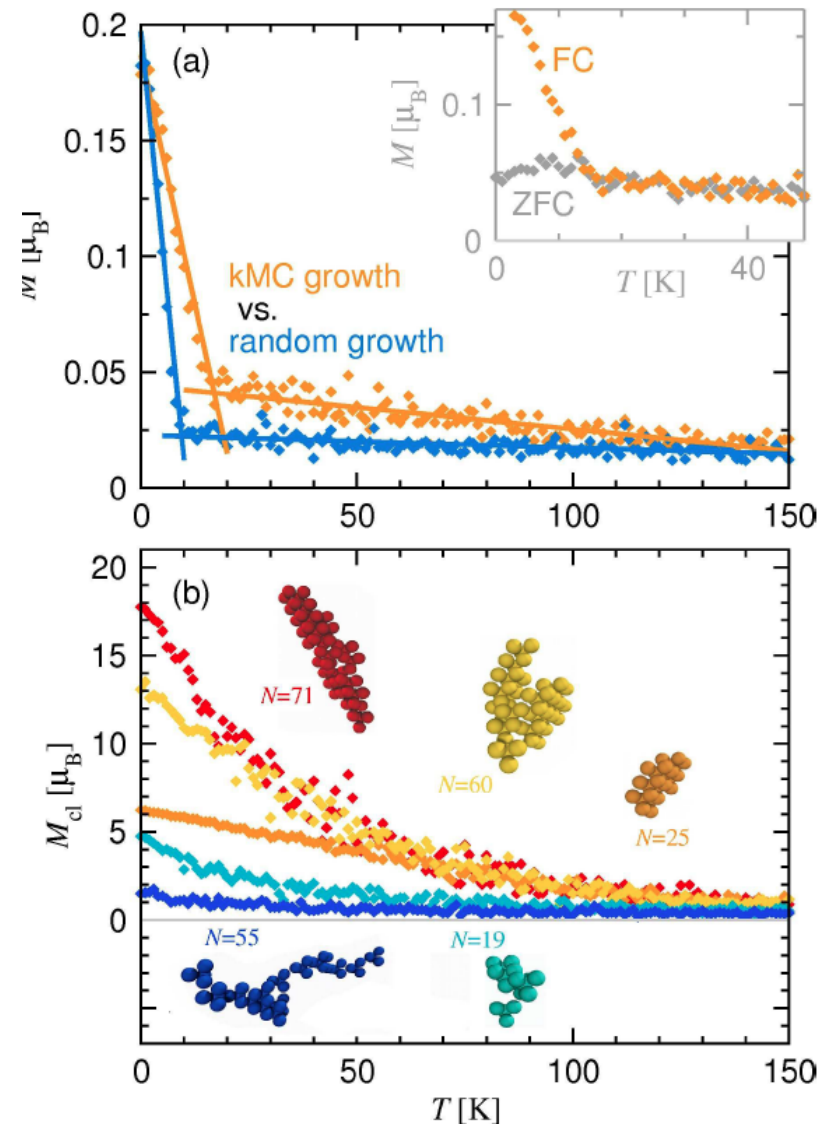


FIG. 8. (Color online) Comparison of XPS and XES measurements of the EuN valence band PDOS with various theories. Solid black line, XPS; thin light blue line, N K-edge XES; solid red line with labels, DMFT of Eu f^5 multiplet PDOS; blue dashed line, N 2s PDOS; pink dash-dotted line, N 2p PDOS; purple dotted line, Eu 4f in LSDA + U . The XES energy scale has been shifted by -396.6 eV.

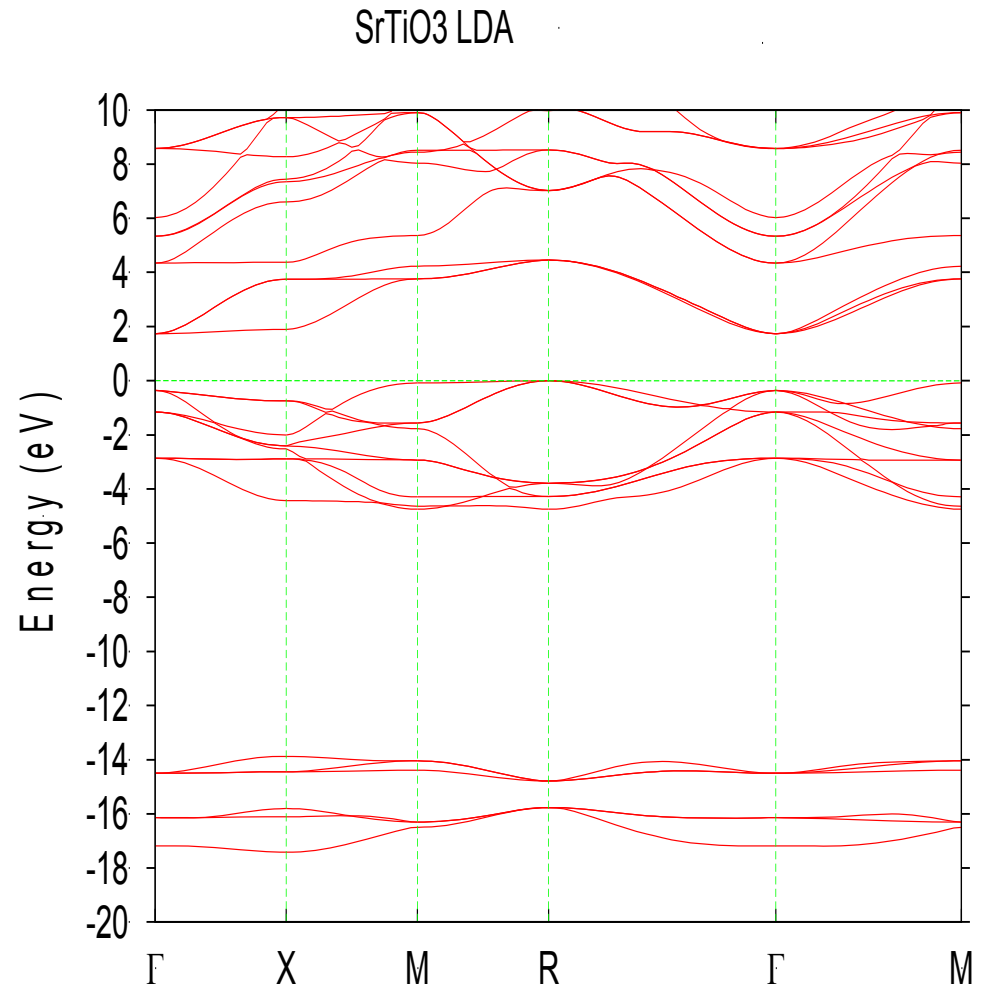
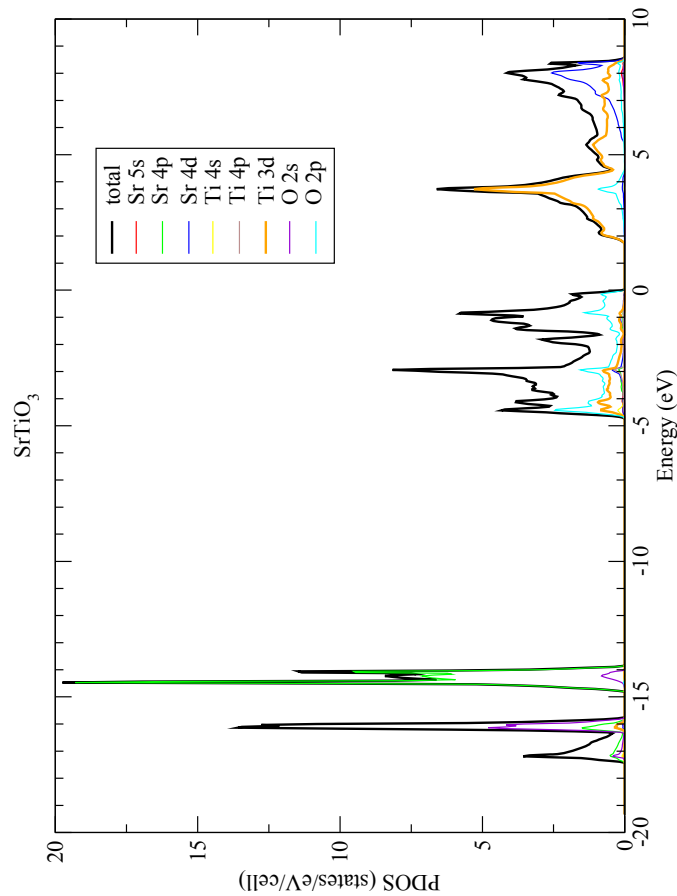
Theory predicts much lower T_c for pure GdN than observed indicating the role of N vacancy impurities

Gd-doped GaN: not a colossal ferromagnet but a superparamagnet

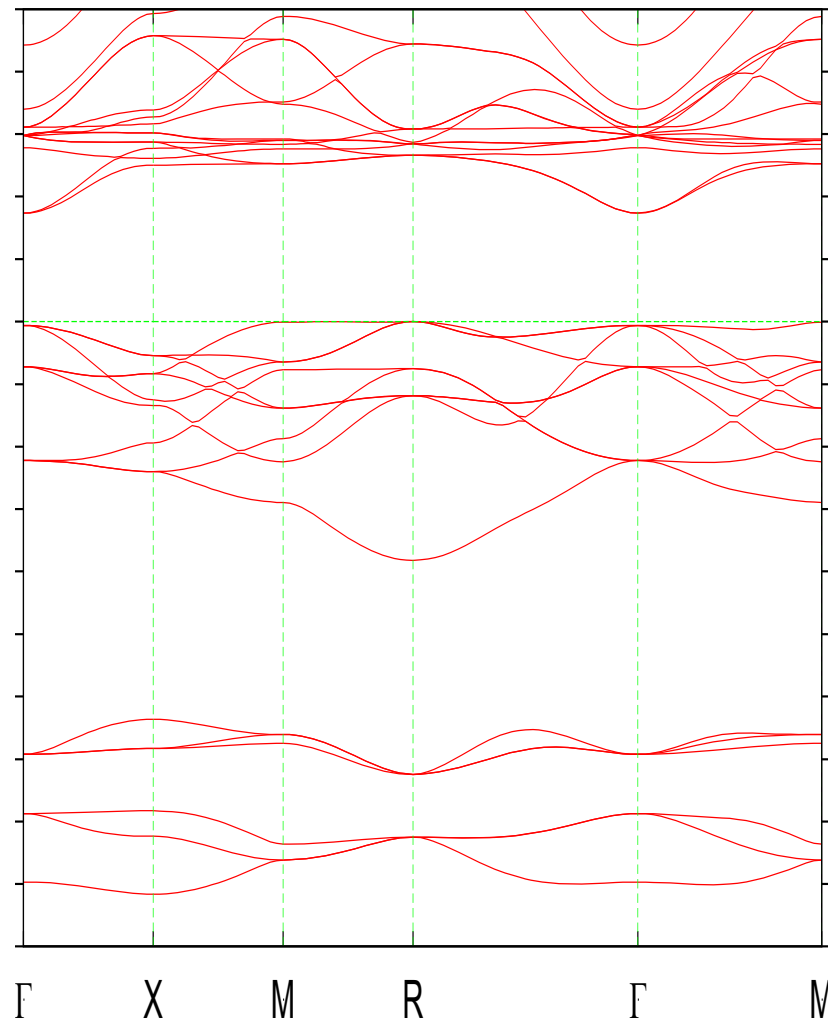
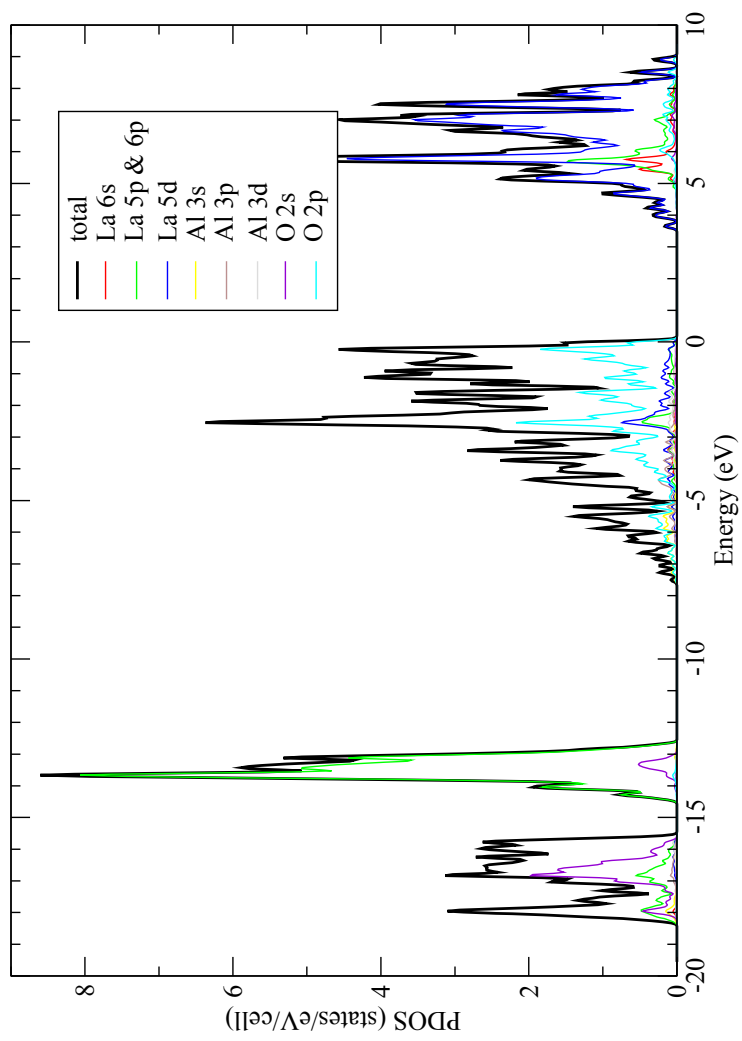
- KKR-nano simulations of large size cells provide statistically averaged exchange interactions between Ga vacancy magnetic moments and with Gd
- Growth simulations show evidence for Ga vacancy clustering
- Monte Carlo simulations of magnetization show two temperature regimes in agreement with experiment and indicate superparamagnetism in clusters rather than ferromagnetism



Preliminary results for LAO and STO



LaAlO₃



Conclusions

- Oxides are a very interesting (but also very broad) family of electronic and multifunctional materials.
- In particular the TM with partially filled d bands in the perovskite ternary oxides lead to multiple correlated phenomena, leading to their multifunctionality
- The basics of the theory of 2DEG formation at interfaces between oxides with different polarities in the layers is understood but many open questions remain

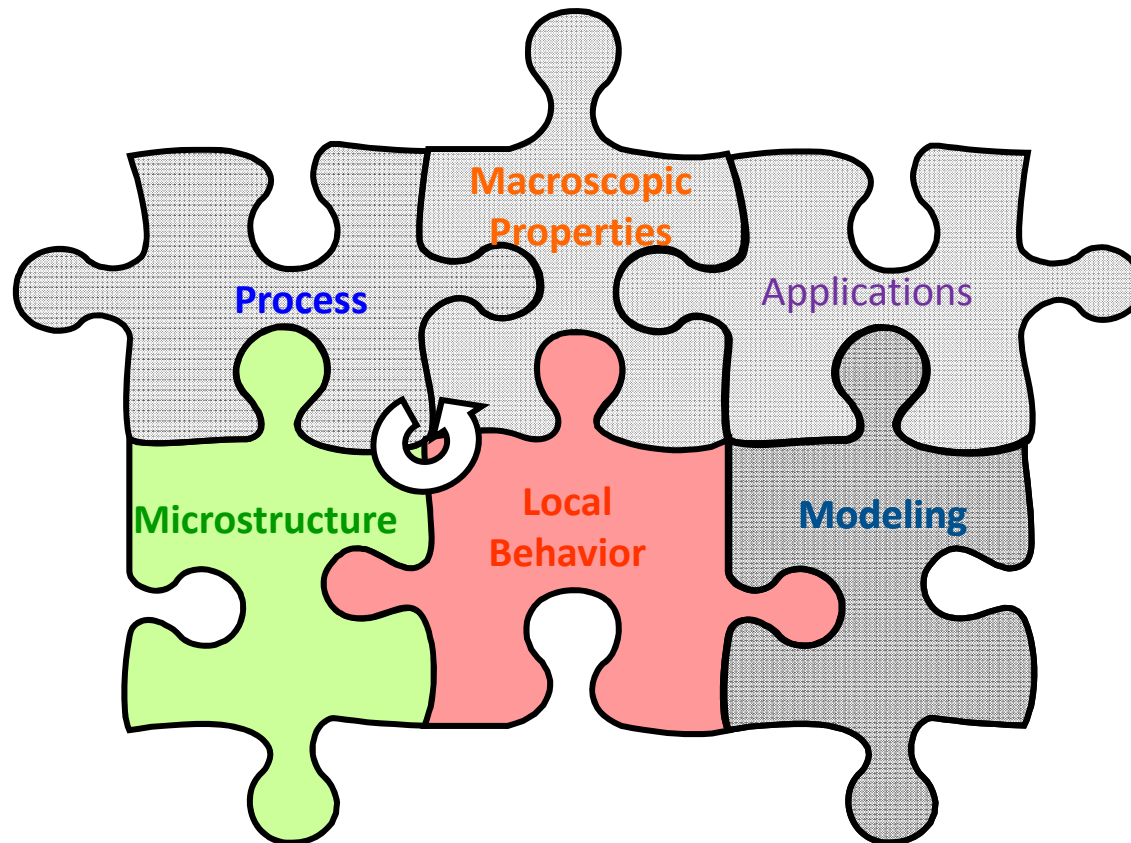
Conclusions continued

- We have determined some focus areas for our research, in particular relating to stoichiometry deviations and strain effects, which will attempt to solve the questions raised by the experiments.
- We have an array of state-of-the art computational methods available.
- We have demonstrated our capability of using these methods and solving important problems on defects and strongly correlated materials in our past research on other materials, including oxides.

Quantitative identification of electro-physical properties of oxide based hetero-interfaces at extreme environments

Nano-structural investigation of $\text{LaAlO}_3/\text{SrTiO}_3$ hetero-interfaces

Marie-Hélène Berger, co-PI – Hicham Zaid, PhD Student
Mines-ParisTech, France



Mines-ParisTech

is a Graduate School
in Science, Engineering and Economics
Established in 1783

2,024 PEOPLE

745 permanent staff

1,279 students

RESEARCH

16 research centers in 5 main scientific fields

-Material Sciences & Engineering

-Applied Mathematics, Computer Science,
Systems and Control

-Process Engineering & Energetics

-Geosciences & Environment Sciences

-Social & Economics Sciences



Centre des Matériaux – EVRY

Mines- ParisTech, CNRS Lab. + ARMINES

National Ranking : A⁺

187 PEOPLE

- 38 Permanent researchers
- 10 Engineers, 22 Technicians
- 9 Masters - 87 PhD – 9 Post-Doc
- 12 Administration staff

RESEARCH

High Temperature Material Behavior

Surfaces, Interfaces & Processing

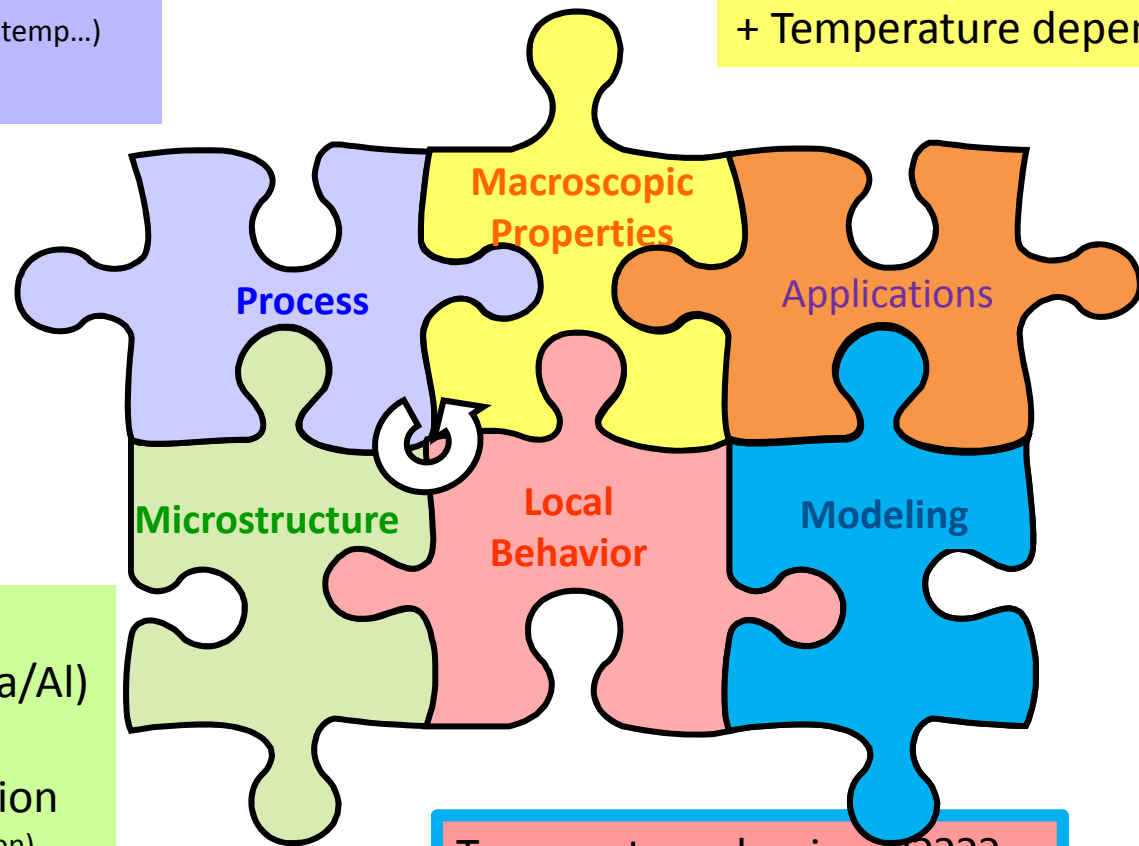
Materials and Mechanics, Fracture Mechanics

Composites, Assembling and Adhesion

Structural Mechanics, Constitutive Behavior

STO Substrate orientation mis-cut angle
STO Surface preparation etching
LAO Target
PLD conditions (p_{O_2} , plume, angle, temp...)
Annealing

Charged carrier density
mobility
+ Temperature dependence



Substrate termination
Stoichiometry of the film (La/Al)
Domains
Strain development/relaxation
(LAO cell dilatation/contraction, dislocation)
Cation distribution at interface
Ti valence profile
Oxygen vacancies
+ Temperature dependence

Transport mechanism ?????
Polar discontinuity
Oxygen deficiency
Lattice distortion
Cationic intermixing

Local investigation of the $\text{LaAlO}_3/\text{SrTiO}_3$ interface structure

Spatial resolution required : atomic resolution

TEM-STEM is the dedicated tool

TEM

// electron beam, E_0

object
(thin)

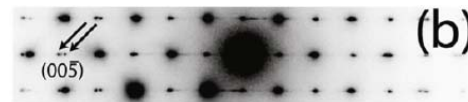
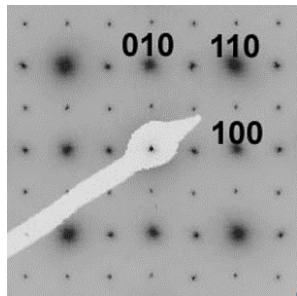
Elastic and coherent
Diffusion

Inelastic Diffusion
 $\Delta E = h\nu$
 $E_0 - \Delta E_i$

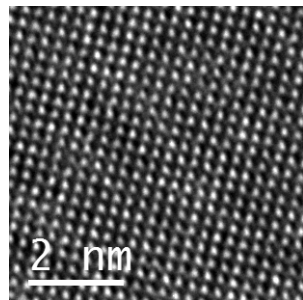
Objective
lens

Back focal
plane

imaging
Image
plane



Chambers et al. 2010

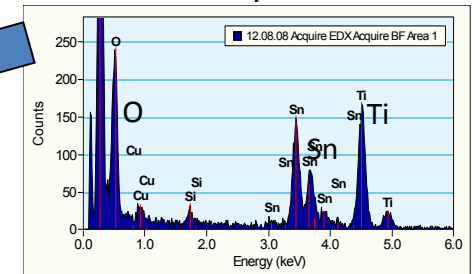


Phase Contrast

• + • + •

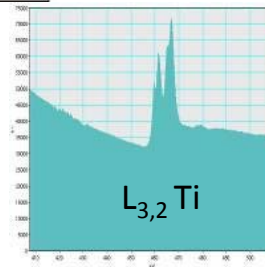
EDX

Chemical
analysis



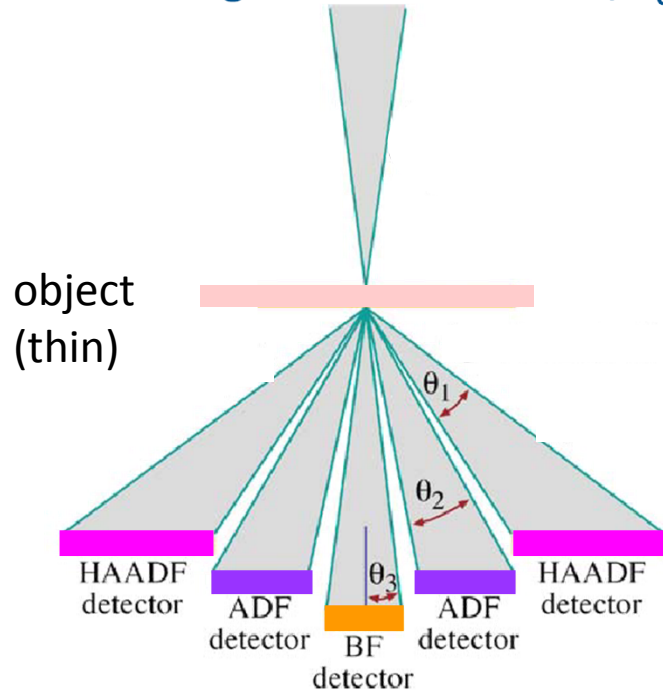
EELS

Chemical environment
Valence state



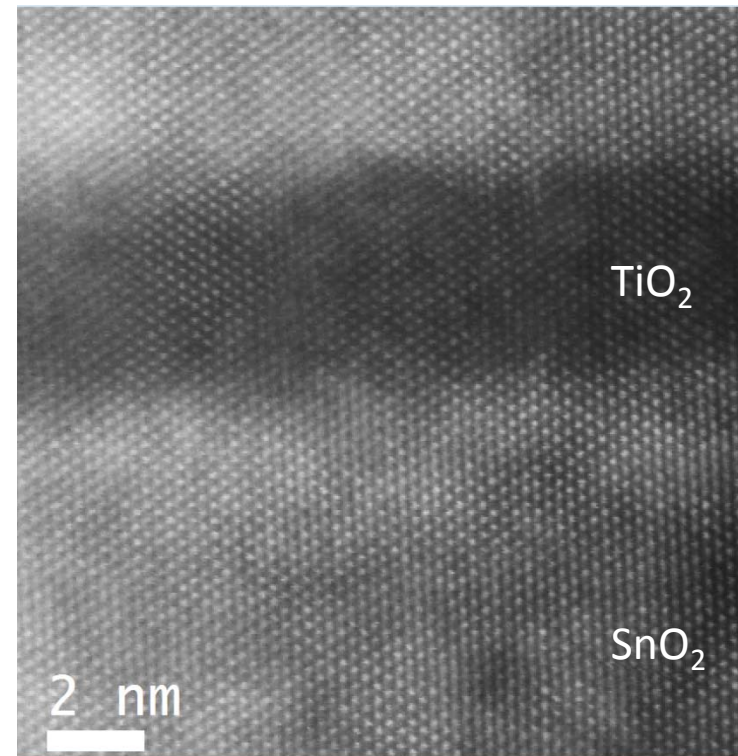
STEM

convergent electron beam, E_0



High Angle Annular Dark Field detector

Elastic Incoherent Diffusion $\propto Z^2$



Example

Self partitioning of a $(\text{Ti,Sn})\text{O}_2$ solid solution by spinodal decomposition

F Dynys - MH Berger – A Sehirlioglu

STEM-HAADF LPS Saclay , F M Walls

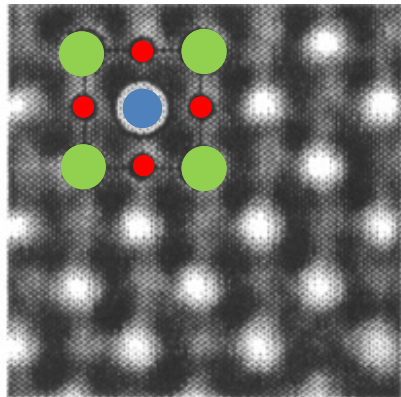
High Resolution TEM vs STEM-HAADF

HRTEM

More sensitive to light elements

→ O visible

Ti and Sr cannot be distinguished

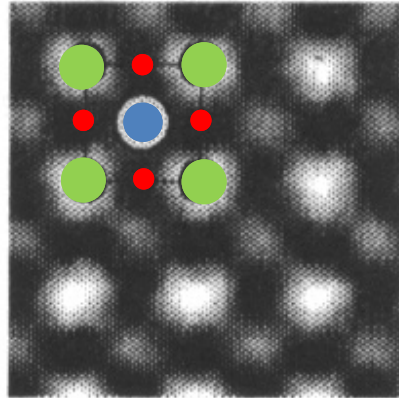


HAADF

O not visible

Z^2 contrast

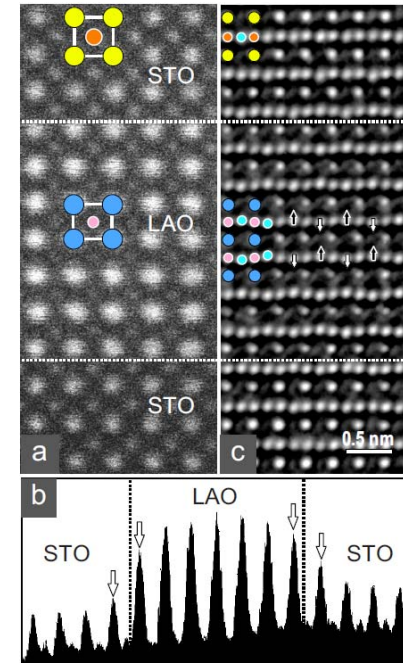
→ Ti and Sr can be distinguished



Christian Kisielowski - Jeanne Ayache - NCEM - Berkeley

STEM HAADF

HRTEM

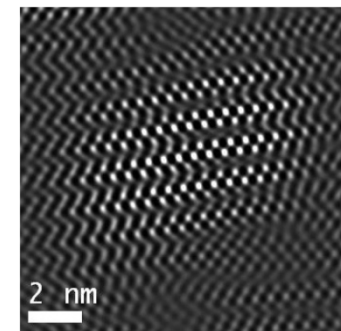
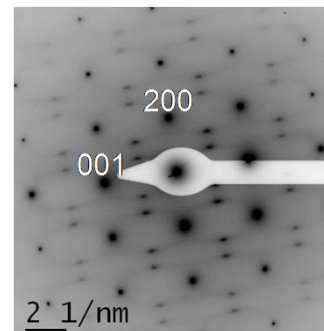
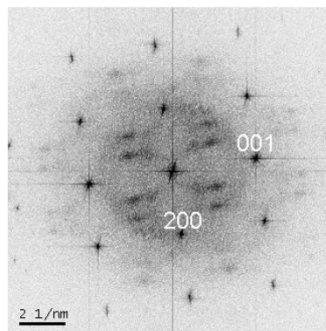
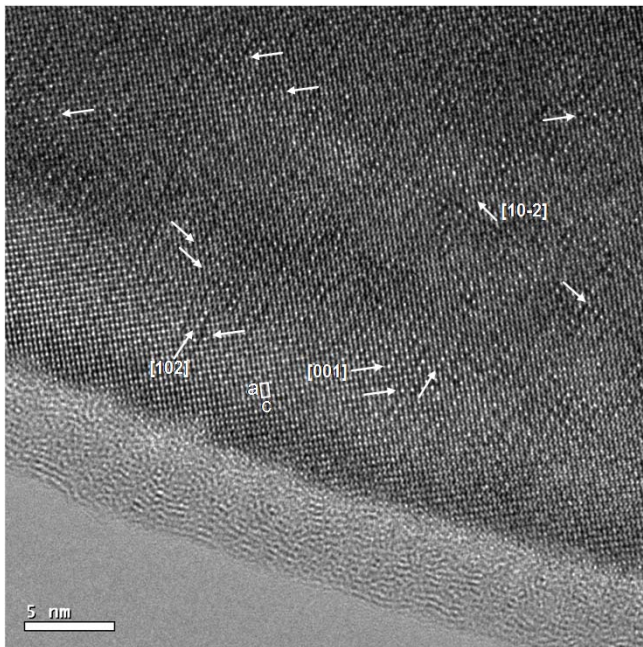


→ Oxygen Octahedron rotation

C. L. Jia,^{1,*} S. B. Mi,¹ M. Faley,¹ U. Poppe,¹ J. Schubert,² and K. Urban¹
PHYSICAL REVIEW B 79, 081405(R) (2009)

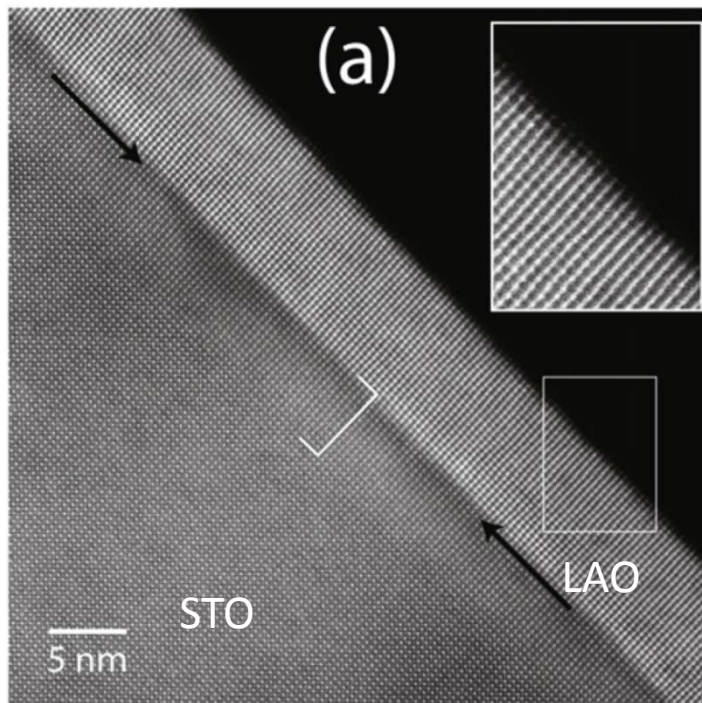
HRTEM study of oxygen vacancy ordering in mullite grown by directional solidification

A Sayir, MH Berger

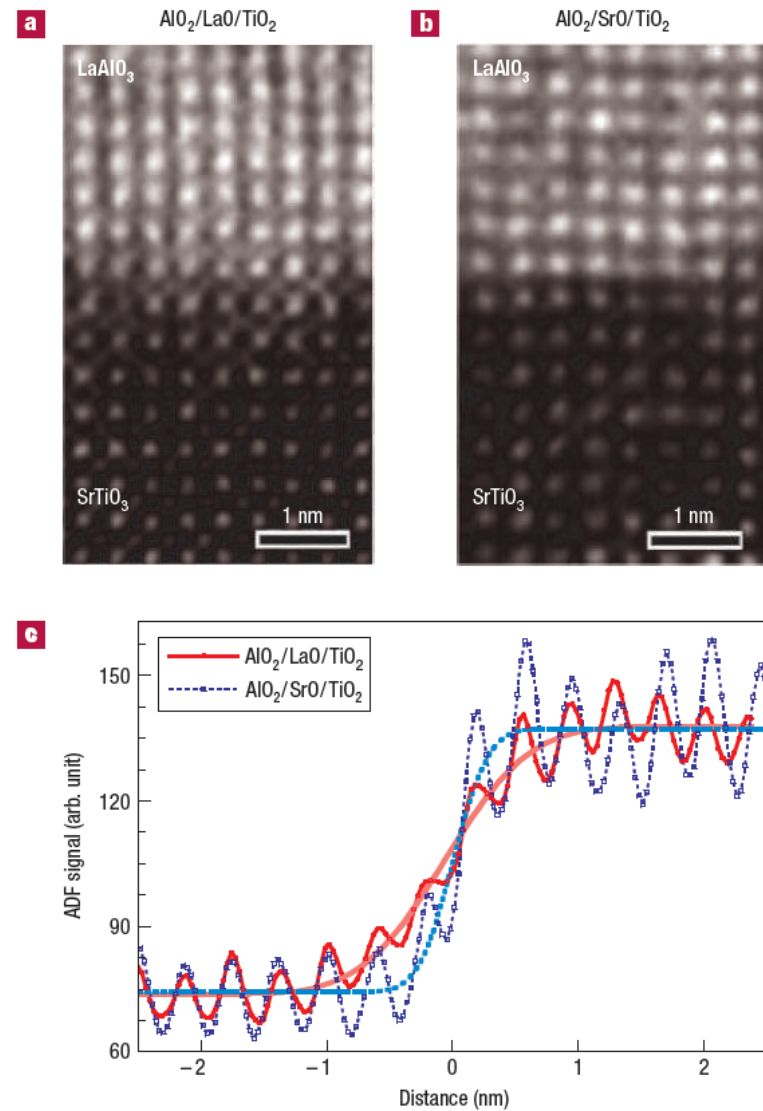


STEM-HAADF

Cation intermixing, interface roughness...

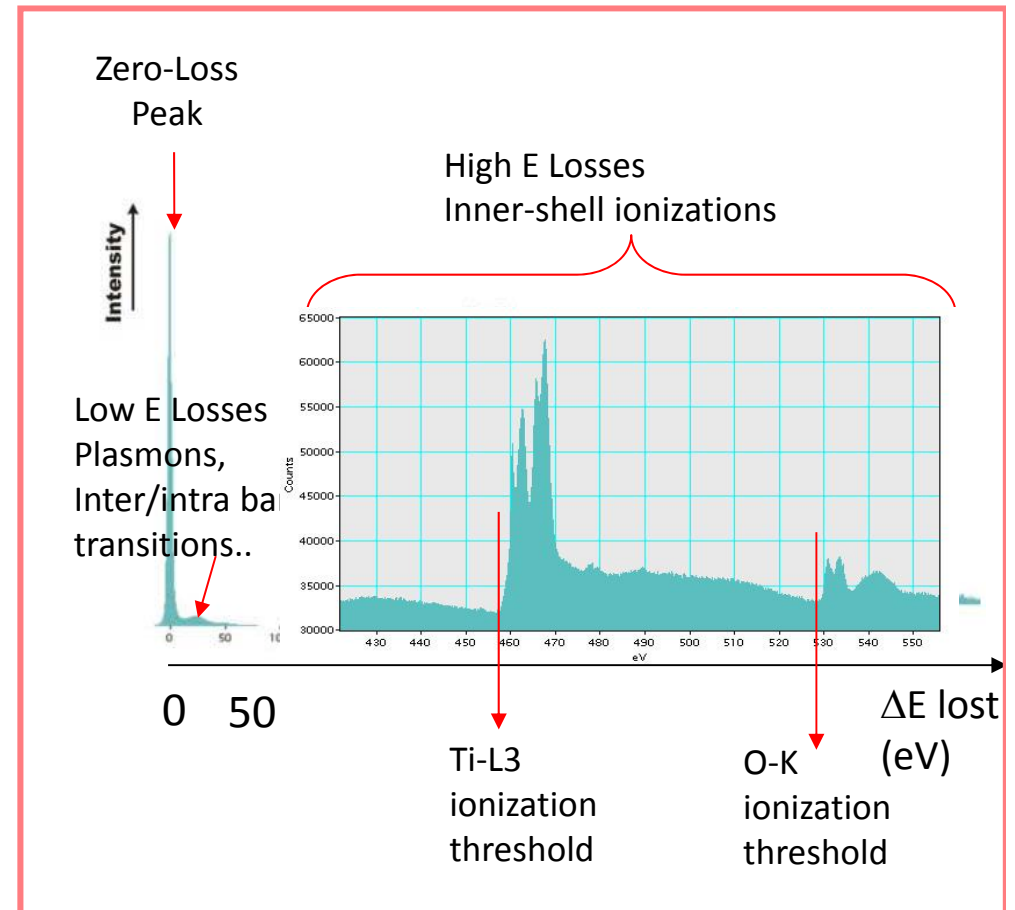
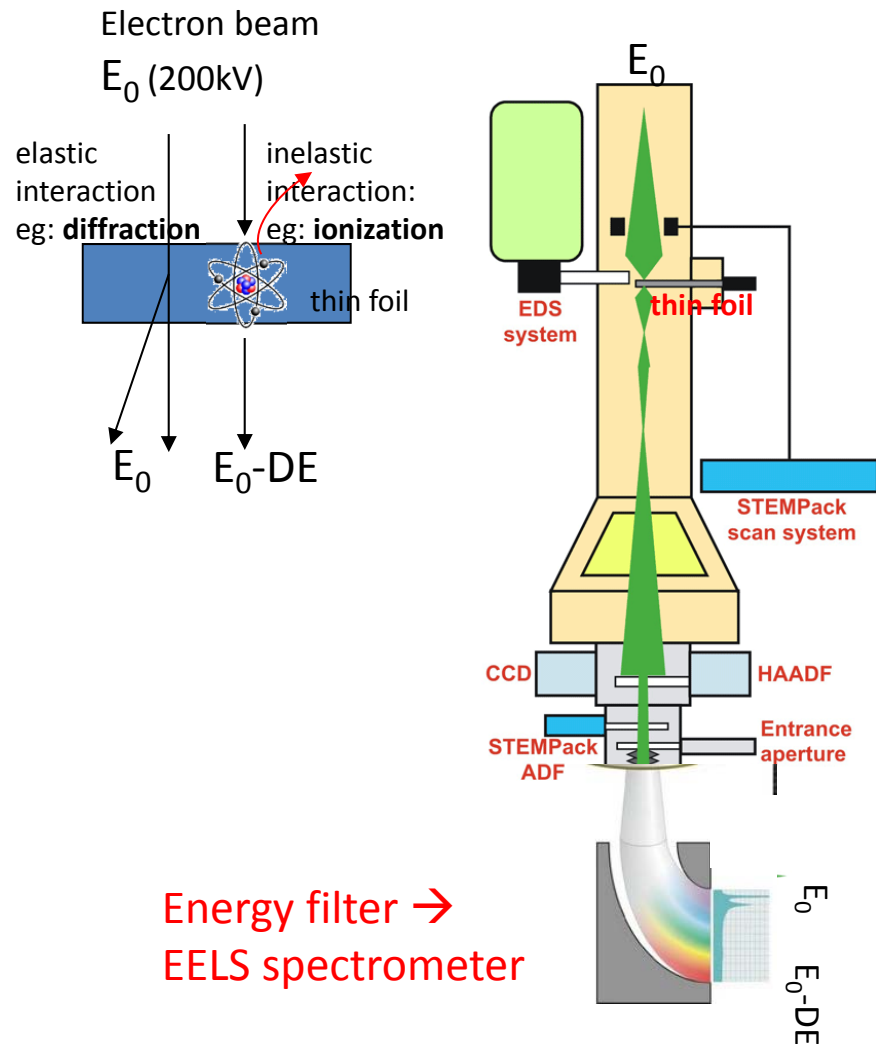


S.A. Chambers et al. / Surface Science Reports 65 (2010) 317–352

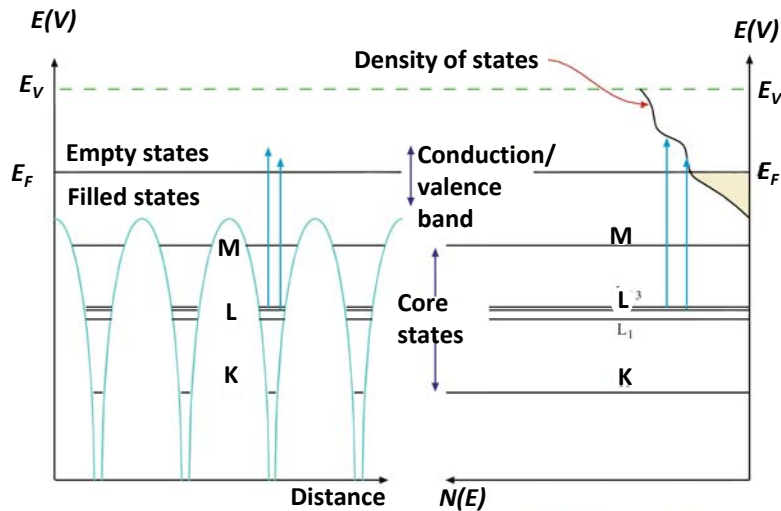


NAOYUKI NAKAGAWA^{1,2}, HAROLD Y. HWANG^{1,2} AND DAVID A. MULLER^{3*}
nature materials | VOL 5 | MARCH 2006 | www.nature.com/naturematerials

Electron Energy Loss Spectroscopy



EELS ELNES: Ti Valence + O Vacancies



Ti L_{23} and O K edges in TiO_2 rutile

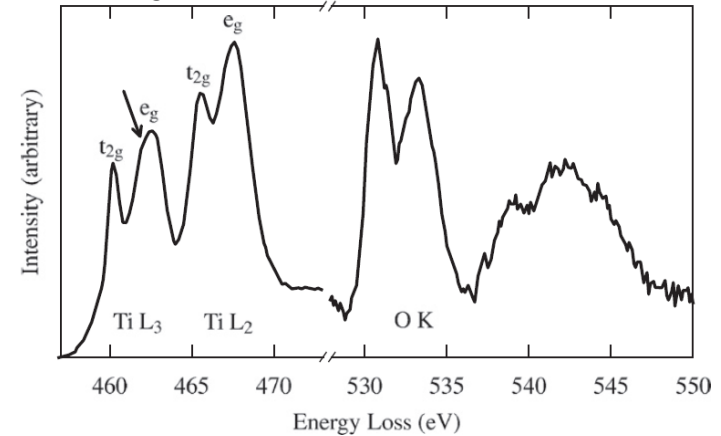


Fig. 3. O-K and Ti- $L_{3,2}$ edges in Ti-rich layers. Note the shoulder on the Ti-L3 e_g peak (arrow) indicating the rutile structure.

Ultramicroscopy 111 (2011) 169–176

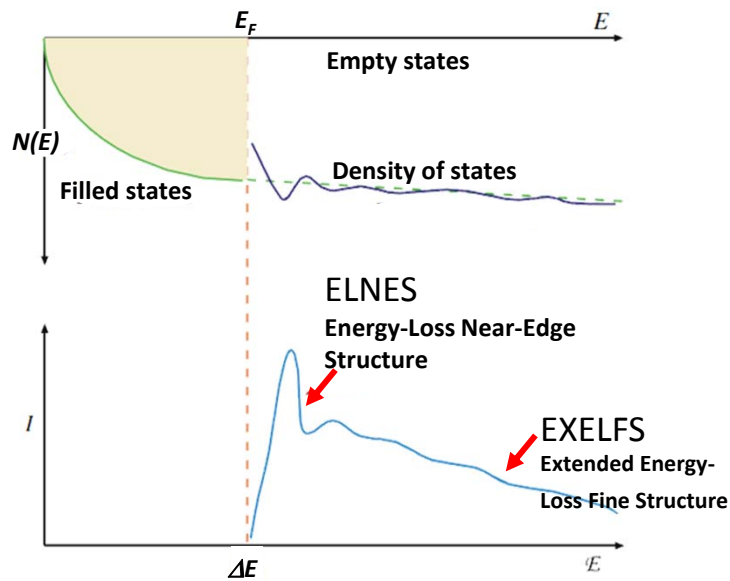
F. de la Peña^{a,1}, M.-H. Berger^b, J.-F. Hochepeid^c, F. Dynys^d, O. Stephan^a, M. Walls^{a,*}

^a Laboratoire de Physique des Solides, Bât. 510, Université Paris-Sud, 91405 Orsay Cedex, France

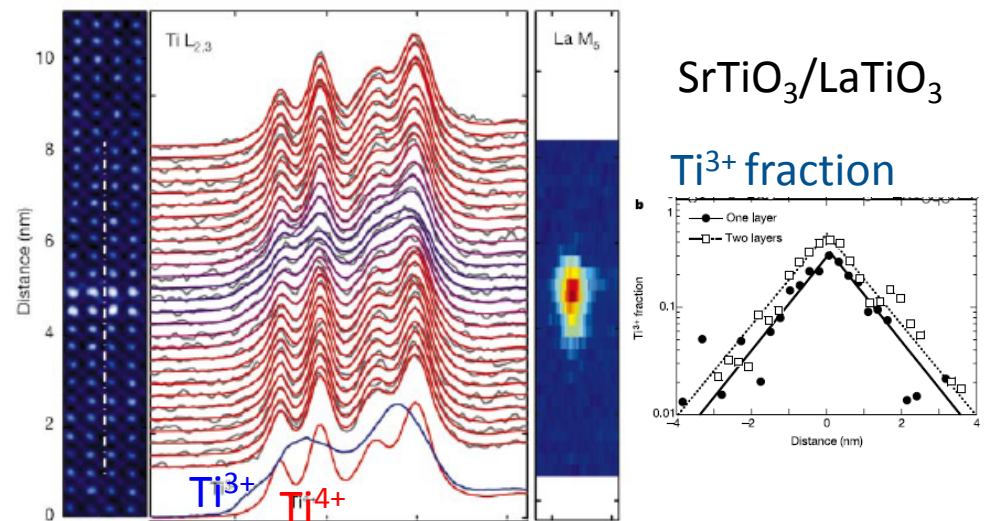
^b MINES—ParisTech, Centre des Matériaux, CNRS UMR 7633, BP 87 91003 Evry Cedex, France

^c MINES—ParisTech, CEP-SCPI, 60bd Saint Michel 75272 Paris, Cedex 06, France

^d NASA Glenn Research Center, 21000 Brookpark Road, Cleveland, OH 44135, USA




Williams & Carter
TEM textbook



A. Ohtomo, D. A. Muller, J. L. Grazul & H. Y. Hwang

NATURE | VOL 419 | 26 SEPTEMBER 2002 | www.nature.com/nature

In summary...

	TEM	Electron Diffract ⁿ	HR-TEM	STEM- HAADF	EELS	EDX	RBS* MEIS**
Epitaxy Domains Twins Dislocations	X	X	X				
Stress		X	X				
Stoichiometry						X	
Atomic displacement			X	X			
Substrate termination				X			
Cation intermixing				X	X		X
Oxygen vacancies			X		X		
Ti valence					X		
High Temp Phase transit ⁿ	X	X	X				
Heating sample holder							

-TEM-STEM HAADF EDX EELS : at Mines-ParisTech 200kV FEG Tecnai FEI F20ST

+ collaboration with LPS Orsay UltraSTEM Nion- Mike Walls

-*Rutherford Back Scattering and **Medium Energy Ion Scattering :

Intermixing study with a depth resolution of one atomic layer

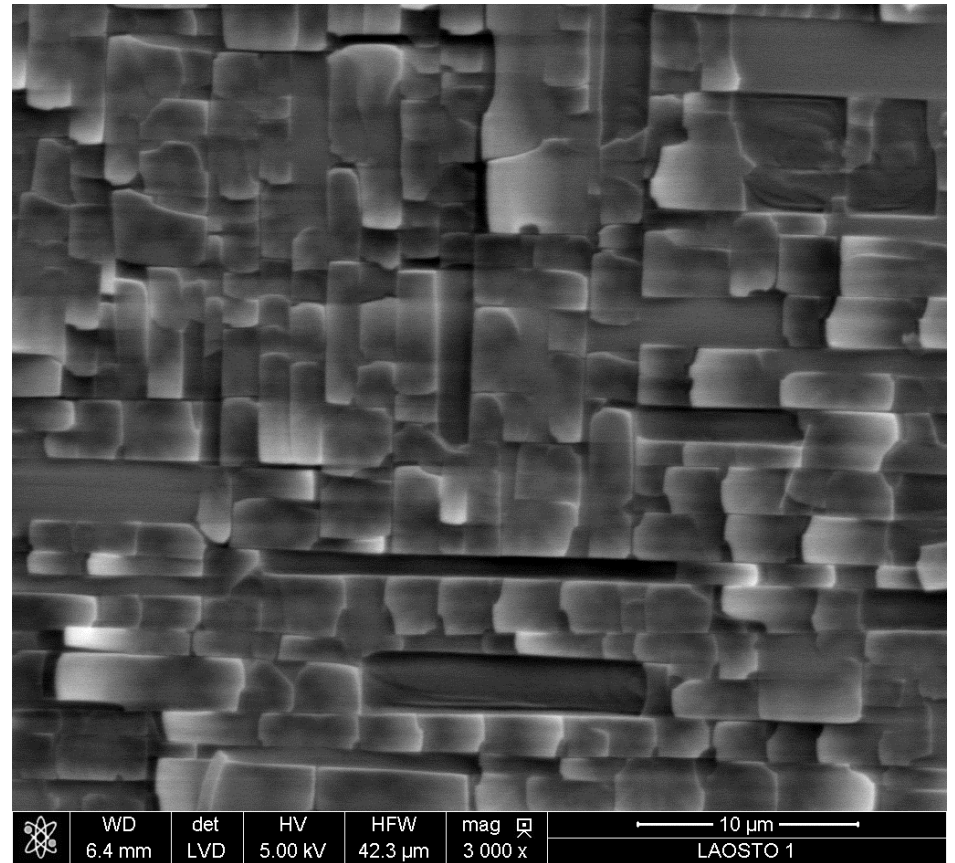
In contact with Denis Jalabert/Pascal Berger CEA-Grenoble/Saclay

We asked Alp to grow a thick film, for easier TEM thin foil preparation...
SEM → Periodic multicracking, decohesion (internal stresses) ... but

Electron Channeling Pattern ... to deepen



SEM-BSE

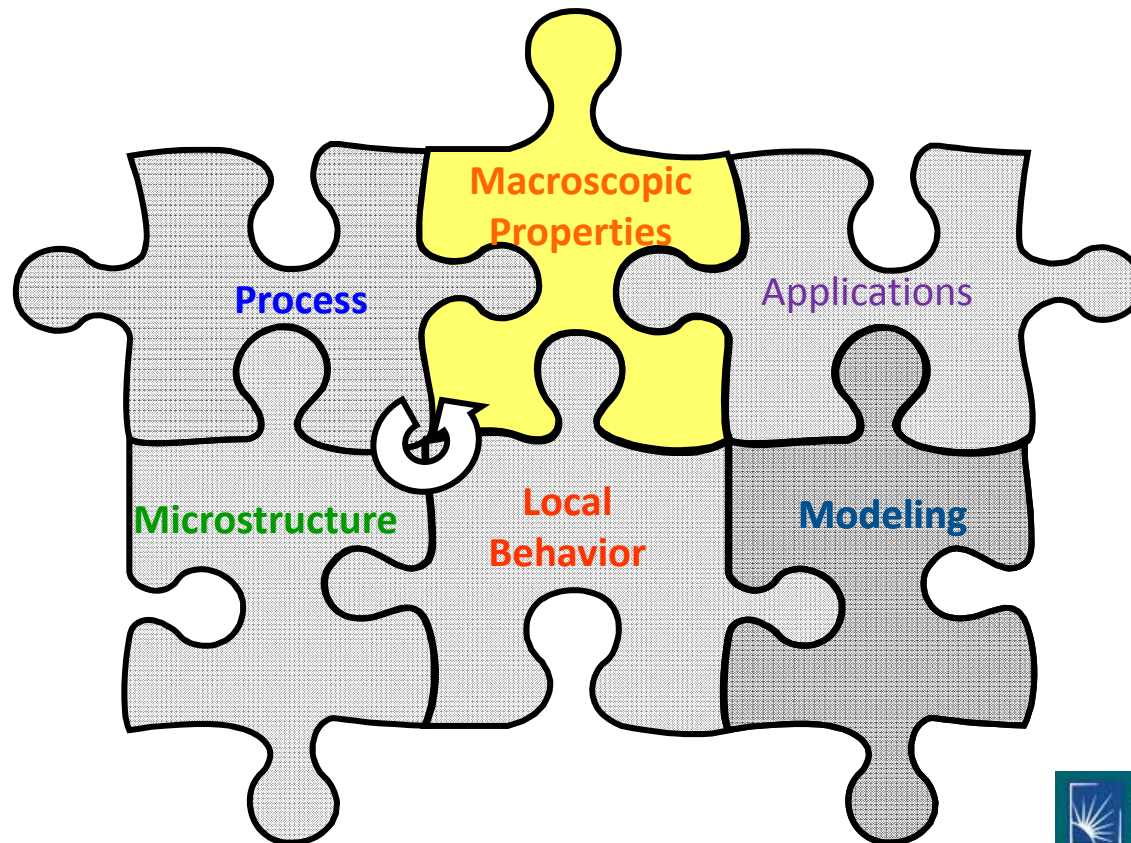


SEM-SE

Quantitative identification of electro-physical properties of oxide based hetero-interfaces at extreme environments

LaAlO₃/SrTiO₃ hetero-interfaces: electrical transport properties

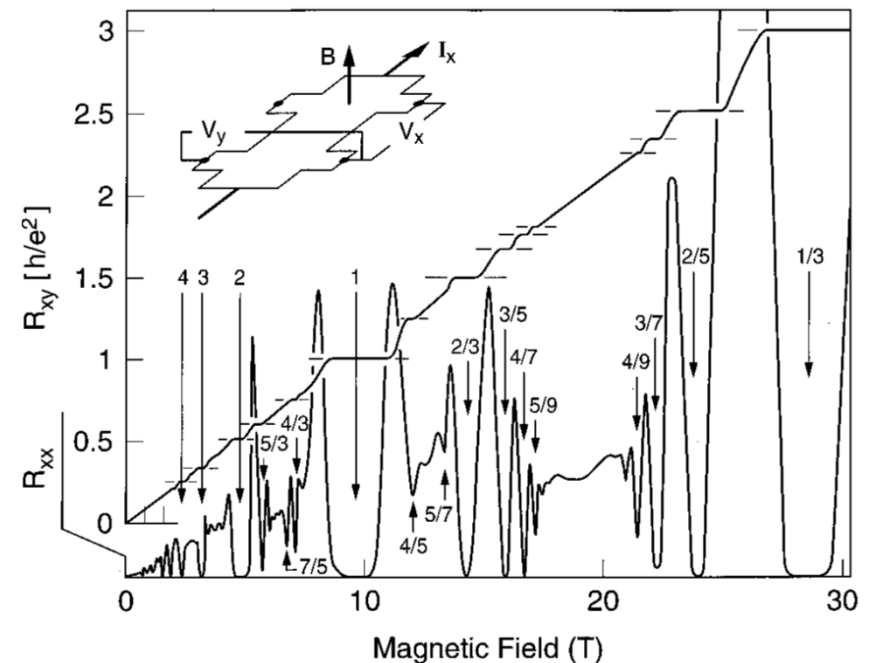
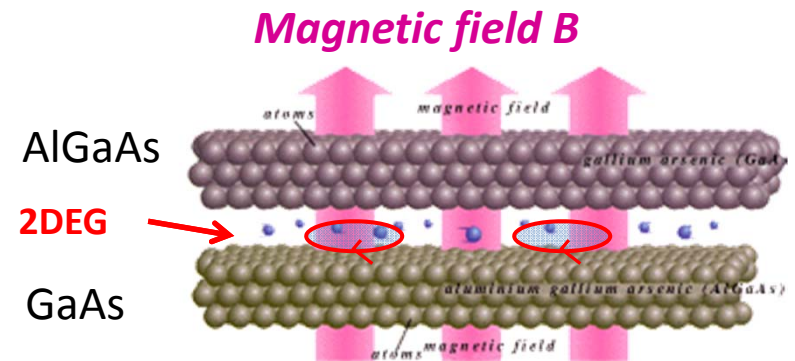
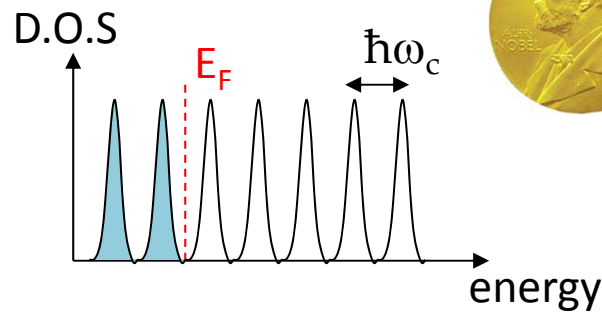
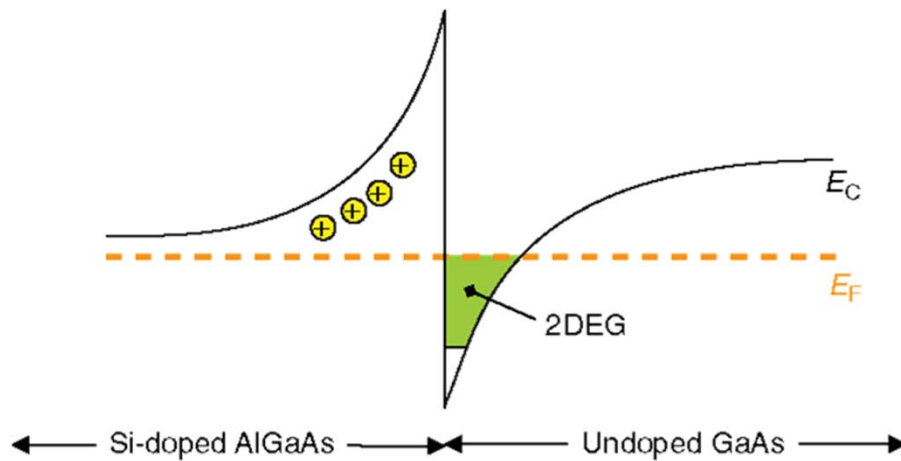
Xuan Gao – Department of Physics, CWRU



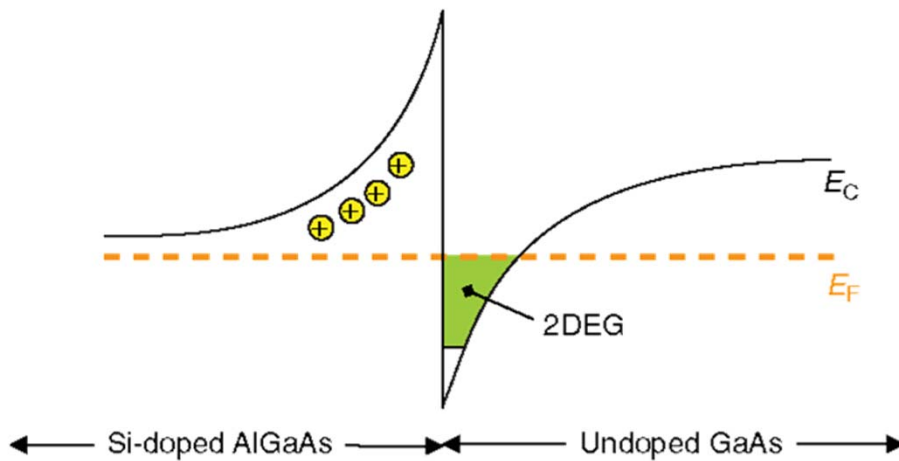
Outline

- STO/LAO hetero-interface transport properties: an overview
- STO/LAO hetero-interface transport properties: outstanding questions (origin of charge) and some initial electrical transport data from our team (dominant effect of O vacancies)
- Conclusions

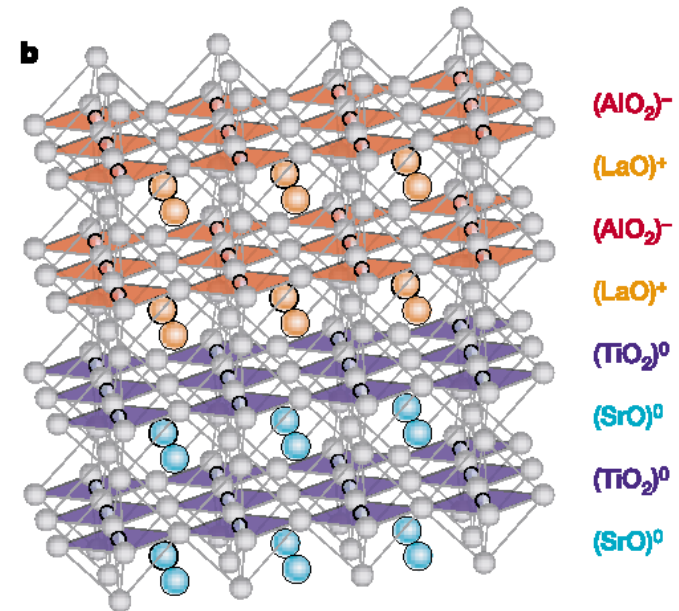
2DEG at conventional semiconductor hetero-interface



Formation of conducting 2DEG formation at oxide hetero-interfaces



Conventional semiconductor hetero-interface



Polar hetero-interface of perovskite oxides

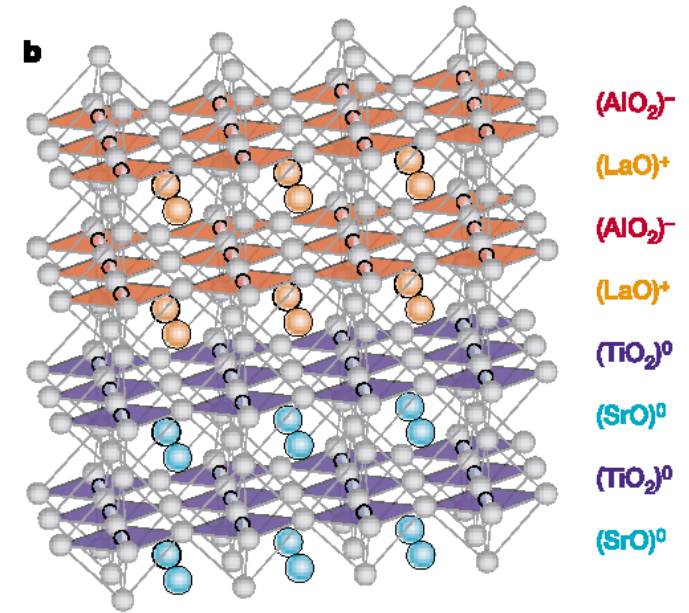
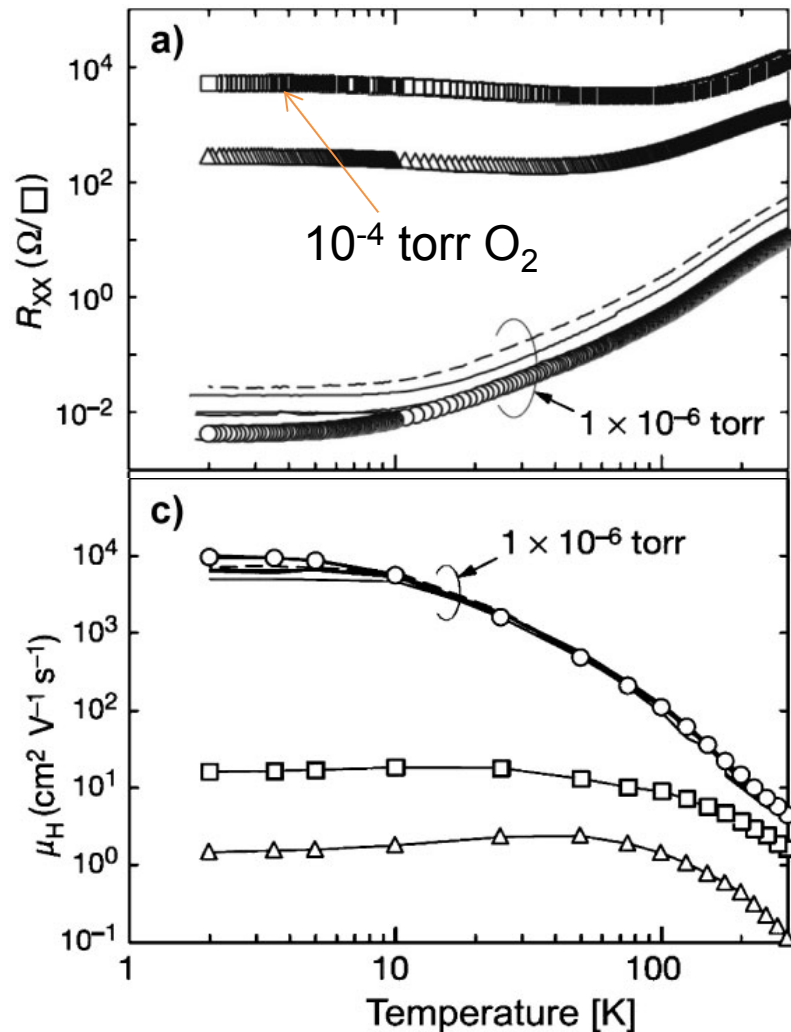
letters to nature

A high-mobility electron gas at the $\text{LaAlO}_3/\text{SrTiO}_3$ heterointerface

A. Ohtomo^{1,2,3} & H. Y. Hwang^{1,3,4}

Ohtomo and Hwang, Nature (2004)

Formation of conducting 2DEG formation at oxide hetero-interfaces



Polar hetero-interface of perovskite oxides

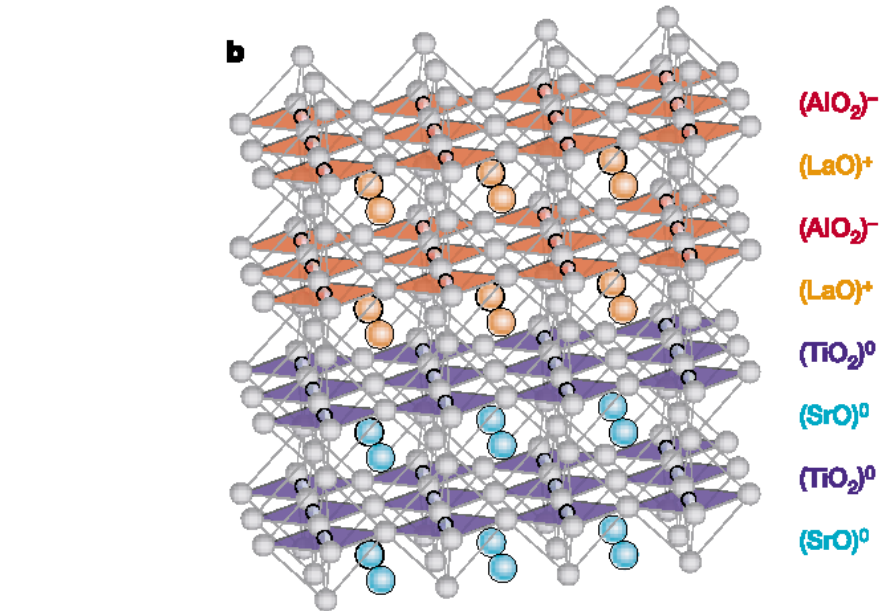
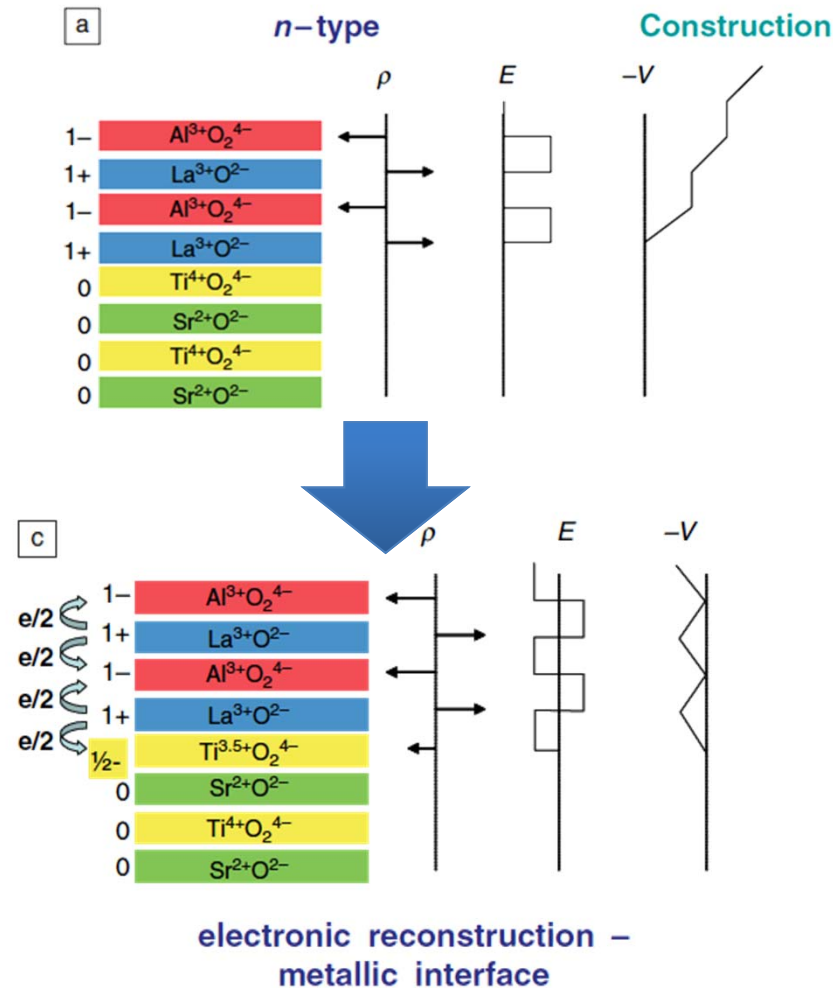
letters to nature

A high-mobility electron gas at the $\text{LaAlO}_3/\text{SrTiO}_3$ heterointerface

A. Ohtomo^{1,2,3} & H. Y. Hwang^{1,3,4}

Ohtomo and Hwang, Nature (2004)

Formation of conducting 2DEG formation at oxide hetero-interfaces



Polar hetero-interface of perovskite oxides

letters to nature

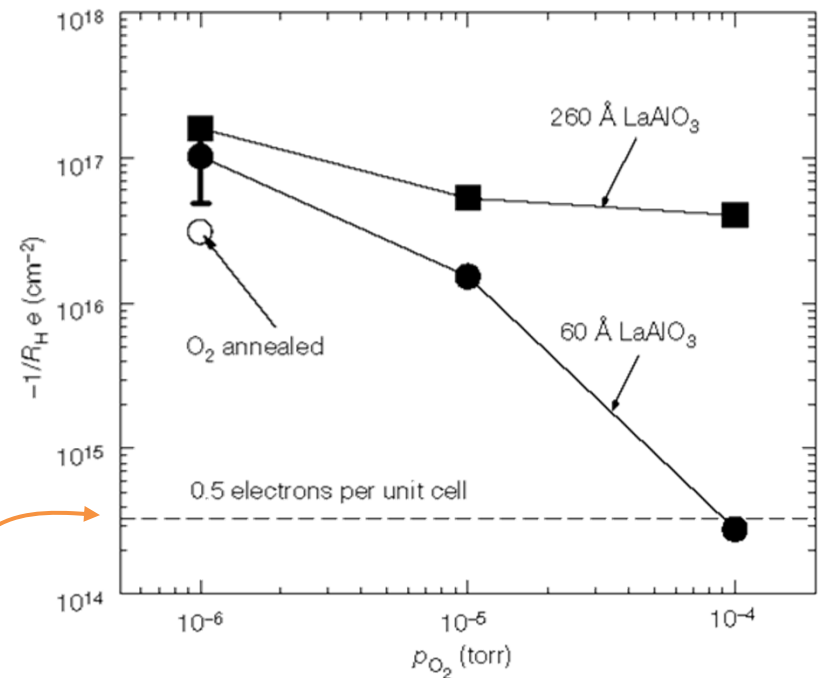
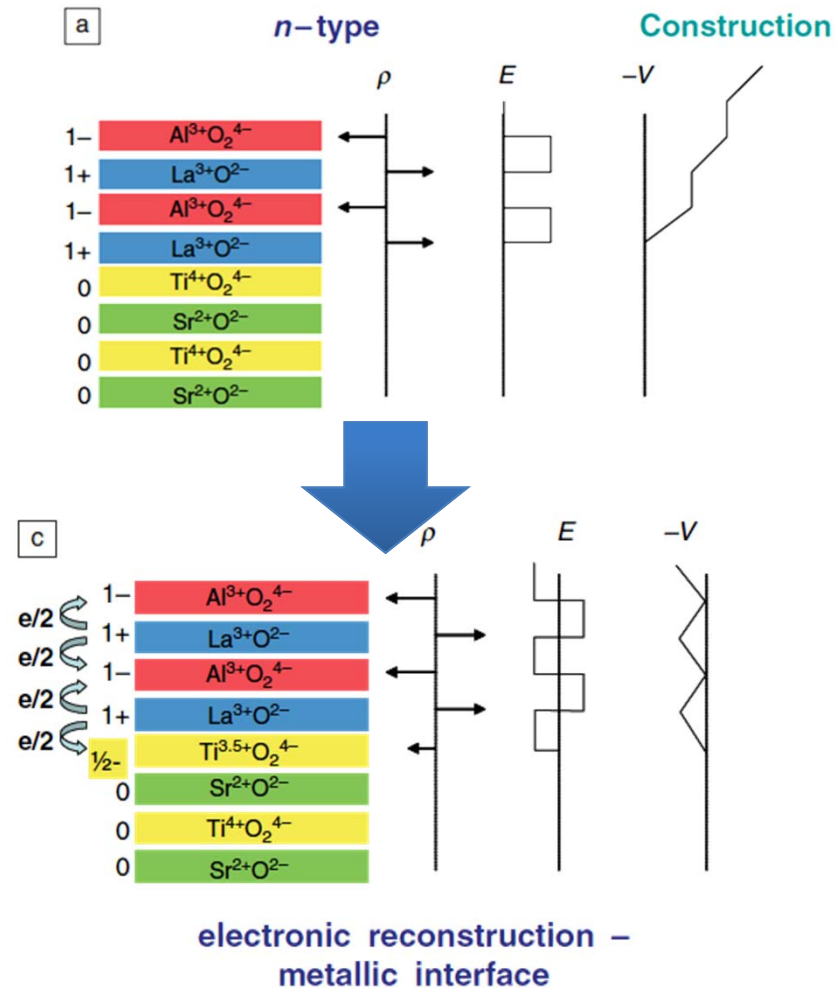
**A high-mobility electron gas at
the LaAlO₃/SrTiO₃ heterointerface**

A. Ohtomo^{1,2,3} & H. Y. Hwang^{1,3,4}

Ohtomo and Hwang, Nature (2004)

Polar catastrophe: $0.5e/\text{unit cell} \rightarrow 3.5 \times 10^{14}/\text{cm}^2$

Formation of conducting 2DEG formation at oxide hetero-interfaces



Polar catastrophe: $0.5e/\text{unit cell} \rightarrow 3.5 \times 10^{14}/\text{cm}^2$

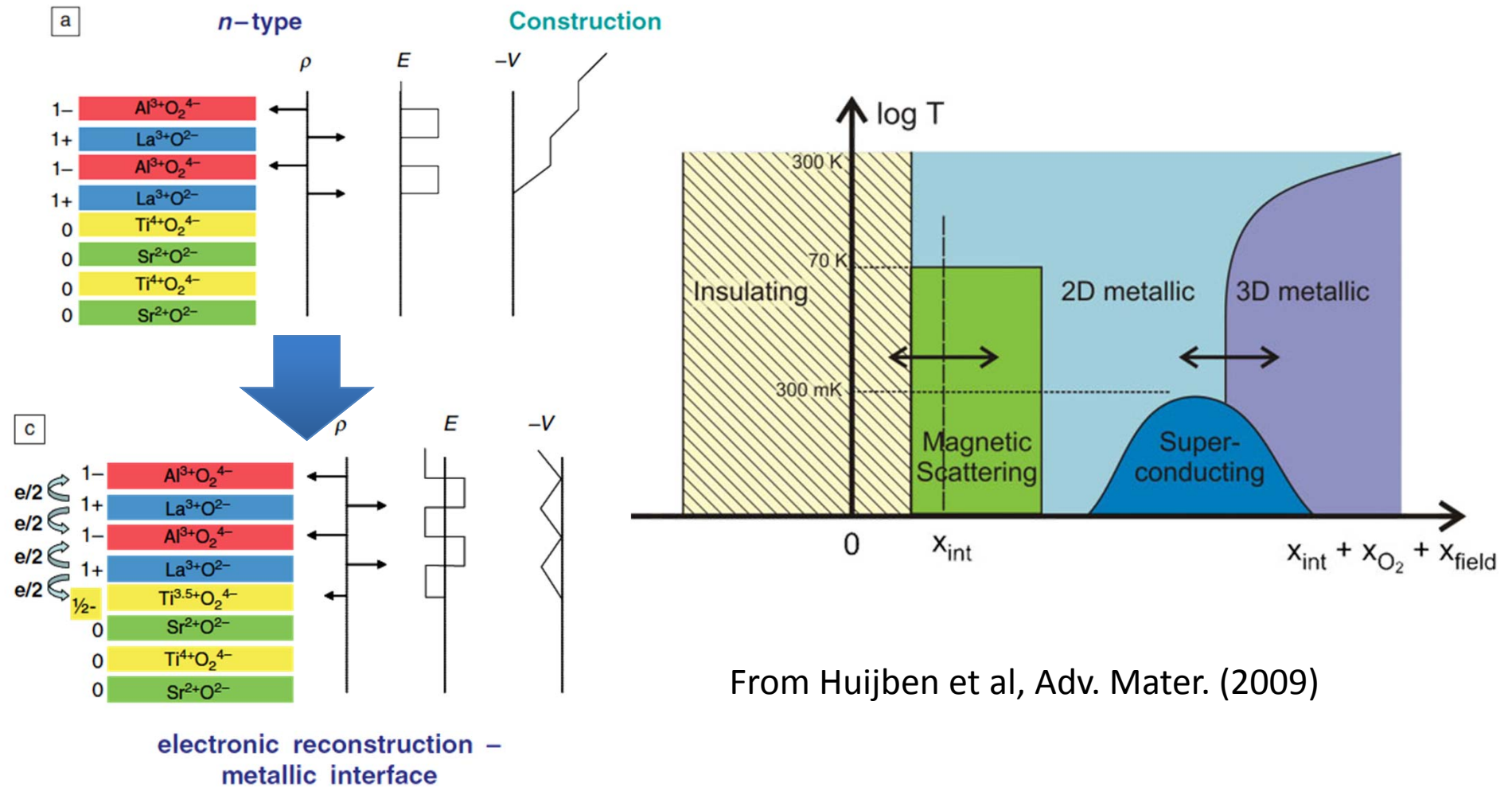
letters to nature

A high-mobility electron gas at the LaAlO₃/SrTiO₃ heterointerface

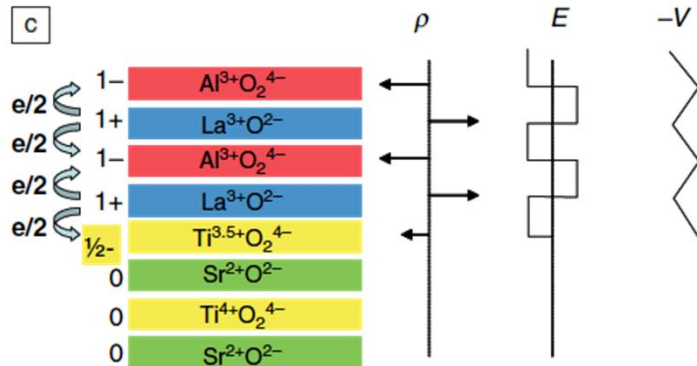
A. Ohtomo^{1,2,3} & H. Y. Hwang^{1,3,4}

Ohtomo and Hwang, Nature (2004)

Emergent phenomena in the 2DEG at LAO/STO hetero-interface

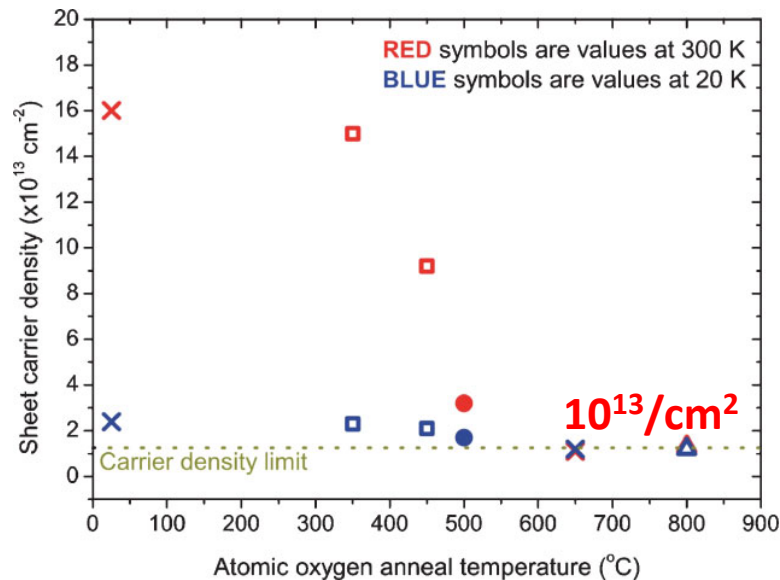


Origin of 2DEG at LAO/STO hetero-interface: extrinsic or intrinsic?



electronic reconstruction –
metallic interface

**Polar catastrophe induced
electronic reconstruction (Intrinsic
origin):**
 $0.5e/\text{unit cell} \rightarrow 3.5 \times 10^{14}/\text{cm}^2$



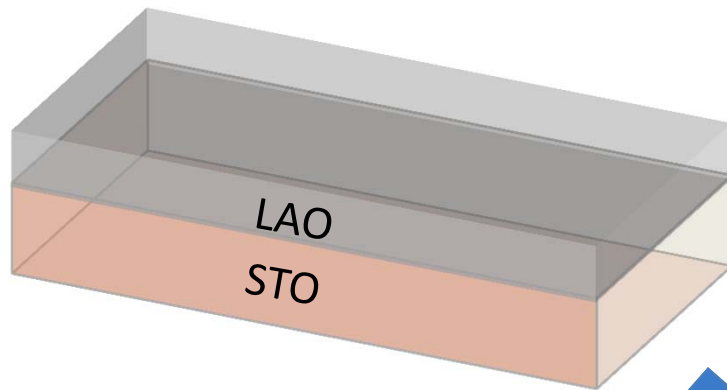
**Oxygen vacancy as extrinsic source
of 2DEG:**
annealing in $\text{O}_2 \rightarrow 10^{13}/\text{cm}^2$

Siemons et al., PRL (2007);
also Herranz et al., PRL, Kalabukhov
et al. PRB.

Focus of our planned research

- Coupling with theory and other material/device study, we will investigate the impact of the following factors on the fundamental transport properties of 2DEG at STO/LAO interface
 - Oxygen vacancies and doping control
 - La-Al stoichiometry
 - Strain effects
 - Electrical properties at extreme conditions (high T, low T, magnetic field), and gate control of conductivity in transistor type of devices

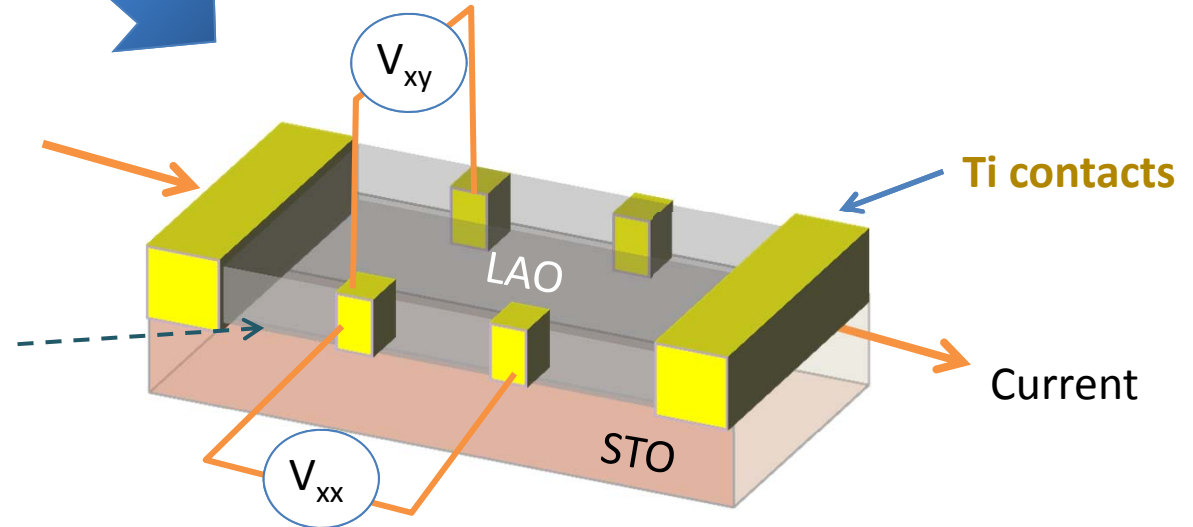
Our electrical measurements on STO/LAO hetero-interfaces: device configuration



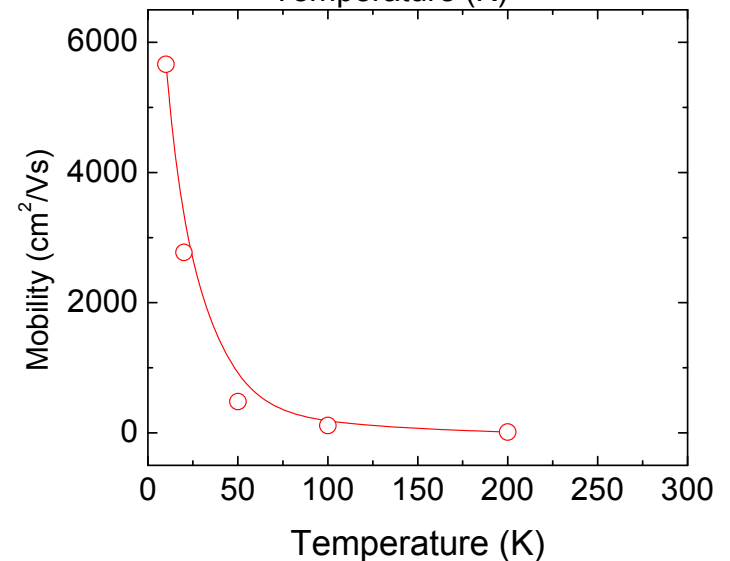
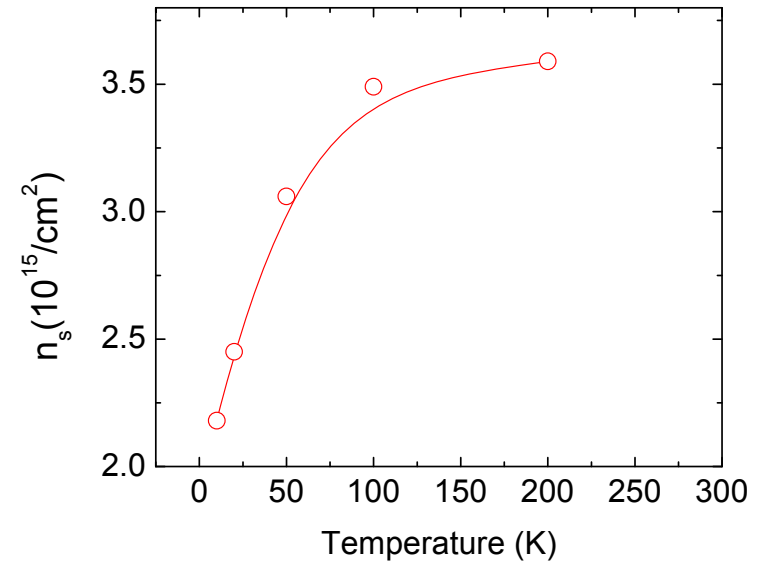
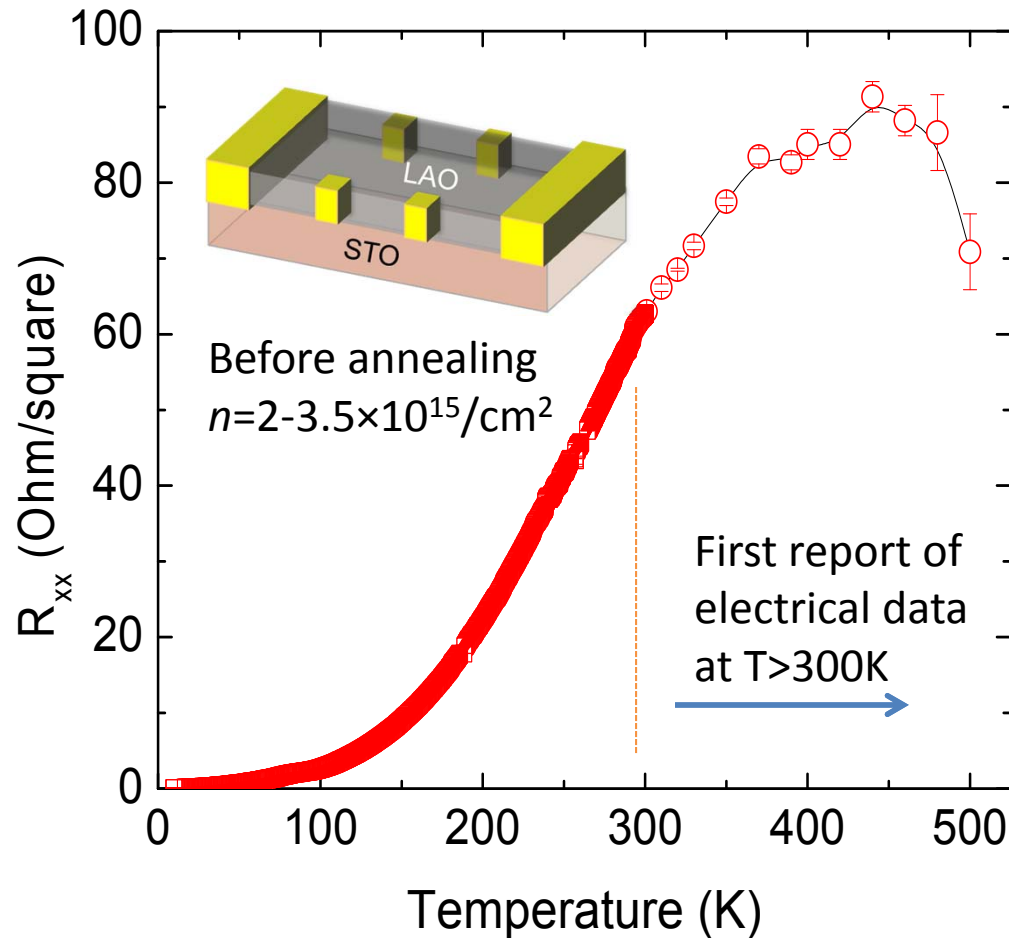
$$R_{xx} \text{ (Ohm/}\square\text{)} = 1/(ne\mu)$$
$$R_{xy} = B/(ne)$$

n : carrier sheet density
 μ : carrier mobility

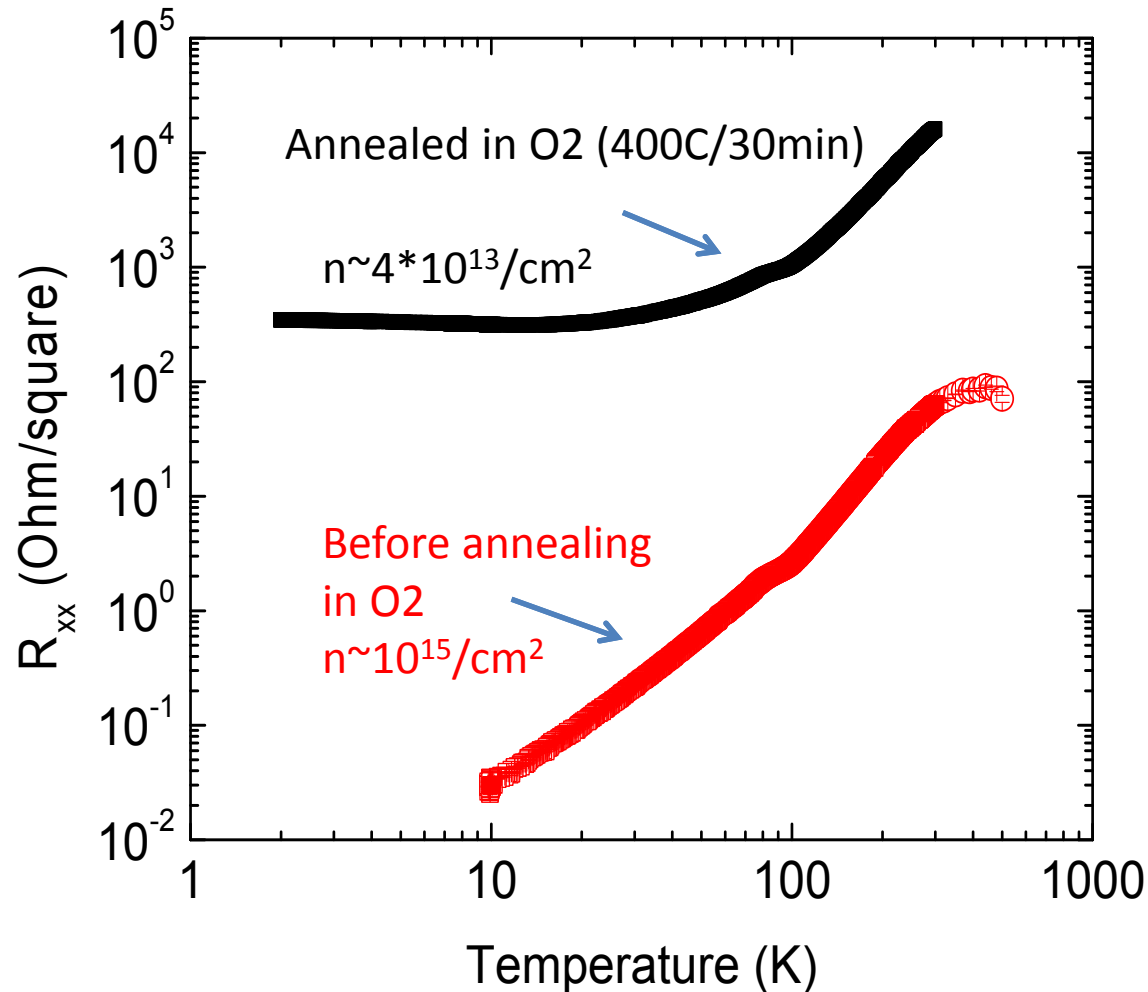
2DEG at hetero-interface



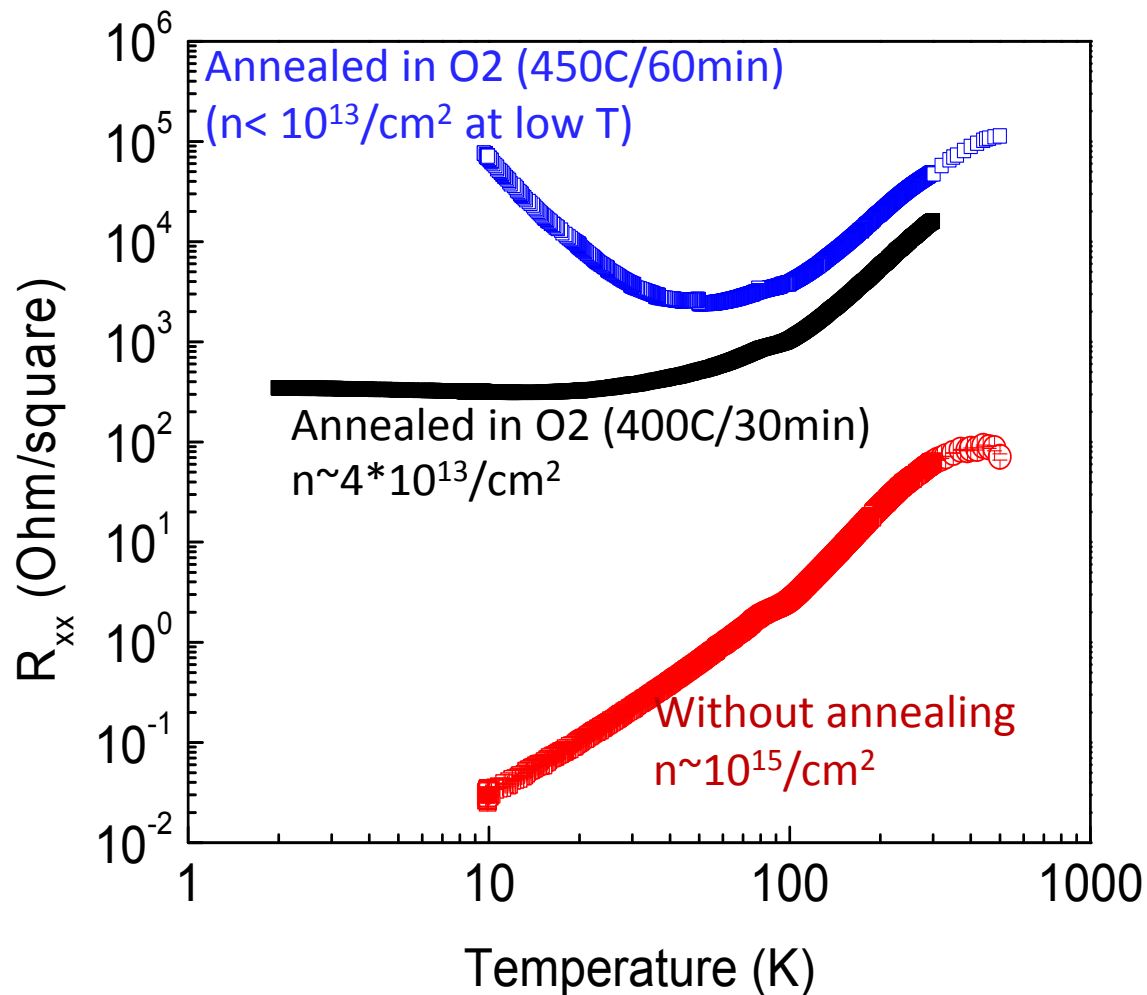
Our electrical data on STO/LAO hetero-interfaces: sample grown in low O_2 pressure



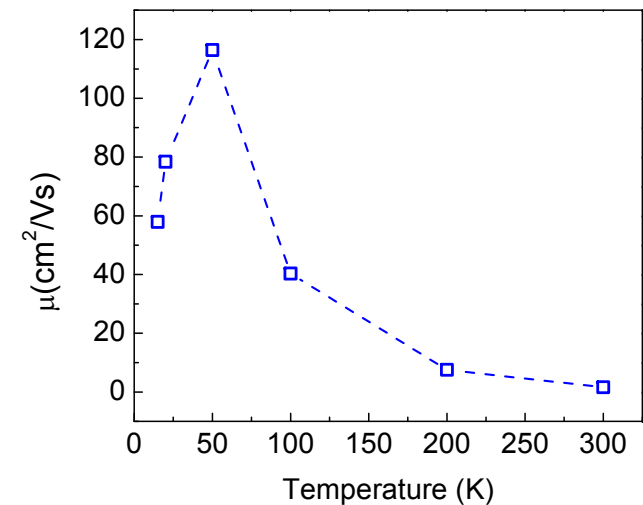
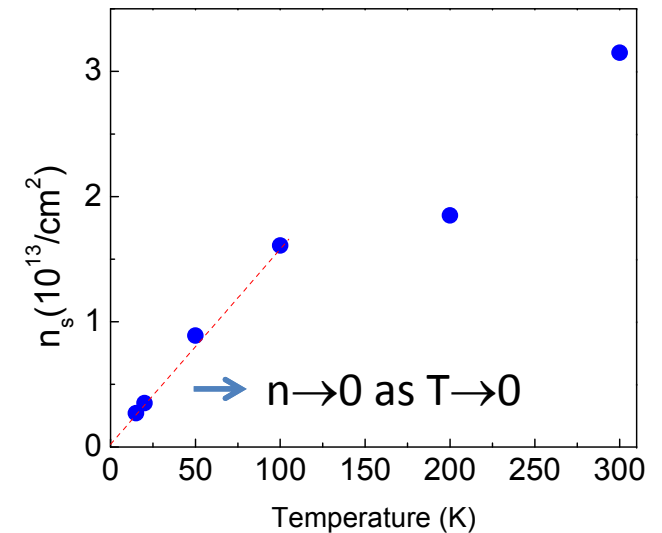
Our electrical data on STO/LAO hetero-interfaces: effect of annealing in O₂



Greatly reduced carrier density by annealing in O_2



After annealing for 1hr:



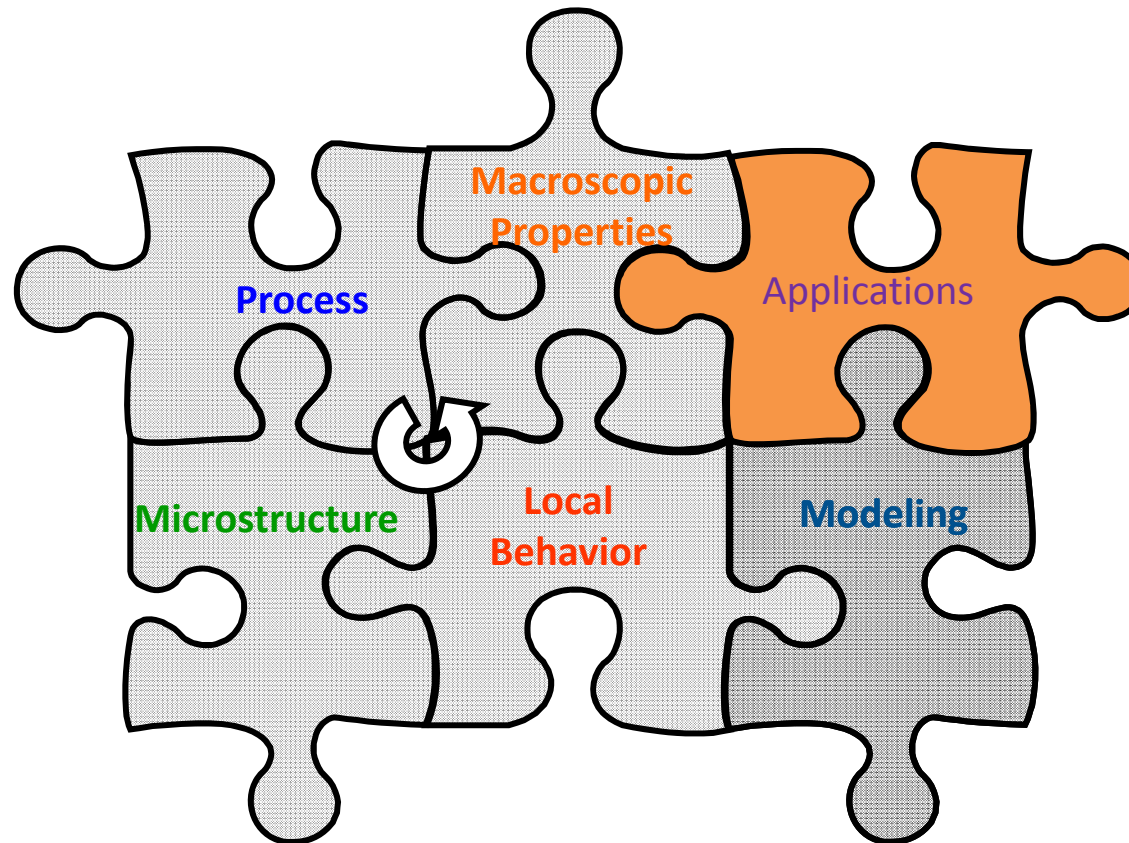
Conclusions

- Electrically conductivity 2DEG at STO/LAO
- Annealing in O₂ can strongly suppress (completely remove) the density of 2DEG: 'extrinsic' origin of 2DEG
- Further synergistic investigations between material structural/composition analysis of interface, theoretical understanding of defect states (O vacancies etc) can help understand the origin of 2DEG; controlled doping/strain/stoichiometry may tune the performance/functionality further.

Quantitative identification of electro-physical properties of oxide based hetero-interfaces at extreme environments

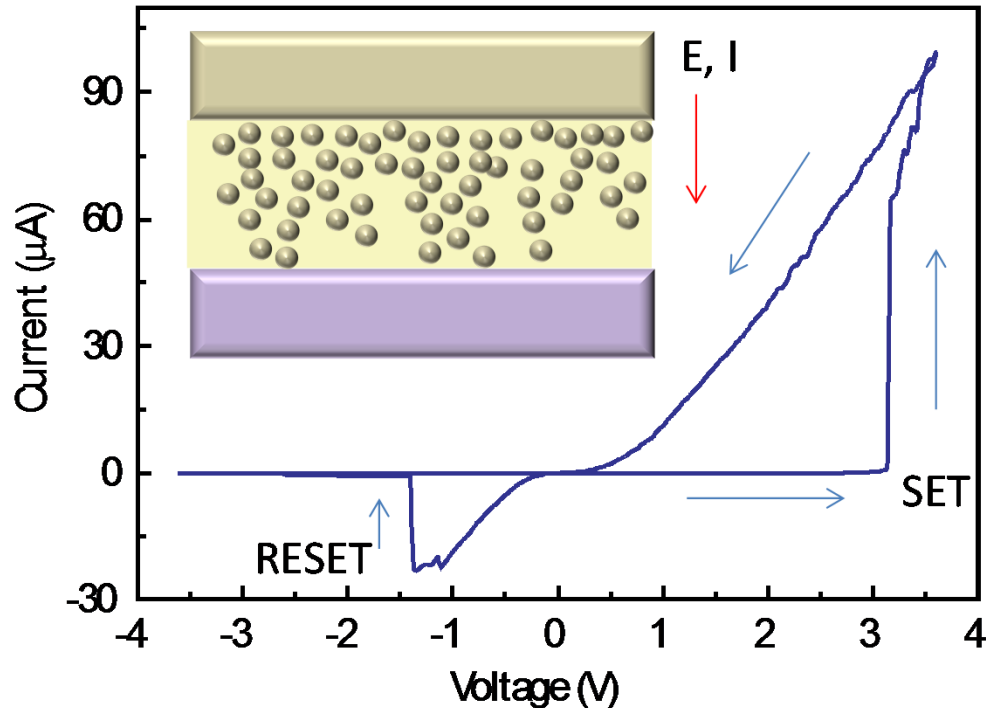
Vacancy Mediated Multifunctional Oxide Devices

Wei Lu – Department of Electrical Engineering and Computer Science, University of Michigan



Introduction

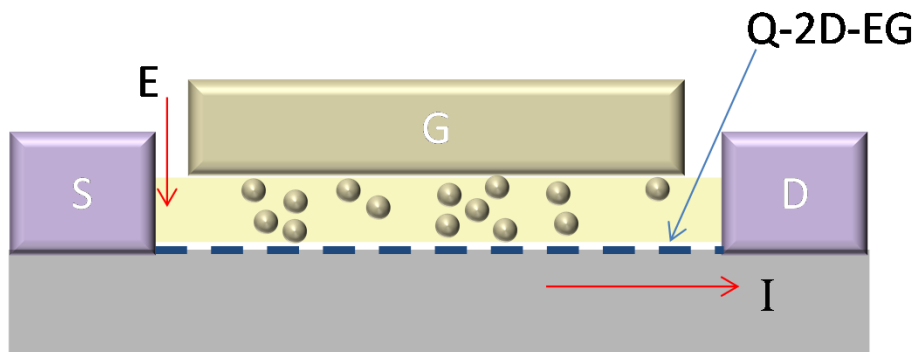
Combining hysteretic resistive switches with HEMT in a single device



- Vertical (gate) direction – resistance switching (memristor) device enabled by oxygen vacancy redistribution.
- Lateral (channel) direction – HEMT based on 2DEG at oxide interface.

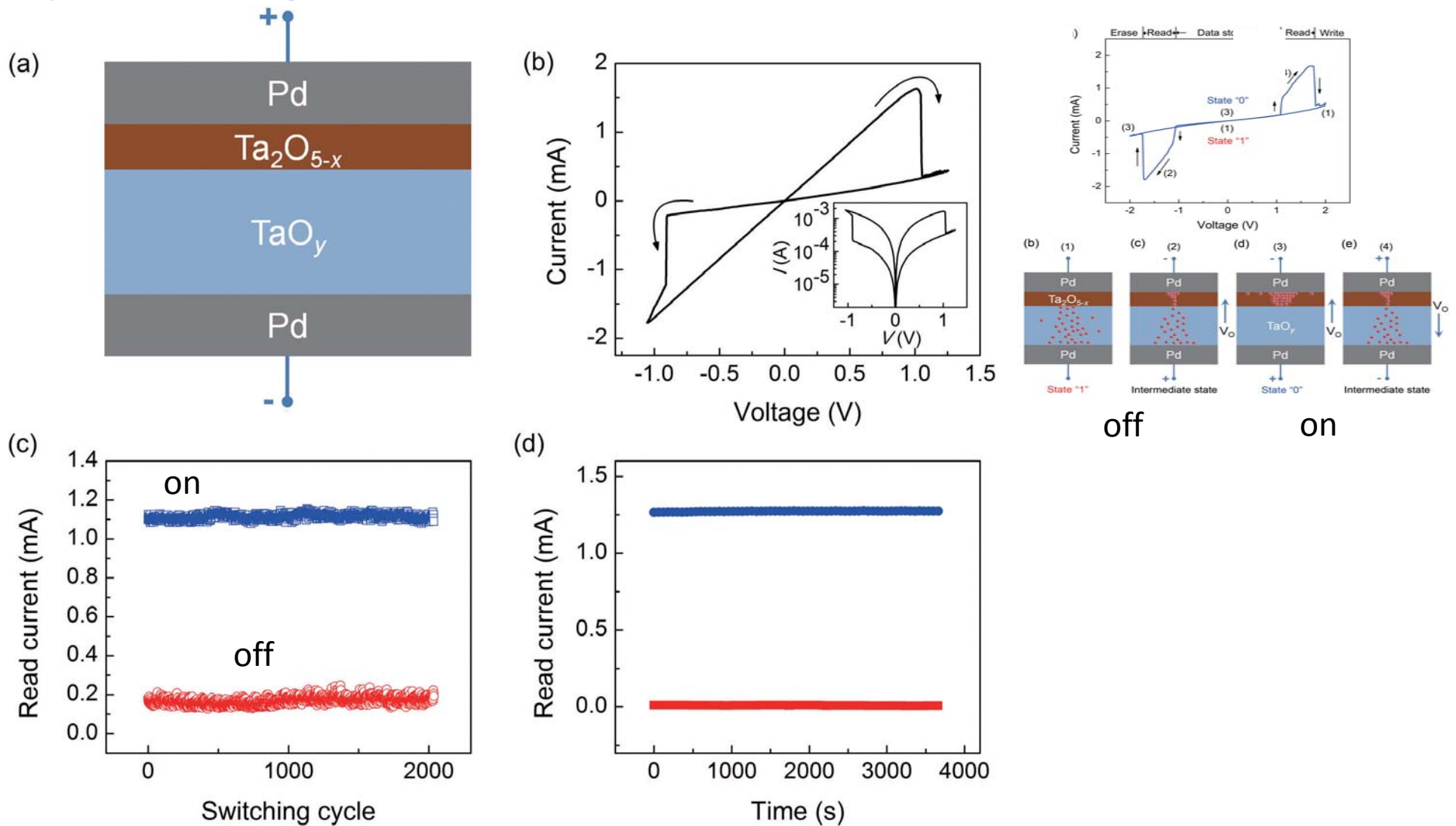
Applications:

- Combining non-volatile memory with fast transistor
- Appears as float-gate type devices but without the “control” gate and much faster (not based on electron tunneling)
- Reconfigurable RF circuits



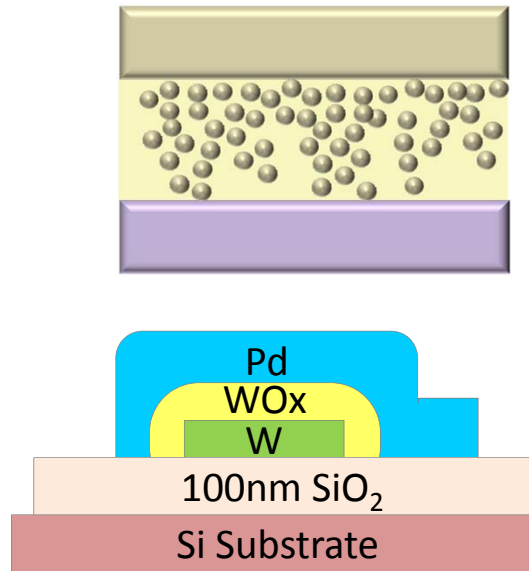
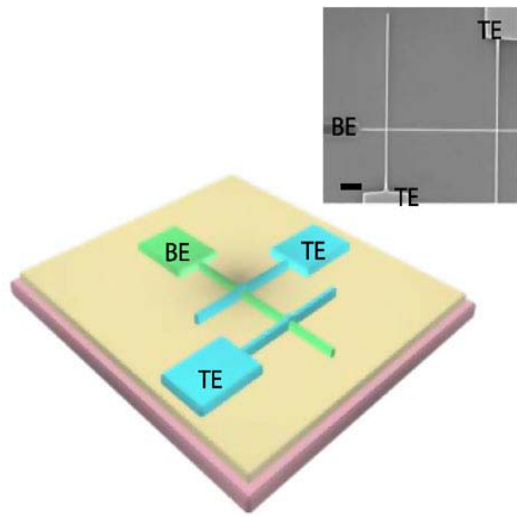
Prior Work - Resistive Switching in TaO_x

Bipolar switching



Y. Yang, P. Sheridan, W. Lu, *App. Phys. Lett.* 100, 203112 (2012)

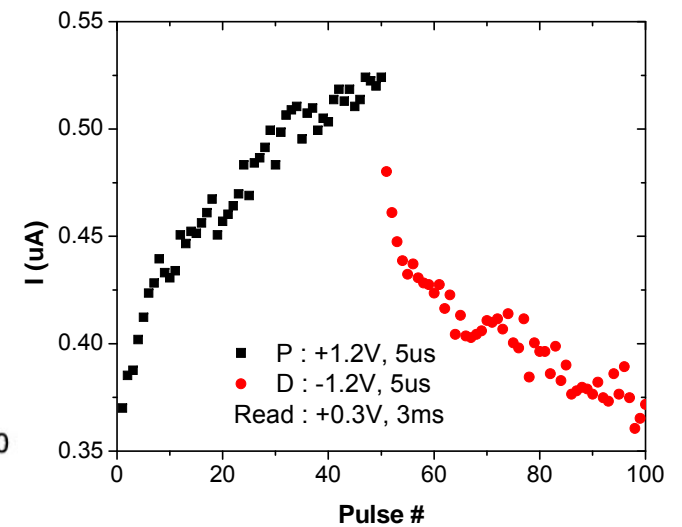
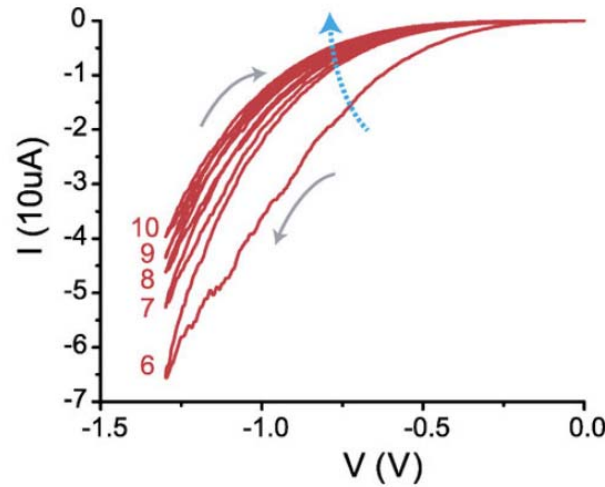
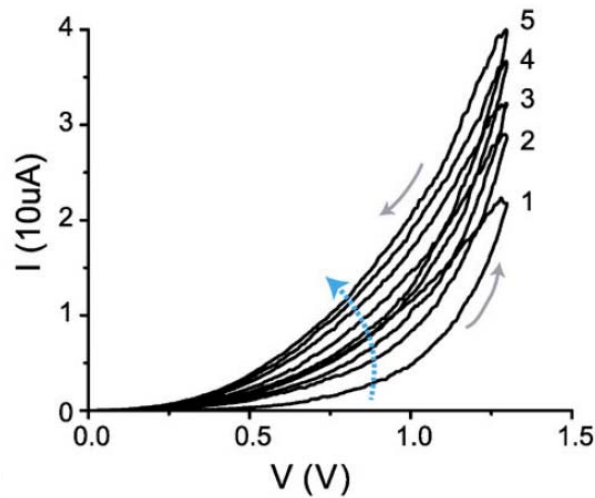
Prior Work - WO_x-Based Device



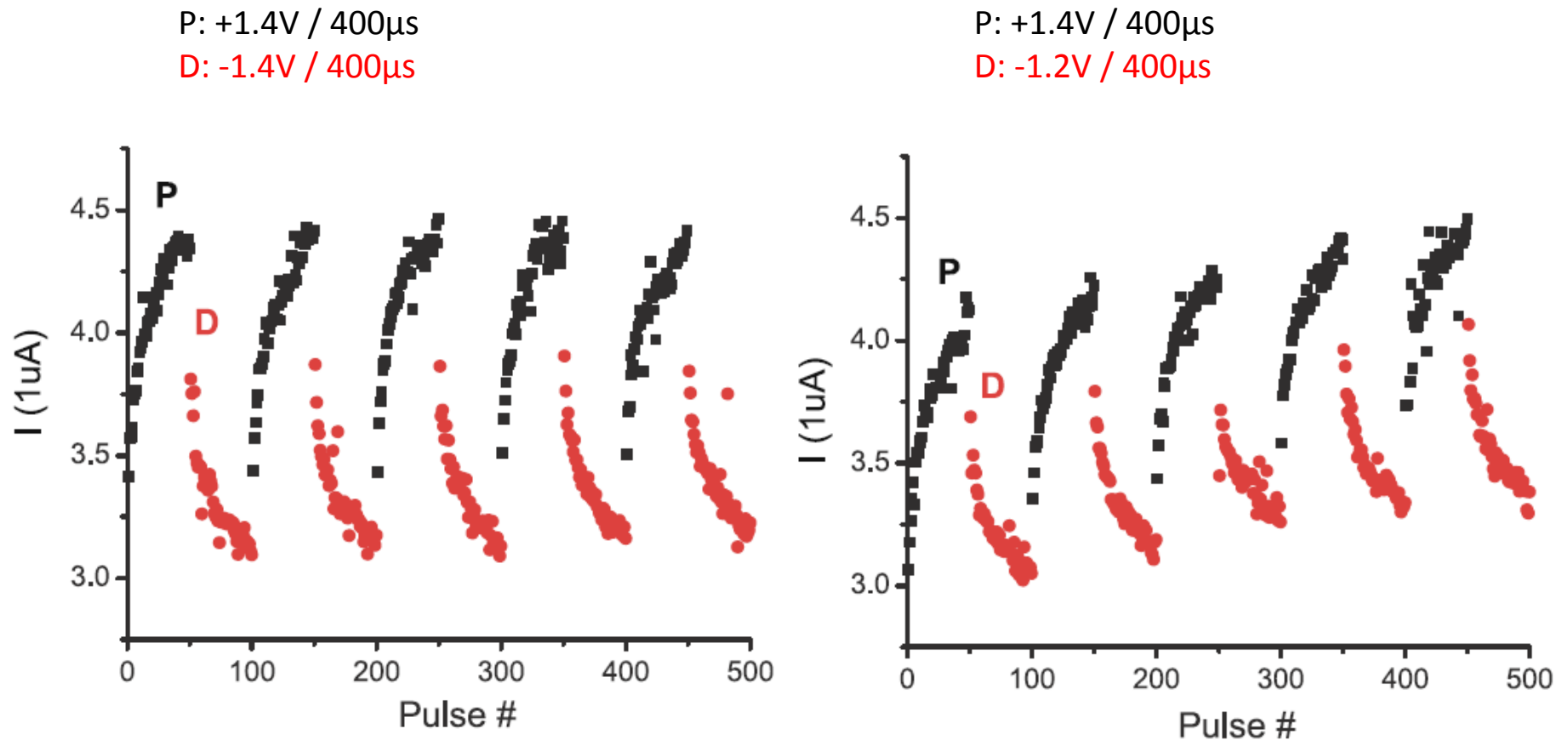
Potential (+V)
Conductance increases
Synaptic weight strengthened

Motion of V_{ox} \updownarrow

Depression (-V)
Conductance decreases
Synaptic weight weakened

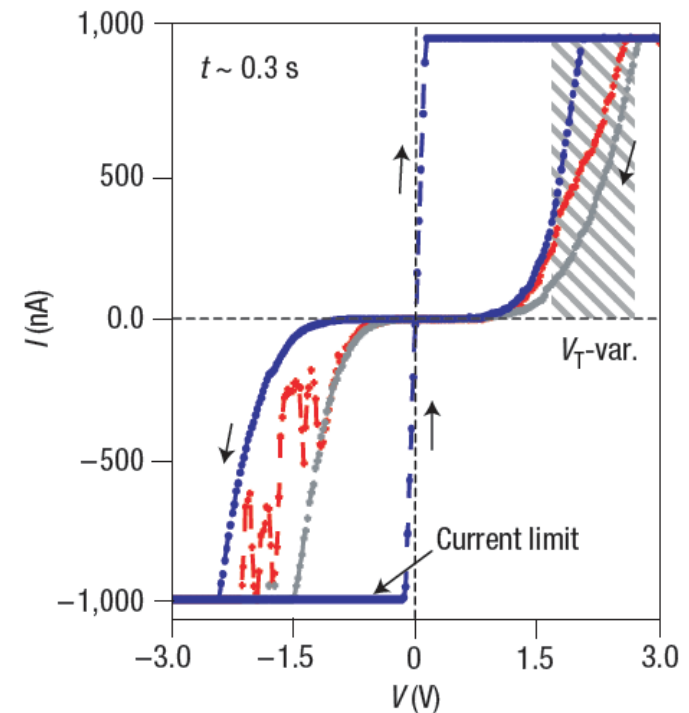
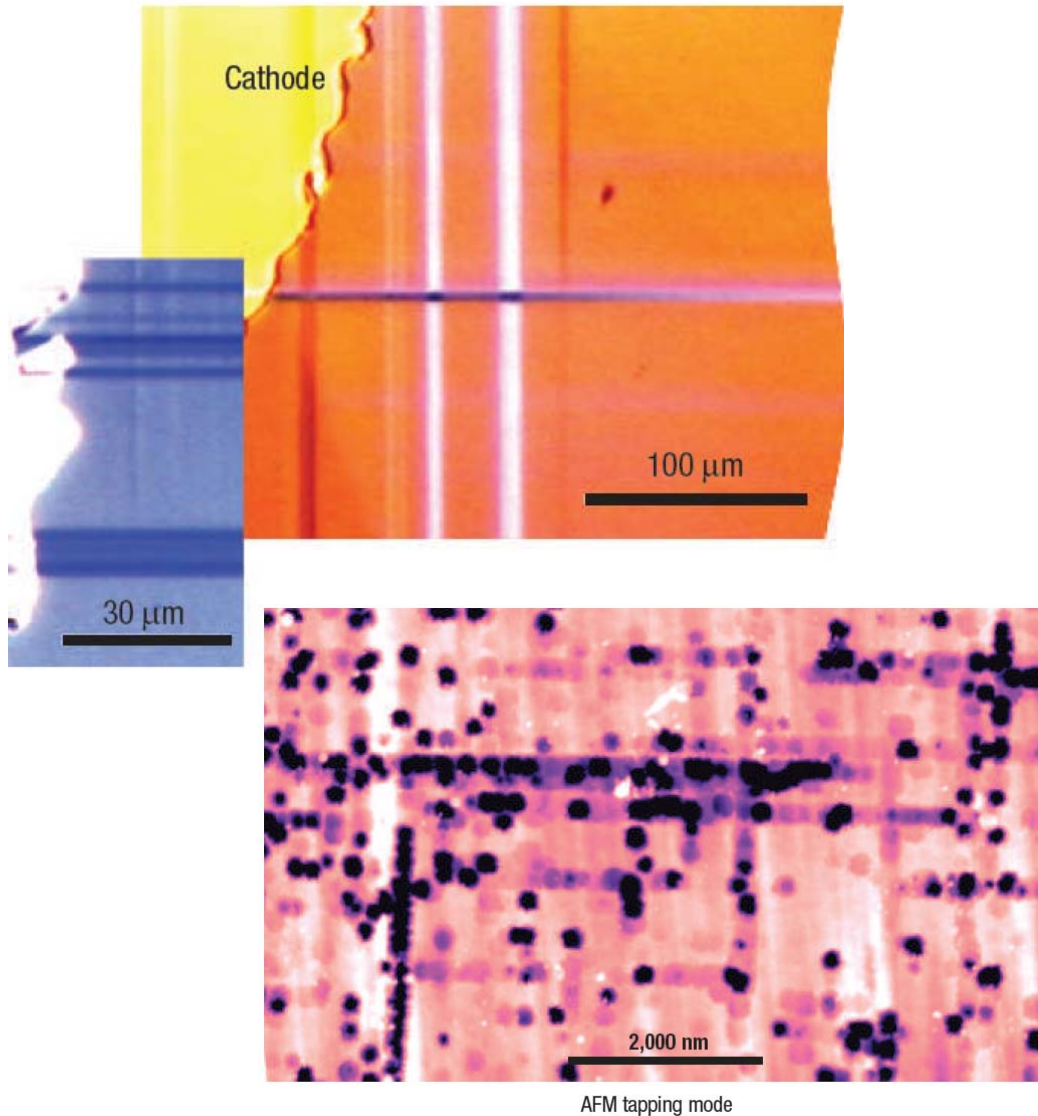


WO_x Memristor Characteristics



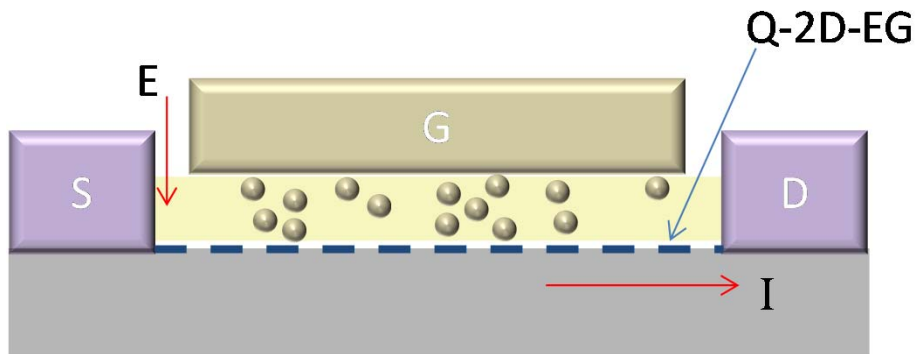
- Resistance change controlled by voltage pulses (pulse height or width)
- Overall conductance determined by the integral of voltage-time

Resistive Switching in Intrinsic TMO



- Oxygen vacancies can be created under high electric bias in intrinsic, single-crystalline STO
- Oxygen move along naturally occurring dislocations and cause resistive switching

Proposed Studies

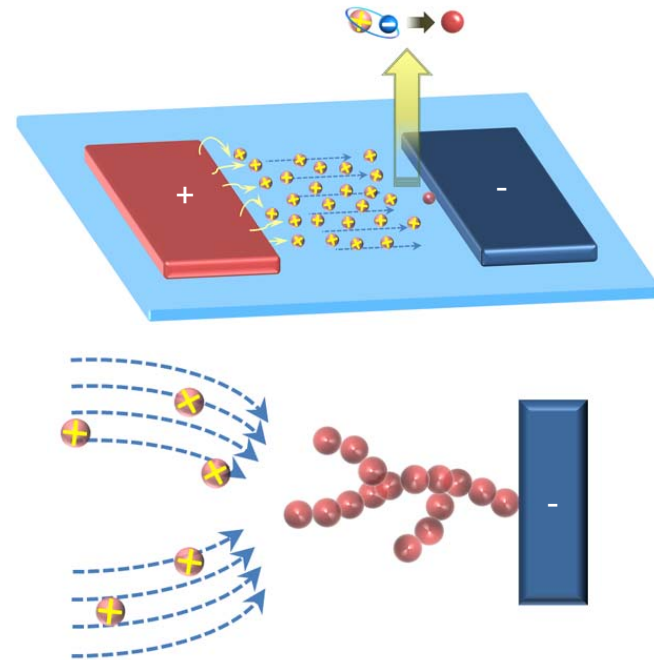
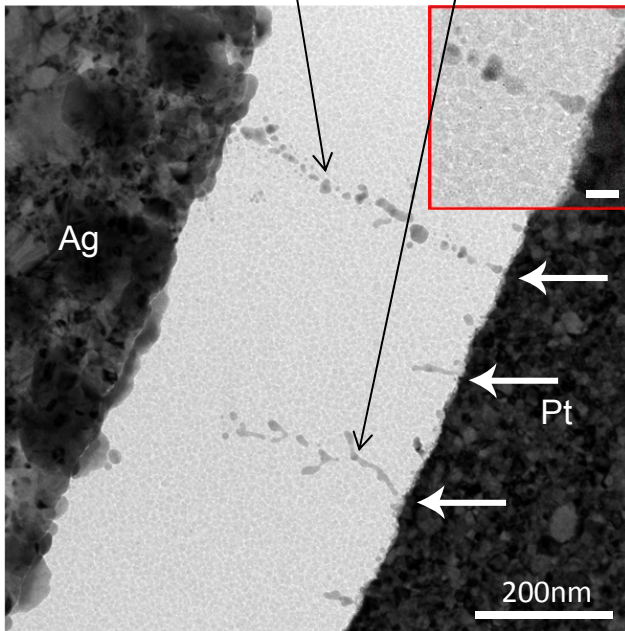


- **Prototype device demonstration**
 - HEMT with plastic V_T
 - E-field requirement
 - device optimization (electrode material, interface)
- **Mechanism verification**
 - Electrode dependence (blocking electrodes vs reactive electrodes)
 - TEM characterizations
 - Analog switching vs. digital switching
- **Modeling**
 - Phenomenological model
 - First-principle model (working with Walter)
- **Application**
 - Simple reconfigurable circuit

Prior work - Observation of Conducting Filaments

- Ag/SiO₂/Pt structure, sputtered SiO₂ film
- The filament grows from the IE backwards toward the AE
- Branched structures were observed with wider branches pointing to the AE

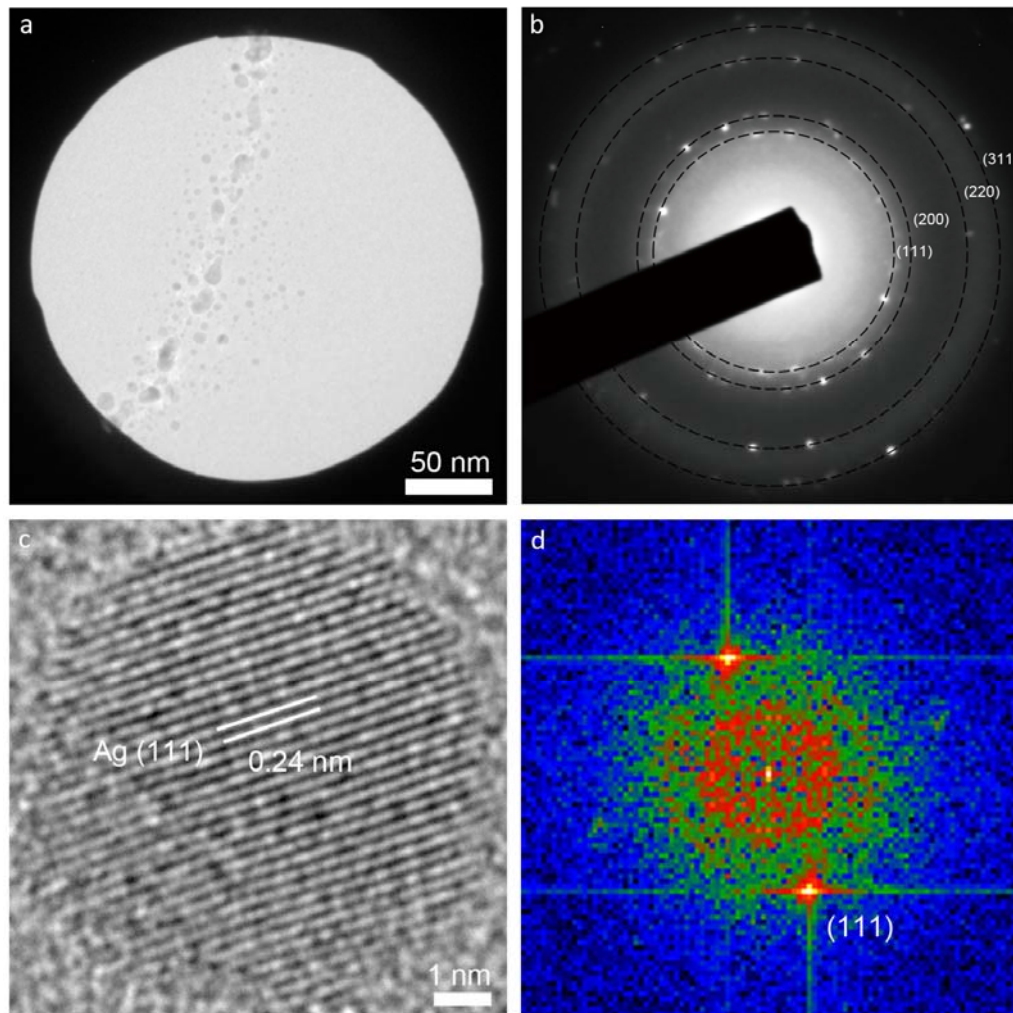
Completed filament Partially formed filaments



Yang, Gao, Chang, Gaba, Pan, and W. Lu, Nature Communications, 3, 732, 2012.

Compositional Analysis of the Filament

Ag filament in SiO_2



The filament was verified to be composed of elemental fcc Ag particles (i.e. not Ag ions or oxides)

Thin Ag filaments are not stable and naturally break into discrete Ag particles

High conductance can be maintained when the particles are closely spaced

Prior Work - Model Development

$$\dot{i} = G(w, v)v$$

$$\dot{w} = f(w, v)$$

First order model:

Two equations describing switching behavior

w : state variable

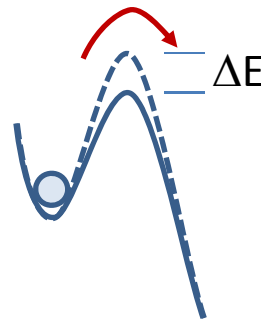
I-V equation, tunneling through a barrier with thickness of $w-l$ with barrier height ψ

$$I = \frac{eA}{2\pi\hbar(w-l)^2} \left[\left(\psi - \frac{eV}{2} \right) e^{-\frac{4\pi(w-l)(2m)^{1/2}}{\hbar} \sqrt{\psi - \frac{eV}{2}}} - \left(\psi + \frac{eV}{2} \right) e^{-\frac{4\pi(w-l)(2m)^{1/2}}{\hbar} \sqrt{\psi + \frac{eV}{2}}} \right] \quad (1)$$

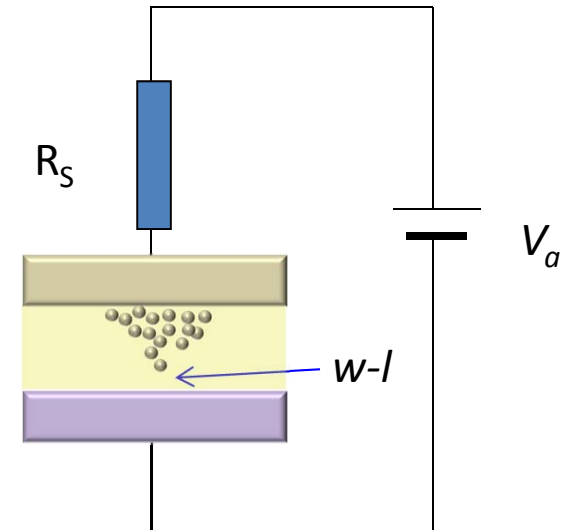
l is the length of the filament, determined by Eq. 2

$$\frac{dl}{dt} = \frac{\Delta d}{\tau_0} \left[e^{\left(\frac{V/E_0}{w-l} \right)} - e^{\left(\frac{-V/E_0}{w-l} \right)} \right] \quad (2)$$

$$E_0 = \frac{2kT}{e\Delta d} \quad \Delta d \text{ is the step length of the filament}$$



RRAM

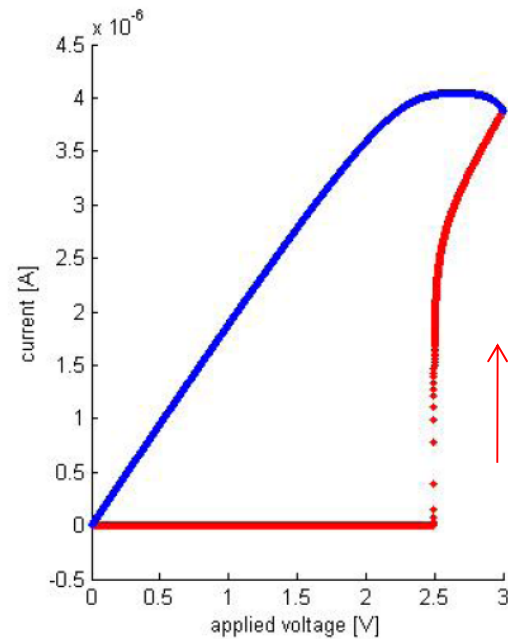
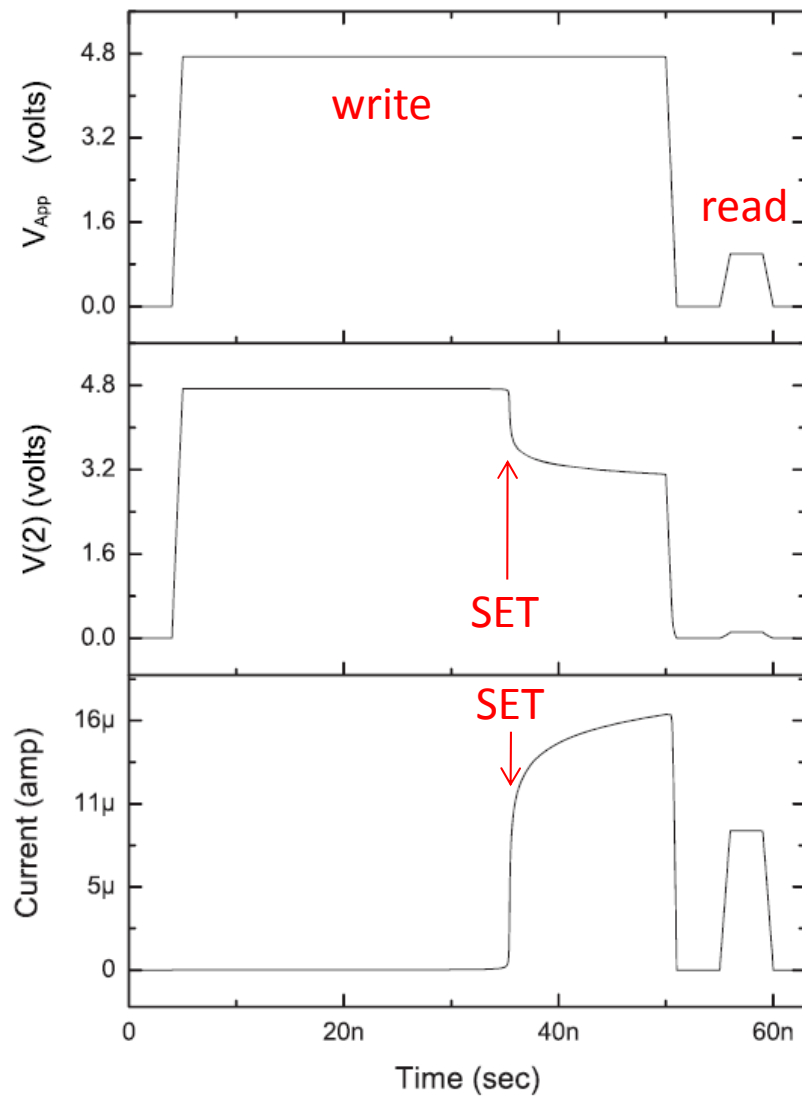


$$V + I \times R_s = V_a \quad (3)$$

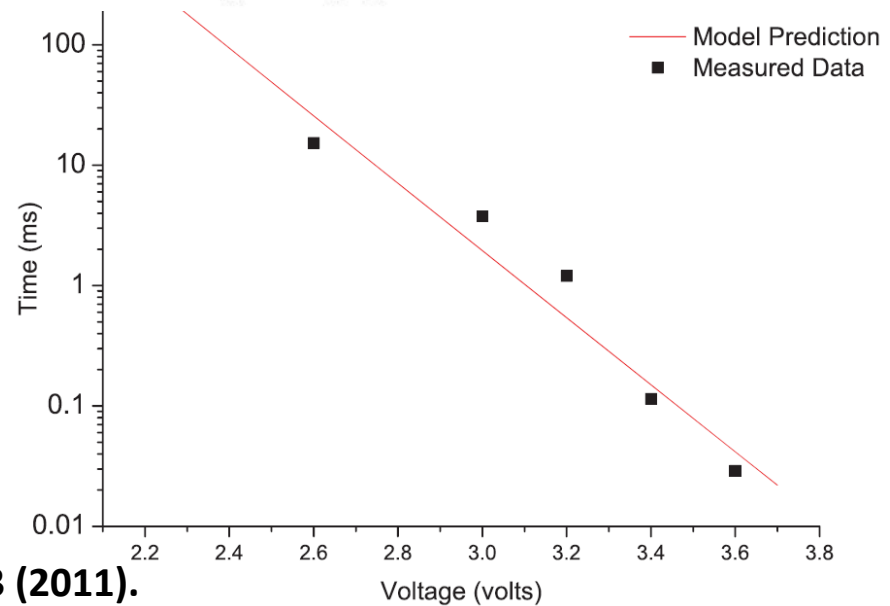
The voltage across the device V is related to I and applied voltage V_a

P. Sheridan, T. Chang, W. Lu, *Nanoscale* 3, 3833 (2011).

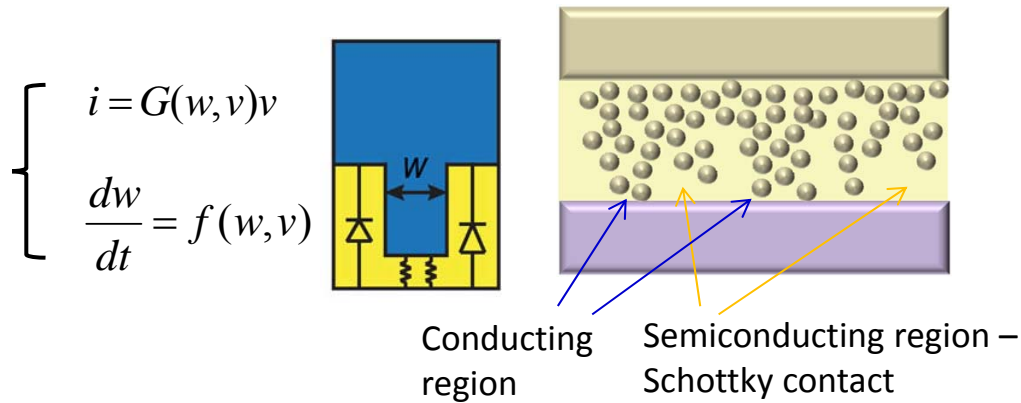
SPICE Model



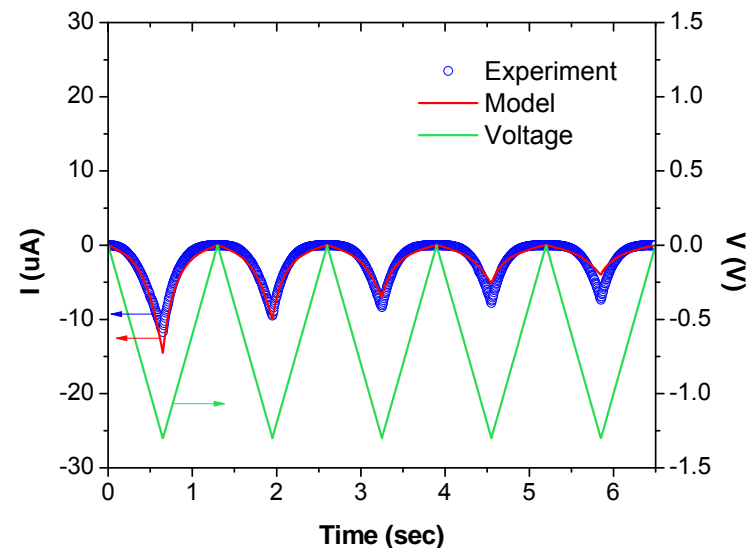
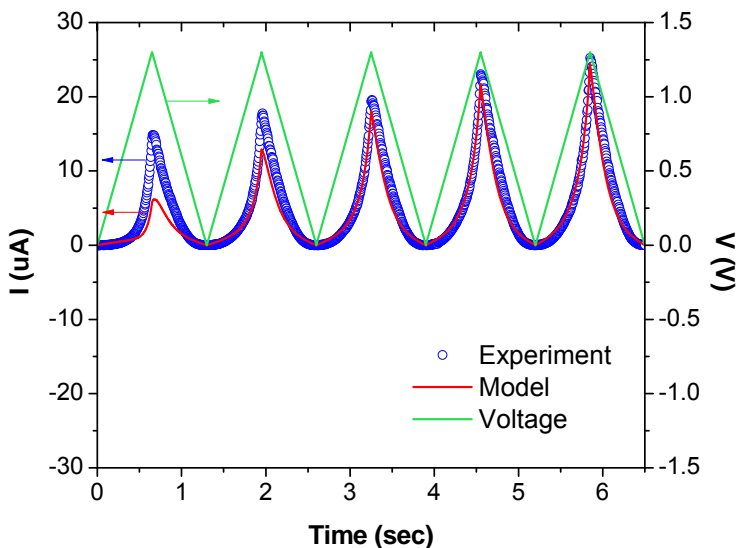
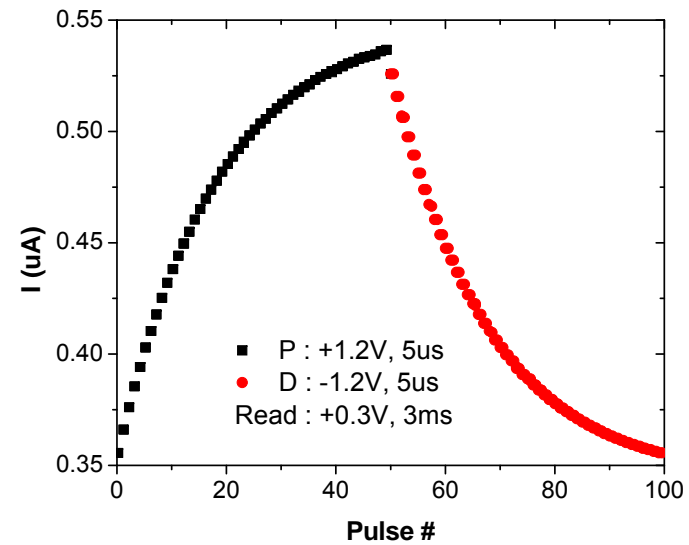
• Cell switching effects captured in SPICE



Analog Memristor Model

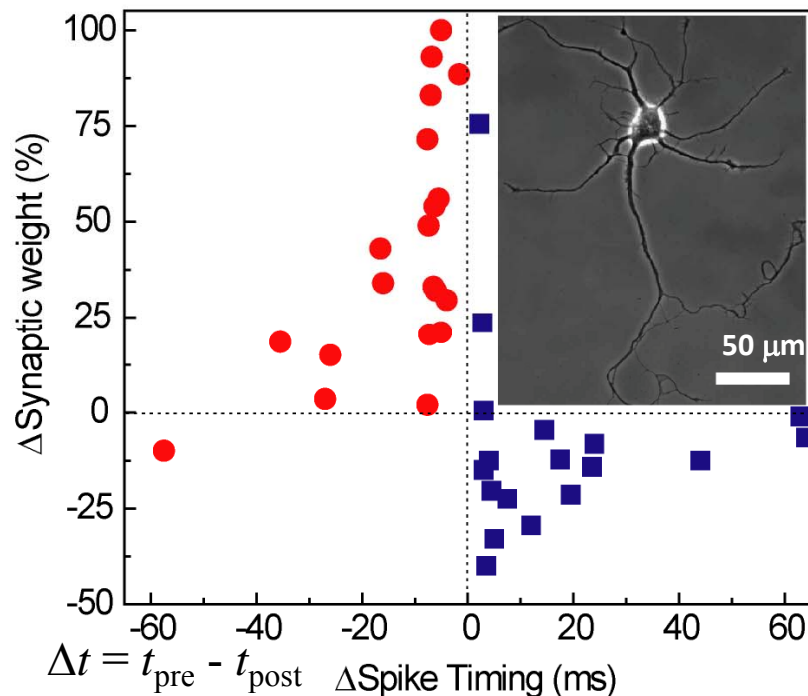


$$\Rightarrow \left\{ \begin{array}{l} i = (1 - w)\alpha[1 - \exp(-\beta v)] + w\gamma \sinh(\delta v) \\ \frac{dw}{dt} = \lambda \sinh(\eta v) - \frac{w}{\tau} \end{array} \right.$$



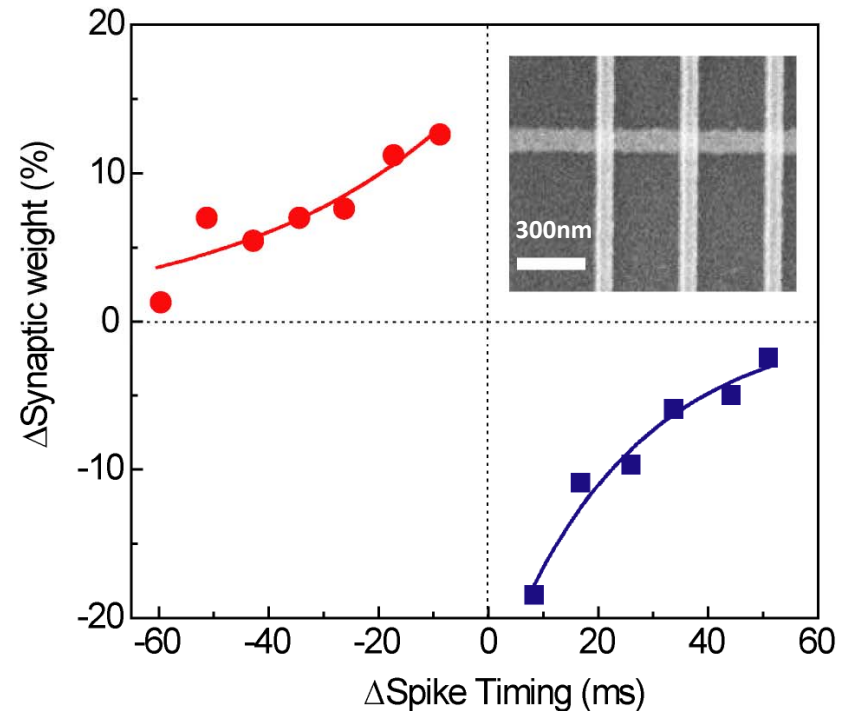
Prior Work - Analog Memristor As Synapse

Bio-system



Re-plotted with permission from G. Q. Bi, M. M. Poo, J. Neurosci. 1998. Inset: neuron image with permission from Kaech, S.; Banker, G. Nature Protocols 2006.

CMOS neuron/memristor synapse



S. H. Jo, T. Chang, I. Ebong, B. Bhavitavya, P. Mazumder, W. Lu, Nano Lett. 10, 1297-1301 (2010).

Prior Work - Integrated Crossbar Array/CMOS System

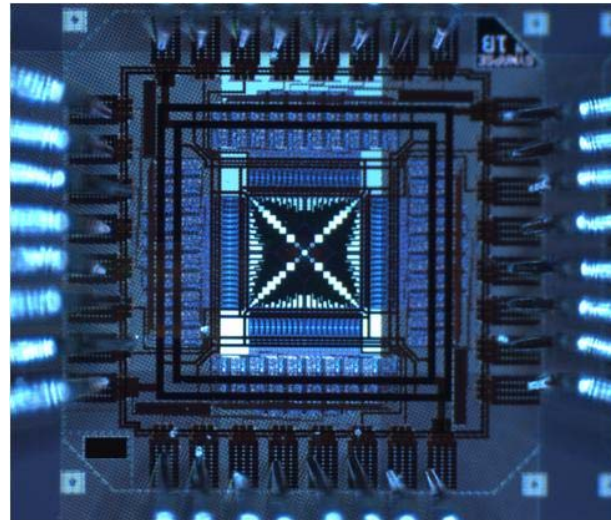
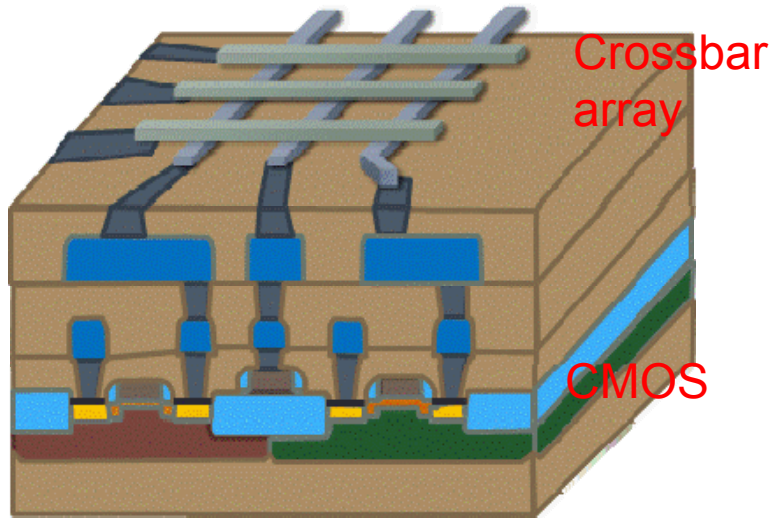
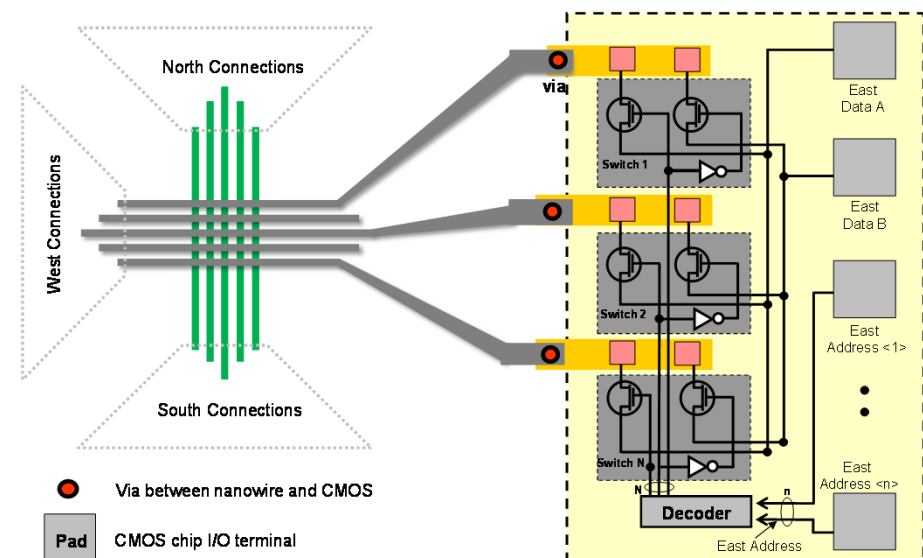
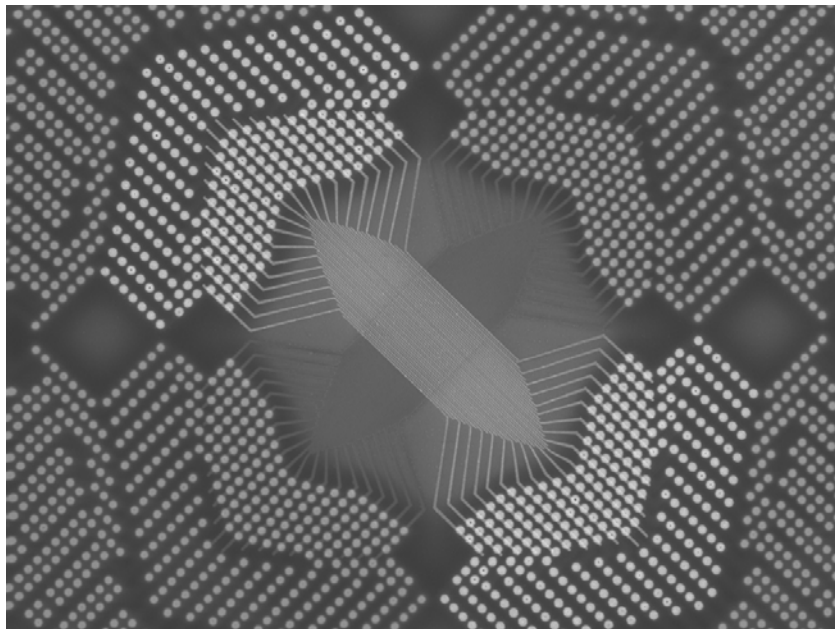
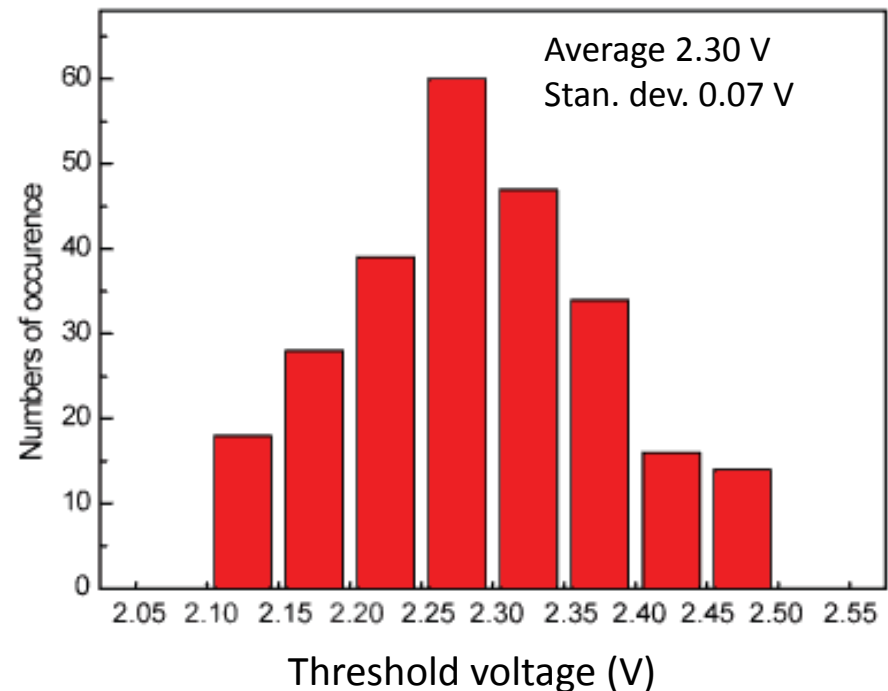
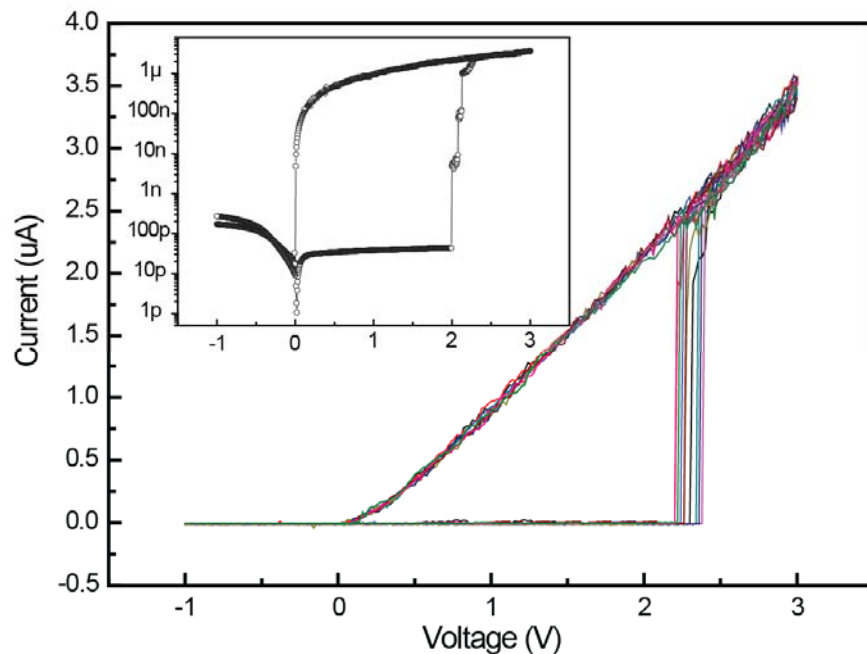


Image of an integrated crossbar/CMOS chip with probe card attached



Integrated Crossbar Array/CMOS System

I-V of the integrated Crossbar/CMOS system, Single device



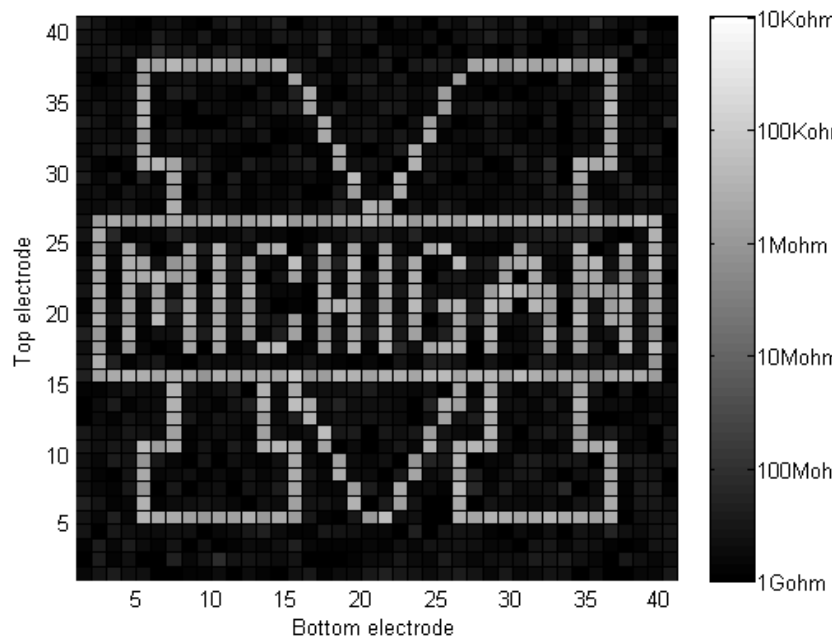
- Tight distribution from 256 devices measured
- Devices shown good on/off and intrinsic diode characteristics

K.-H. Kim, S. Gaba, D. Wheeler, J. M. Cruz-Albrecht, T. Hussain, N. Srinivasa, W. Lu,
Nano Lett., 12, 389–395 (2012).

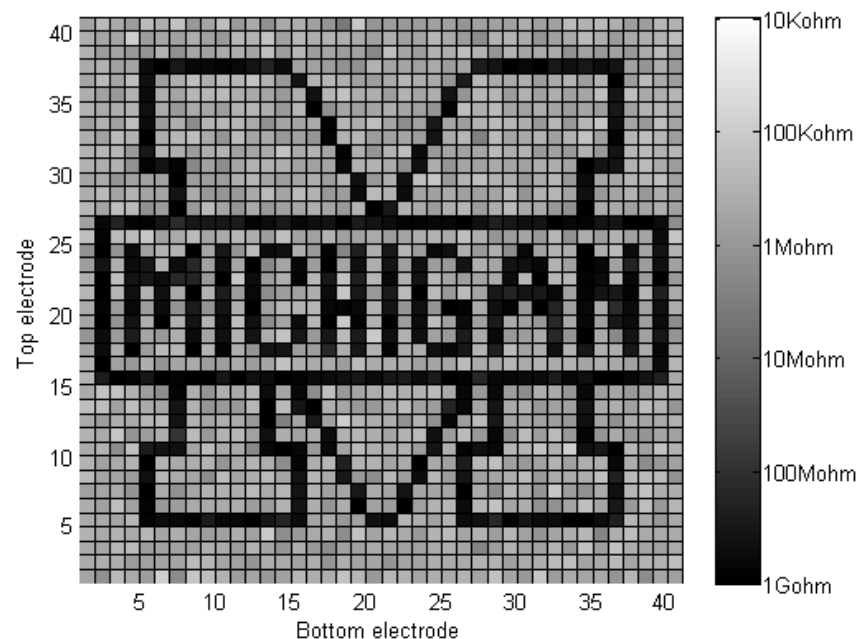
Integrated Crossbar Array/CMOS System

- Crossbar array operation, array written followed by read
- Programming and reading through integrated CMOS address decoders
- Each bit written with a single 3.5V, 100us pulse

Stored/retrieved image 1



Stored/retrieved image 2



Results from a 40x40 crossbar array integrated on CMOS

K.-H. Kim, S. Gaba, D. Wheeler, J. M. Cruz-Albrecht, T. Hussain, N. Srinivasa, W. Lu,
Nano Lett., 12, 389–395 (2012).

Conclusions

- Oxygen vacancy can be generated and move along dislocations at extreme environments
- Oxygen vacancy redistribution along the gate direction can modulate 2DEG conduction
- Multi-functional HEMT will be explored that combine configurability with high-performance
- Detailed experimental and modeling studies will be carried out to explore the underlying mechanism and demonstrate prototype devices

Summary

The proposed approach is a fully integrated schedule that will provide the electrical property measurements on the exact same films that are characterized for non-stoichiometry, interface strain, intermixing, point defects and dislocations.

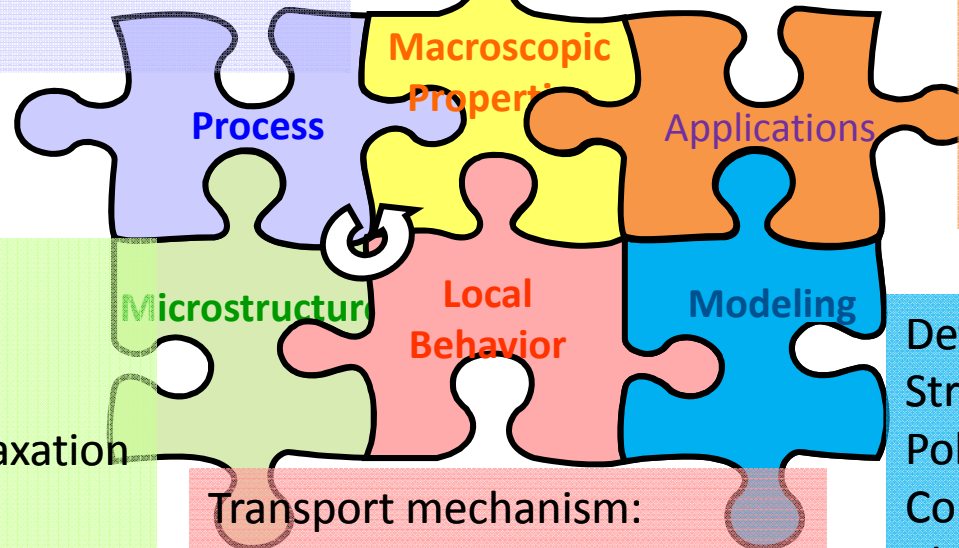
A strong international team has been built to address these challenges:

STO Substrate orientation
STO Surface preparation
Target material
Deposition conditions (p_{O_2} , plume, angle, temp...)
Annealing

Charged carrier density
mobility
Temperature dependence
Electrode/interface/substrate

Defect based devices
Resistive switching
Modeling and
experimental
prototype devices.

Substrate termination
Local stoichiometry
Domains
Strain development/relaxation
Intermixing
Ti valence profile
Point defects
+ Temperature dependence



Transport mechanism:
Polar discontinuity
Dipoles
Scattering sites
Domain boundaries

Defects and Impurities
Strain
Polarization
Compositional variations
Charge balance
mechanisms.
Charge carrier
development